Report DOT-FR-10026

TECHNICAL FEASIBILITY OF MAGNETIC LEVITATION AS A SUSPENSION SYSTEM FOR HIGH-SPEED GROUND TRANSPORTATION VEHICLES. VOL. II (APPENDIX)

John R. Reitz, Robert H. Borcherts, L. C. Davis,
Dennis F. Wilkie
Scientific Research Staff, Ford Motor Company

Administered by:
Transportation Research and Planning Office
Ford Motor Company
23400 Michigan Avenue
Dearborn, Michigan 48124

February 1972
Final Report (Task I) February 1971 - February 1972

Prepared for:
U. S. Department of Transportation
Federal Railroad Administration
400 Seventh Street, S.W.
Washington, D.C. 20591

TECHNICAL REPORT STANDARD TITLE PAGE

1. Report No.	2. Government Accession No.	3. Recipient's Catalog No.

4. Title and Subtitle
Technical Feasibility of Magnetic Levitation as a Suspension System for High-Speed Ground Transportation Vehicles

5. Report Date
February 1972

6. Performing Organization Code

7. Author(s)
John R. Reitz, Principal Investigator, Robert H. Borcherts, L. Craig Davis, Dennis F. Wilkie

8. Performing Organization Report No.

9. Performing Organization Name and Address
Ford Motor Company
Transportation Research and Planning Office
23400 Michigan Avenue
Dearborn, Michigan 48124

10. Work Unit No.

11. Contract or Grant No.
DOT-FR-10026

12. Sponsoring Agency Name and Address
U. S. Department of Transportation
Federal Railroad Administration
400 Seventh Street, S.W., Room 5416
Washington, D.C. 20591

13. Type of Report and Period Covered
Final Report (Task I)
Feb. 1971 - Feb. 1972

14. Sponsoring Agency Code

15. Supplementary Notes

16. Abstract

This report examines the technical feasibility of magnetic levitation as a suspension system for high-speed ground transportation vehicles in the 300 mph cruise speed range. Of the various magnetic suspensions which have been proposed only one appears to provide all of the desired features: good ride quality, moderate guideway tolerance, basic stability, and moderate drag forces. This is the high clearance (~ 10 inch vehicle-track clearance) suspension using superconducting magnets in the vehicle and a conducting, nonmagnetic, continuous guideway. If a high tolerance track can be successfully laid and maintained, then the low clearance suspension using magnetic attraction forces (being developed by Messerschmitt-Bölkow-Blohm and Krauss-Maffei in Germany) becomes a strong contender.

Analyses of ride quality show the importance of a high clearance suspension in smoothing track irregularities without allowing the vehicle to come into contact with the track. All magnetic suspensions are poorly damped relative to vehicle perturbation, so some type of active or passive control is necessary. Methods for increasing passive damping have been explored in the present report.

A preliminary design for a vehicle magnet using a superconducting coil is given.

Vol. I. Main body of report
Vol. II. Technical appendices

17. Key Words	18. Distribution Statement
Magnetic levitation, magnetic lift and drag forces, vehicle dynamics, ride quality, superconducting magnets	Unlimited

19. Security Classif. (of this report)	20. Security Classif. (of this page)	21. No. of Pages	22. Price
Unclassified	Unclassified		

Form DOT F 1700.7 (8-69)

TECHNICAL APPENDICES

A. Forces on Moving Magnets Due to Eddy Currents, J. R. Reitz (J. Appl. Phys. 41, 2067 (1970)).

B. Analysis of Motion of Magnetic Levitation Systems: Implications for High-Speed Vehicles, L. C. Davis and D. F. Wilkie (J. Appl. Phys. 42, 4779 (1971)).

C. Force on a Coil Moving Over a Conducting Surface, Including Edge and Channel Effects, R. H. Borcherts and L. C. Davis.

D. Force on a Rectangular Coil Moving Above a Conducting Slab, J. R. Reitz and L. C. Davis.

E. Dynamics, Control and Ride Quality of a Magnetically Levitated High Speed Vehicle, D. F. Wilkie.

F. Passive Damping, L. C. Davis.

G. Dynamic Response at an Expansion Joint in the Track, J. R. Reitz.

H. Magnet Calculations, R. H. Borcherts.

Reprinted from JOURNAL OF APPLIED PHYSICS, Vol. 41, No. 5, 2067–2071, April 1970

Forces on Moving Magnets due to Eddy Currents

JOHN R. REITZ
Scientific Research Staff, Ford Motor Company, Dearborn, Michigan 48121
(Received 15 August 1969; in final form 8 January 1970)

A magnet or a current-carrying coil, moving with constant velocity above a conducting plate, will experience magnetic lift and drag forces from the eddy currents induced in the plate. The lift and drag forces are calculated for various coil geometries on the assumption that the conducting plate is thin. For this model, the lift at high speeds approaches the force between the coil and its "image" located directly below it, and the drag force falls off as (velocity)$^{-1}$. The ratio of lift to drag is found to be independent of coil geometry, but the velocity dependence of the lift is greatly affected by the geometry. The ratio of lift to coil weight can be as high as 2000 for a superconducting coil moving at 300 mph at 0.1 m above a conducting plate. The relevance of the calculation to magnetically supported high-speed vehicles is discussed.

I. INTRODUCTION

Among the various proposals for new forms of high-speed ground transportation, several of these suggest that vehicle support might be achieved by means of magnetic fields.[1–4] In addition, magnetic levitation has also been proposed for a high-velocity rocket sled.[5,6] Except for Polgreen's system,[3] which uses a permanent-magnet roadbed, vehicle support is to be provided by magnetic forces on current-carrying coils located in the vehicle, these forces resulting from eddy currents induced in the conducting roadbed.

In the simplest type of system utilizing magnetically supported vehicles the roadbed consists of a conducting plate (aluminum or copper) backed by a conventional (nonconducting) roadbed. There are several calculations in the literature which bear on this situation. Two basic studies[7,8] treat long current-carrying wires moving parallel to and above a conducting plate, and both of these show that at high speeds the lift force on the wire approaches that produced by the "image" of the current-carrying wire and that the drag force decreases asymptotically toward zero. In the first calculation, Hannakam[7] treated two long parallel wires carrying currents in opposite directions moving perpendicular to their lengths over a "thin" conducting plate. In the second case, Klauder[8] investigated the forces on a single current-carrying wire moving over a thick conducting slab. Neither of these calculations treated complete current circuits so that no considerations of coil geometry were possible.[9] In order to understand better the parameters which govern the lift and drag forces on a magnet (or coil) moving above a conducting plate, it was felt that calculations of induced eddy currents and their associated fields for several magnet geometries would be useful. This forms the basis for the present paper.

Calculations will be made for the lift and drag forces on various magnets moving with velocity v at fixed height z_0 above a thin conducting plate. The method of

calculation (the image-wake method), which is described in Sec. II, is easy to apply to realistic magnet geometries. In Sec. III the method is applied to several geometries, including the magnetic dipole, parallel current-carrying wires, large rectangular coils, and coil arrays. The limitation of the thin-plate model and its applicability to high-speed transportation is discussed in Sec. IV. Section V discusses achievable lift-to-weight ratios using superconducting coils and the power requirement to overcome magnetic drag forces.

II. EDDY CURRENTS IN A THIN PLANE SHEET

Consider a thin plane sheet of infinite extent of conductivity σ and thickness δ. Let this plate coincide with the x–y plane. The exciting field will be represented by a vector potential $\mathbf{A}'(x, y, z, t)$ due to sources in the upper half-space ($z>0$). The field from eddy currents in the conductor will be represented by a vector potential $\mathbf{A}(x, y, z, t)$. The conducting plate is assumed thin compared to the skin depth for the dominant frequencies in the exciting field; under these conditions the current density in the plate is independent of the z coordinate. This is the method considered by Hannakam[7] who used a Fourier integral method to determine the eddy currents produced by a pair of moving wires, but a simpler method of solution appropriate to this problem has been discussed by Smythe.[10] We shall limit the discussion to source currents moving parallel to the x–y plane; under these circumstances both $\mathbf{A}$ and $\mathbf{A}'$ have no z component.

From Faraday's Law, Ohm's Law, and Ampere's Circuital Law (neglecting displacement currents), it is found that the vector potential satisfies the following equation[10]:

$$\partial(\mathbf{A}'+\mathbf{A})/\partial t = w\partial\mathbf{A}/\partial z, \tag{1}$$

where

$$w = 2/\sigma\mu_0\delta \tag{2}$$

(in mks units) has the dimensions of a velocity. Since $\mathbf{A}'$ is known, Eq. (1) may be used to obtain $\mathbf{A}$ in the sheet. Consider a sudden change in the exciting field $\mathbf{A}'$; the right-hand side of (1) is finite, so that

$$d(\mathbf{A}'+\mathbf{A}) \to 0 \quad \text{as} \quad dt \to 0. \tag{3}$$

In other words a sudden change in the exciting field produces eddy currents which maintain the instantaneous field in the plate. The eddy currents subsequently decay. Suppose that the exciting field from a source at z_0 and originally time independent is changed from

$$\mathbf{A}_1' = \mathbf{f}_1(x, y, z-z_0) \quad \text{for} \quad t<0$$

to

$$\mathbf{A}_2' = \mathbf{f}_2(x, y, z-z_0) \quad \text{for} \quad t>0. \tag{4}$$

At $t=+0$, the $\mathbf{A}$ field in the plate is

$$(\mathbf{A})_{t=0} = -\mathbf{f}_2(x, y, z-z_0) + \mathbf{f}_1(x, y, z-z_0). \tag{5a}$$

This field can be visualized as being produced by two images at z_0, and its form is appropriate for extension into the lower half-space. It is evident that (5a) prevents the instantaneous propagation of a change in $\mathbf{A}'$ from proceeding through the plate. Another possible prescription for the $\mathbf{A}$ field in the plate at $t=+0$ (since $\mathbf{f}$ due to a source at z_0 depends only upon current geometry and $|z-z_0|$) is

$$(\mathbf{A})_{t=0} = -\mathbf{f}_2(x, y, z+z_0) + \mathbf{f}_1(x, y, z+z_0). \tag{5b}$$

This field can be visualized as produced by two images below the sheet. Equation (5b) can be extended into the upper half-space; combined with (5a) it gives the $\mathbf{A}$ field the necessary symmetry.

$\mathbf{A}' = \mathbf{f}_2(x, y, z-z_0)$ is independent of time, so that for $t>0$ Eq. (1) reduces to

$$\partial\mathbf{A}/\partial t = w(\partial\mathbf{A}/\partial z). \tag{6}$$

This equation may be used to solve the eddy current decay. A solution of (6) which reduces to (5b) at $t=0$ is

$$\mathbf{A} = -\mathbf{f}_2(x, y, z+z_0+wt) + \mathbf{f}_1(x, y, z+z_0+wt). \tag{7}$$

This potential may be visualized as produced by a pair of images moving away from the midplane with velocity w. Since the tangential component of $\mathbf{A}$ is continuous at the plate surface and Eq. (7) satisfies Laplace's equation in the upper half-space, (7) provides a solution in the region in and above the conducting plate.

The eddy current configuration in a thin plate and its time-dependent decay has thus been replaced by a set of receding images. In order to solve problems involving moving magnets, we replace the uniform motion by a series of sudden jumps and then proceed to the limit of continuous motion. The force on the magnet due to the currents can be evaluated as the force provided by the image system. The wake of images produced by a magnetic dipole moving above a thin conducting plate is shown in Fig. 1.

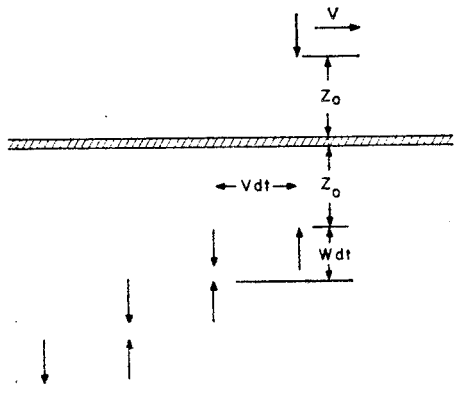

FIG. 1. Schematic view of the "wake of images" produced by a magnetic dipole moving with velocity v at height z_0 above a thin conducting sheet. The image wake extends to $-\infty$ with the images receding vertically with velocity w. For clarity, the images are separated by a finite-time interval dt.

III. EXAMPLES OF FORCES ON MOVING MAGNETS AND COILS

In this section are calculated the forces on several different magnets moving with uniform velocity v at constant height z_0 above a thin conducting plate characterized by the parameter $w=2/\mu_0\sigma\delta$.

A. Magnetic Monopole

We first consider a monopole at height z_0 above the conducting plate. The monopole is the limit of a long thin bar magnet or solenoid oriented perpendicular to the plate. The pole strength q has the dimensions of magnetic moment per unit length. The vertical component of magnetic field at the pole from the nth image pair, which has receded a distance $wn\tau$, is

$$\Delta B_z=\frac{\mu_0 q}{4\pi}\left(\frac{2z_0+nw\tau}{[(nv\tau)^2+(2z_0+nw\tau)^2]^{3/2}}-\frac{2z_0+nw\tau}{[(nv\tau+v\tau)^2+(2z_0+nw\tau)^2]^{3/2}}\right). \quad (8)$$

Letting $n\tau\rightarrow t$ and $\tau\rightarrow dt$, we obtain

$$B_z=\frac{3\mu_0 v^2 q}{4\pi}\int_0^\infty\frac{(2z_0t+wt^2)\,dt}{[v^2t^2+(2z_0+wt)^2]^{5/2}}. \quad (9)$$

The lift force $F_L=qB_z$ is found to be

$$F_L=(\mu_0 q^2/16\pi z_0^2)[1-w/(v^2+w^2)^{1/2}]. \quad (10)$$

The drag force F_D may be calculated from the component of magnetic field in the direction of motion of the monopole. We find

$$F_D=(w/v)F_L. \quad (11)$$

The maximum lift from Eq. (10) is that due to a single image located directly below the monopole. This will be called the ideal lift.

B. Magnetic Dipole

We next consider a dipole of moment m, oriented vertically, at height z_0 above the plate. Since a dipole can be considered constructed of two monopoles we can use the result of Sec. A to obtain

$$F_L=(3\mu_0 m^2/32\pi z_0^4)[1-w/(v^2+w^2)^{1/2}] \quad (12)$$

and

$$F_D=(w/v)F_L. \quad (13)$$

Here again the lift approaches the ideal lift from a single image.

C. Long Straight Wire

The third example is a long straight wire carrying current I moving perpendicular to its length at constant height z_0 ($z_0\ll$length of wire). The lift and drag forces (per unit length of wire) are found to be

$$F_L=(\mu_0 I^2/4\pi z_0)[v^2/(v^2+w^2)], \quad (14)$$

$$F_D=(w/v)F_L. \quad (15)$$

D. Two Parallel Wires

A slightly more interesting case from the preceding one is that of two parallel wires separated by distance $2c$ carrying equal but oppositely directed currents I, moving perpendicular to their lengths at constant height z_0. In addition to the forces found under case C we also have a force on each wire from the image system of the other. And because the rear wire sees more of the second image system than the front wire there is a turning couple on the system. We find (forces per unit length of wire)

$$F_L=(\mu_0 I^2/2\pi)[c^2/z_0(c^2+z_0^2)][v^2/(v^2+w^2)], \quad (16)$$

$$F_D=(w/v)F_L, \quad (17)$$

and

$$\text{Torque}=z_0F_D \quad (18)$$

in a direction such as to lift the rear wire.

E. Large Rectangular Coil

More interesting for vehicle levitation are large flat coils. We shall consider a rectangular coil of N turns with dimensions $a\times b$ moving in the plane of the coil at constant height z_0 above the conducting plate. The b dimension is taken in the direction of motion. The number of turns N is considered to be small enough that all turns are at approximately the same height z_0. The mutual inductance between the coil and one of its images can be calculated from Neumann's formula[11]; for the mutual inductance between the coil and that image separated by a vertical distance z and a horizontal distance in the direction of motion x:

$$M=\frac{\mu_0 N^2}{2\pi}\Big\{2a\sinh^{-1}\frac{a}{(x^2+z^2)^{1/2}}-a\sinh^{-1}\frac{a}{[(x+b)^2+z^2]^{1/2}}-a\sinh^{-1}\frac{a}{[(x-b)^2+z^2]^{1/2}}+(x+b)\sinh^{-1}\frac{x+b}{z}$$
$$+(x-b)\sinh^{-1}\frac{x-b}{z}-2x\sinh^{-1}\frac{x}{z}-(x+b)\sinh^{-1}\frac{x+b}{(z^2+a^2)^{1/2}}-(x-b)\sinh^{-1}\frac{x-b}{(z^2+a^2)^{1/2}}+2x\sinh^{-1}\frac{x}{(z^2+a^2)^{1/2}}$$
$$-4(a^2+x^2+z^2)^{1/2}+4(x^2+z^2)^{1/2}+2[a^2+z^2+(x+b)^2]^{1/2}-2[z^2+(x+b)^2]^{1/2}+2[a^2+z^2+(x-b)^2]^{1/2}-2[z^2+(x-b)^2]^{1/2}\Big\}, \quad (19)$$

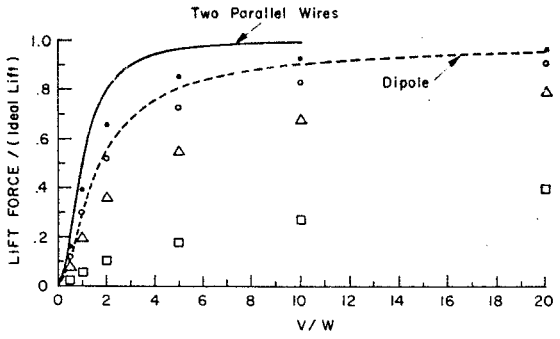

FIG. 2. Lift force (expressed as fraction of ideal lift) for several different coil geometries as a function of coil speed v moving parallel to and above a thin conducting sheet. — Two long parallel wires carrying equal but opposite currents moving perpendicular to their lengths. -- Magnetic dipole. The other results are for rectangular coils of dimensions $b\times a$ at height $z_0=0.05a$ (the b dimension is in the direction of motion): ● $b=0.5a$, ○ $b=a$, △ $b=2a$, □ $b=10a$.

and the force on the coil due to the image is

$$\mathbf{F}=\pm I^2\,\mathrm{grad}M, \tag{20}$$

the sign being determined by the relative sense of the currents. The lift and drag forces may be obtained by summing the appropriate component of (20) over the image system. This procedure has been carried out for several coil geometries, the final summation over the image wake being done numerically.

The lift forces on various rectangular coils moving at constant height above the conducting plate are shown in Fig. 2 as a function of v/w. The actual calculations shown are for $z_0=0.05a$, but since they are normalized to the ideal lift (the force between the coil and its image located directly below it) the results change only slowly with z_0. The ideal lift is given in Table I. As seen from the figure, a rectangular coil with its small dimension in the direction of motion is more effective in producing lift at moderate speeds than is a coil with the other aspect ratio. Drag forces have also been calculated; in all cases

$$F_D=(w/v)F_L, \tag{21}$$

a not unexpected result since a large coil can be imagined as being constructed from dipoles.

F. Coil Array

Calculations were also made for a two-coil array, the two rectangular coils of the array being separated in the direction of motion. If the two coils are not too far apart there is interaction between each coil and the image system of the other, which can produce either more or less lift depending upon the relative sense of the currents. As an example, consider two rectangular coils with $b/a=0.5$; b is the dimension in the direction of motion. If these are separated by a distance $10a$ (in the direction of motion) there is very negligible interaction between the coils for speeds less than $10w$. For $v/w=20$ the lift is changed by 0.5%; this represents an increase in lift if the currents in the coils circulate in opposite senses. If the two coils are separated by $0.6a$ and the currents circulate oppositely, the lift is increased by 15% at $v/w=1$ and by 9.2% at $v/w=10$. The drag is still given by Eq. (21).

IV. LIMITATIONS OF THE MODEL

The model we have been using to calculate lift and drag forces is that of the thin conducting plate. For this model all drag forces fall off as v^{-1} in the high-velocity range, i.e., propulsive power to overcome electromagnetic drag is independent of speed in the high-velocity range. The parameter w is inversely proportional to the thickness of the plate so that a larger thickness pushes F_L and F_D farther into the asymptotic range. However, the various frequency components of the electromagnetic disturbance of the moving magnet will be shielded by skin depth considerations, and prevent a uniform distribution of currents across the thickness of the plate. As a first approximation, one might replace the plate thickness by the skin depth when the former exceeds the latter and apply the thin-plate theory described here.[12] Since skin depth is proportional to $\omega^{-1/2}=(v/\text{appropriate length})^{-1/2}$, drag forces will switch over to a $v^{-1/2}$ dependence at the higher velocities.

To get some idea of the importance of these considerations, we make a few numerical calculations. For a 1-cm-thick plate at room temperature

$$w(\text{copper})=2.7\text{ m/sec},$$

$$w(\text{aluminum})=4.5\text{ m/sec}.$$

The electromagnetic disturbance of a moving magnet will have a broad frequency spectrum. The dominant frequency for a magnet moving with velocity v at distance z_0 above the plate will be $\omega=v/z_0$. For $v=134$ m/sec (300 mph) and $z_0=0.1$ m the skin depth at this frequency is

$$\delta_S(\text{copper})=0.45\text{ cm},$$

$$\delta_S(\text{aluminum})=0.58\text{ cm}.$$

One is therefore in the region controlled by skin depth at

TABLE I. Repulsive force (ideal lift) between a rectangular coil of dimensions $a\times b$ and its image situated directly below it at distance $2z_0$. Factor in table is to be multiplied by $(\mu_0N^2I^2/2\pi)\times(\text{perimeter}/2z_0)$.

$2z_0/a$	$b/a=0.5$	1	2	10
0	1.0000	1.0000	1.0000	1.0000
0.1	0.8601	0.9009	0.9316	0.9742
0.2	0.7143	0.8041	0.8601	0.9340
0.3	0.5771	0.7108	0.7870	0.8822
0.4	0.4591	0.6228	0.7143	0.8224
0.5	0.3633	0.5417	0.6438	0.7583

this velocity and plate thickness. The transition from thin-plate to skin-depth behavior should occur at speeds around 30 m/sec for a 1-cm thick plate.

The calculations of the preceding section show that at high velocities the lift force approaches that from the magnet's image (the ideal lift) and the ratio of drag to lift is w/v. If we substitute the skin depth $\delta_S = (2/\omega\sigma\mu_0)^{1/2} = (2z_0/v\sigma\mu_0)^{1/2}$ for the plate thickness we find

$$F_D/F_L = (2/\sigma\mu_0 v z_0)^{1/2}. \tag{22}$$

Klauder[8] has calculated lift and drag on a current-carrying wire moving over a thick plate. He finds that the currents in the plate decrease as a function of distance below the surface, more rapidly at the higher velocities. He further finds that the lift approaches the ideal lift at high speeds. The ratio of drag to lift is not a simple function, but in the high-velocity limit he finds (converting his result to mks units)

$$F_D/F_L = (\pi/4\sigma\mu_0 v z_0)^{1/2}, \tag{23}$$

which is of the same order but somewhat smaller than (22). It thus appears that the thin-plate model can be used to study effects of magnet geometry on the lift and drag forces on fast moving magnets provided one uses the skin depth for the effective plate thickness. At lower velocities the eddy currents are distributed throughout the plate thickness and approach the true current distribution of the thin-plate model.

V. ACHIEVABLE LIFT-TO-WEIGHT RATIO AND ESTIMATE OF ELECTROMAGNETIC DRAG

In this section we examine the lift-to-weight ratio for a large flat coil to determine the feasibility of magnetic suspension. Impressive results can be achieved with superconducting coils and these have in fact been proposed by Powell and Danby[2] for high-speed transport. From data for commercially available superconducting wire, 32 000 m of wire which will carry a critical current of 50 A weighs 30 kg. This may be wound into a 1-m-diam coil with a current-carrying cross section of about 16 cm^2. The ideal lift force on the coil from its image at $2z_0 = 0.2$ m is 6.50×10^5 N $= 6.62\times10^4$ kg. This is a lift-to-weight ratio of 2200. This ratio will be degraded by added weight for Dewars and associated cryogenic equipment, and by the finite-speed lift factor, but the ratio appears large enough to warrant serious consideration for magnetic support in high-speed transportation systems. Problems relating to the stability of persistent-mode superconducting coils against vibration and other demagnetizing effects have not been explored.

Finally, a few remarks about the power requirement to overcome electromagnetic drag are in order. In all cases the F_D/F_L ratio is given by w/v; this is independent of coil geometry. For the thick plate case F_D/F_L is given by (23) and probably is also independent of coil geometry except for height above surface. The power requirement:

$$\text{Power} = F_D v = F_L w = (\text{weight})\, w. \tag{24}$$

If we take $w = 6$ m/sec (this might be appropriate for copper when the thickness is controlled by the skin depth and the speed is 300 mph), then for an automobile-size vehicle the power requirement is 90 kW or about 120 hp. [This becomes 76 hp if one uses Eq. (23).] For larger vehicles the drag scales as the weight. This result is less than, but the same order as aerodynamic drag losses at 300 mph for a well-designed vehicle and thus represents a significant power requirement. It also mitigates against a decisive reduction in drag by running the vehicle system in a partially evacuated tube.

A different type of conducting roadbed has been proposed by Powell and Danby.[2] In their system the conducting part of the roadbed consists of large separated coils (of the same size as coils in the vehicle). Eddy current in each coil is limited by a diode and series inductance. By limiting both the direction and magnitude of the induced currents, these authors claim to reduce electromagnetic drag relative to lift by an order of magnitude. Such a scheme certainly warrants further investigation.

ACKNOWLEDGMENTS

The author would like to thank Dr. A. H. Silver and Dr. R. H. Borcherts for several helpful discussions.

[1] *Survey of Technology for High Speed Ground Transport* (U.S. Dept. of Commerce, Washington, D.C., June 1965), Pt. 1, p. V-180.

[2] J. R. Powell and G. R. Danby, Amer. Soc. Mech. Engrs. Paper 66-WA/RR-5 (1966).

[3] G. R. Polgreen, Proc. Inst. Mech. Engrs. (London) **181**, 145 (1966–67).

[4] H. T. Coffey, F. Chilton, and T. W. Barbee, Jr., J. Appl. Phys. **40**, 2161 (1969).

[5] *The Hypervelocity Rocket Sled* (Stanford Res. Inst., Stanford, Cal., 1968), Contract A7(04-3)-115.

[6] C. A. Guderjahn, S. L. Wipf, H. J. Fink, R. W. Boom, K. E. MacKenzie, D. Williams, and T. Downey, J. Appl. Phys. **40**, 2133 (1969).

[7] L. Hannakam, Elektrotech. Z. **A86**, 427 (1965).

[8] L. T. Klauder, Jr., Amer. J. Phys. **37**, 323 (1969).

[9] Several approximate calculations for current-carrying coils have been made. Guderjahn *et al.* (Ref. 6) applied Hannakam's results to rectangular coils by modifying the asymptotic lift to the appropriate value; they did not, however, calculate how the speed dependence of the lift and drag varies with coil geometry. Some experimental results for lift and drag on rectangular coils are given by these authors. Coffee *et al.* (Ref. 4) have given semiphenomenological expressions for forces on coils moving over a thick plate.

[10] W. R. Smythe, *Static and Dynamic Electricity* (McGraw-Hill Book Co., New York, 1950), 2nd ed., p. 402.

[11] See, e.g., J. R. Reitz and F. J. Milford, *Foundations of Electromagnetic Theory* (Addison-Wesley Publ. Co., Reading, 1967), 2nd ed., p. 176.

[12] This prescription for correcting the thin-plate model was used by Guderjahn *et al.* (Ref. 6).

Reprinted from:
JOURNAL OF APPLIED PHYSICS VOLUME 42, NUMBER 12 NOVEMBER 1971

Analysis of Motion of Magnetic Levitation Systems: Implications for High-Speed Vehicles

L. C. Davis and Dennis F. Wilkie
Scientific Research Staff, Ford Motor Company, Dearborn, Michigan 48121
(Received 7 April 1971; in final form 21 June 1971)

To study the motion of a magnetically suspended high-speed vehicle, a simple example (the long wire above a thin conducting plate) is considered in detail. The lift and drag forces on the magnet (long wire) are derived for arbitrary motion above the plate. The stability of the system is analyzed for typical parameters (velocity = 300 mph, height = 0.1 m). By using a Laplace-transform technique, it is shown that two types of modes occur (in the linearized equations of motion). One mode is a vertical oscillation with an amplitude that grows slowly in time. The other mode is an unbounded increase in the horizontal velocity error. This latter instability results from the fact that the drag force decreases with increasing velocity at high speeds. In this connection, an error is pointed out in a recent publication in which it was claimed that the system is stable. Detailed consideration of the effects of horizontal acceleration and vertical velocity on the magnetic forces is given. The effects of aerodynamic drag and the need for active control of the system are also discussed.

I. INTRODUCTION

The lift and drag forces on various magnets moving with a uniform velocity at a constant height above a thin conducting plate have been calculated by Reitz.[1] These forces result from the eddy currents induced in the plate by the moving magnetic field. The plate is assumed to be infinite in extent with thickness small compared to the skin depth for the dominant frequencies involved and small compared to the height of the magnet above the plate. These assumptions allow a simple image-wake solution for the magnetic forces.

The image-wake method can be extended to arbitrary motion of a magnet. Bailey and Norwood[2] have made such an extension and claimed to show that the equilibrium of the magnet is stable, i.e., the magnet will return to its equilibrium height and velocity if it experiences small perturbations from its previously steady motion. However, we shall point out an error in their analysis and demonstrate that the equilibrium of a magnet in steady motion is unstable. It is important to determine the stability and transient response of such magnetic systems due to the current interest in the use of magnetic levitation for the suspension of high-speed vehicles.[1,3] Subsequently, if these responses are found to be unacceptable, the need for active control will become apparent.

For simplicity, we mostly consider the long wire in this paper, although much of our analysis pertains to the translational degrees of freedom of any magnet. Because we can analyze this case exactly, we can determine the validity and the limitations of approximate techniques which we then can use to analyze more complicated magnet configurations. (In addition, the long wire was considered by Bailey and Norwood[2] and by Reitz.[1]) We also give some general formulas for estimating the corrections to our approximations for any magnet configuration.

In Sec. II we derive the forces on a long wire with arbitrary motion using a slightly different technique than Bailey and Norwood[2] used. In Sec. III we show that our force expressions agree with those of Reitz[1] for the case of steady motion of a long wire. Section IV contains an analysis of the motion of a long wire subject to a small disturbance from previously steady motion. This analysis is based upon a linearization of the forces obtained by replacing the velocity and height in the formulas for the forces resulting from steady motion with the instantaneous velocity and height (referred to as the instantaneous approximation). Although not exact, such an analysis is a useful starting point for understanding the rather complicated results of the exact analysis given in Sec. IV. The exact analysis is made by applying the Laplace transform to the linear approximation of the forces obtained in Sec. II. The error made by Bailey and Norwood[2] in their analysis, which also utilized the Laplace transform, is discussed in Sec. II. The range of validity and the limitations of the instantaneous approximation are also discussed in Sec. II. In Sec. VI we give further justification of the instantaneous approximation for the long wire and show how to determine the size of the corrections to the approximate force expressions for any magnet.

In Sec. VII the results of a numerical study of the motion resulting from an application of the nonlinear forces obtained by the corrected instantaneous approximation (Sec. VI) are given. The ef-

fects of aerodynamic drag on the stability of the equilibrium are discussed, and numerical results are given to illustrate this. Some aspects of the control of the motion of magnetic systems are discussed in Sec. VIII. In Sec. IX we summarize the conclusions which follow from the results presented in the paper.

II. MAGNETIC FORCES FOR ARBITRARY MOTION

In this section we derive the forces on a long wire with arbitrary motion above a thin conducting plate (or sheet) using a somewhat different technique than that used by Bailey and Norwood.[2] The coordinate system for this problem is shown in Fig. 1. We let the thin plate coincide with the x-y plane (infinite in extent). The position of the wire is given by $(x_0(t), z_0(t))$ with the wire remaining parallel to the y axis at all times, i.e., only motion in the x-z plane is to be considered. Let δ be the thickness of the plate and σ the conductivity. The boundary condition at the top of the plate is[4] $(z = +0)$

$$\frac{\partial^2(\Omega+\Omega')}{\partial t\partial z} = w\frac{\partial^2\Omega}{\partial z^2}, \tag{2.1}$$

where

$$w = 2/\mu_0\sigma\delta, \tag{2.2}$$

and the magnetic scalar potential is the sum of two terms: Ω' due to the wire (or in general any source) and Ω due to the eddy currents induced in the plate. In the region external to the plate, Ω satisfies Laplace's equation.

Consider first a source potential Ω' which is suddenly switched on at $t = 0$:

$$\begin{aligned}\Omega'(x,y,z,t) &= 0, \qquad t<0\\ &= f(x,y,z), \quad t>0.\end{aligned} \tag{2.3}$$

For $t < 0$, Ω is zero since no eddy currents have been induced. Integrating (2.1) from $t < 0$ to some time $t_1 > 0$, we find

$$\frac{\partial\Omega}{\partial z}(x,y,+0,t_1)+\frac{\partial\Omega'}{\partial z}(x,y,+0,t_1) = w\int_0^{t_1}\frac{\partial^2\Omega}{\partial z^2}(x,y,+0,t)\,dt. \tag{2.4}$$

As $t_1 \to +0$, the right-hand side of (2.4) vanishes, so that immediately following the time when the source is switched on,

$$\frac{\partial\Omega}{\partial z}(x,y,+0,+0) = -\frac{\partial\Omega'}{\partial z}(x,y,+0,+0) = -\frac{\partial f}{\partial z}(x,y,+0). \tag{2.5}$$

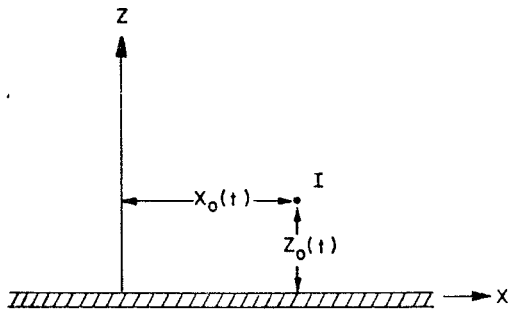

FIG. 1. Coordinate system describing position of wire. Current flows perpendicular to x-z plane. Motion of wire is in x-z plane.

At subsequent times, Ω' is independent of time so for $t > 0$,

$$\frac{\partial^2\Omega}{\partial t\partial z}(x,y,+0,t) = w\frac{\partial^2\Omega}{\partial z^2}(x,y,+0,t). \tag{2.6}$$

It can be shown that a solution which satisfies (2.6) and Laplace's equation and which vanishes at infinity is

$$\Omega(x,y,z,t) = f(x,y,-z-wt), \quad z>0. \tag{2.7}$$

The solution below the plate is found by requiring $\Omega(x,y,z,t) = -\Omega(x,y,-z,t)$, which follows from the symmetry of the problem.

Let us now consider a source potential $\Omega'(x,y,z,t)$ with an arbitrary time dependence. At time t' during an interval dt', a change

$$\frac{\partial\Omega'}{\partial t'}(x,y,z,t')\,dt'$$

occurs in Ω'. This change gives rise to eddy currents which contribute to Ω at time $t > t'$ an amount [according to (2.7)]

$$\frac{\partial\Omega'}{\partial t'}(x,y,-z-w(t-t'),t')dt', \quad z>0.$$

Adding up all such contributions, we find

$$\Omega(x,y,z,t) = \int_{-\infty}^{t}\frac{\partial\Omega'}{\partial t'}(x,y,-z-w(t-t'),\ t')dt'. \tag{2.8}$$

Making a change of variable from t' to $\tau = t - t'$, we have, after some manipulation,

$$\Omega(x,y,z,t) = \Omega'(x,y,-z,t) + w\int_0^{\infty}\frac{\partial}{\partial z}[\Omega'(x,y,-z-w\tau,t-\tau)]\,d\tau. \tag{2.9}$$

Equation (2.9) is valid for an arbitrary source. In particular, for a long wire,

$$\Omega'(x, y, z, t)=\frac{\mu_0 I}{2\pi}\tan^{-1}\frac{x-x_0(t)}{z-z_0(t)}. \tag{2.10}$$

Let us find the magnetic field $\vec{B}(x, y, z, t)$ which is related to Ω by

$$\vec{B}(x, y, z, t)=-\nabla\Omega(x, y, z, t). \tag{2.11}$$

Substituting (2.10) into (2.9) and taking the gradient, we obtain

$$\vec{B}(x, y, z, t)=-\vec{b}(x-x_0(t),\ z+z_0(t))$$
$$-w\int_0^\infty \frac{\partial\vec{b}}{\partial z}(x-x_0(t-\tau),\ z+w\tau+z_0(t-\tau))\,dt, \tag{2.12}$$

where

$$b_x(x, z)=-\frac{\mu_0 I}{2\pi}\frac{z}{x^2+z^2}, \tag{2.13a}$$

$$b_z(x, z)=\frac{\mu_0 I}{2\pi}\frac{x}{x^2+z^2}, \tag{2.13b}$$

and

$$b_y(x, z)=0. \tag{2.13c}$$

The force per unit length of wire is given by (dropping the y variable since there is no y dependence)

$$F_z=IB_x(x_0(t),\ z_0(t)), \tag{2.14a}$$

$$F_x=IB_z(x_0(t),\ z_0(t)), \tag{2.14b}$$

and

$$F_y=0. \tag{2.14c}$$

III. STEADY MOTION

If the wire is moving uniformly in the x direction (perpendicular to its length) with velocity v at a constant height h, then

$$x_0(t)=vt,\qquad z_0(t)=h. \tag{3.1}$$

From (2.12) and (2.14) we find

$$F_z=-Ib_x(0, 2h)-wI\int_0^\infty \frac{\partial b_x}{\partial z}(v\tau, 2h+w\tau)\,d\tau, \tag{3.2a}$$

$$F_x=Ib_z(0, 2h)+wI\int_0^\infty \frac{\partial b_z}{\partial z}(v\tau, 2h+w\tau)\,d\tau. \tag{3.2b}$$

Differentiating (2.13), substituting into (3.2), and performing the integrations, we obtain the lift force

$$F_L(v, h)=F_z=\frac{\mu_0 I^2}{4\pi h}\frac{v^2}{v^2+w^2} \tag{3.3a}$$

and the drag force

$$F_D(v, h)=-F_x=(w/v)F_L, \tag{3.3b}$$

in agreement with Reitz.[1]

IV. ANALYSIS OF STABILITY: INSTANTANEOUS APPROXIMATION

The force expressions in Eq. (3.3) are strictly valid only for a wire which has undergone steady motion (uniform velocity in the x direction at constant height) throughout its time history. However, if accelerations in the x direction and vertical velocities are small enough, we expect that the force expressions obtained by replacing v by $\dot{x}_0(t)$ and h by $z_0(t)$ in (3.3) will result in an approximate description of the motion of a wire undergoing arbitrary motion. We refer to this approximation as the instantaneous approximation. (The conditions under which this approximation is valid and its limitations are discussed further in Secs. V and VI.) Of course, such an approximation is not valid for any general dynamical system. But the nature of the force on a long wire due to eddy currents induced in a thin conducting plate is such that the instantaneous approximation is quite accurate. It is also useful as a guide in understanding the results of the exact analysis.

In this section we study only small departures from steady motion, analyzing the stability of the system with a small-signal or linear version of the equations. We write the dynamical equations for a wire moving under the influence of gravity, a propulsive force, and the magnetic force as

$$m\ddot{z}_0=-mg+F_L(x_0, z_0), \tag{4.1a}$$

$$m\ddot{x}_0=F_P-F_D(x_0, z_0), \tag{4.1b}$$

where m is mass per unit length, g is the gravitational constant = 9.8 m/sec^2, and F_P is the propulsive force which is assumed to be constant. The motion of the wire is assumed to be

$$x_0(t)=vt+x_1(t), \tag{4.2a}$$

$$z_0(t)=h+z_1(t), \tag{4.2b}$$

where $x_1(t)$ and $z_1(t)$ are small deviations from the steady motion. Substituting into (4.1), we find the equilibrium point to be given by

$$0=-mg+F_L(v, h), \tag{4.3a}$$

$$0=F_P-F_D(v, h). \tag{4.3b}$$

The linear equations are

$$m\ddot{z}_1=\frac{\partial F_L}{\partial v}(v, h)\dot{x}_1+\frac{\partial F_L}{\partial h}(v, h)z_1, \tag{4.4a}$$

$$m\ddot{x}_1=-\frac{\partial F_D}{\partial v}(v, h)\dot{x}_1-\frac{\partial F_D}{\partial h}(v, h)z_1. \tag{4.4b}$$

We assume a solution of the form $z_1=z_{10}e^{pt}$, $\dot{x}_1=\dot{x}_{10}e^{pt}$. This gives

$$\left(mp^2-\frac{\partial F_L}{\partial h}(v, h)\right)z_{10}-\frac{\partial F_L}{\partial v}(v, h)\dot{x}_{10}=0, \tag{4.5a}$$

$$\frac{\partial F_D}{\partial h}(v, h) z_{10} + \left(mp + \frac{\partial F_D}{\partial v}(v, h) \right) \dot{x}_{10} = 0. \tag{4.5b}$$

For these equations to have a solution, the determinant of the coefficients must vanish, giving the secular equation

$$\left(mp^2 - \frac{\partial F_L}{\partial h}(v, h) \right) \left(mp + \frac{\partial F_D}{\partial v}(v, h) \right) + \frac{\partial F_D}{\partial h}(v, h) \frac{\partial F_L}{\partial v}(v, h) = 0. \tag{4.6}$$

From (3.3) and (4.3), we have

$$mg = \frac{\mu_0 I^2}{4\pi h} \frac{v^2}{v^2 + w^2}, \tag{4.7a}$$

$$F_P = (w/v) mg, \tag{4.7b}$$

$$\frac{\partial F_L}{\partial h}(v, h) = -\frac{mg}{h}, \tag{4.7c}$$

$$\frac{\partial F_L}{\partial v}(v, h) = \frac{2w^2 mg}{v(v^2 + w^2)}, \tag{4.7d}$$

$$\frac{\partial F_D}{\partial h}(v, h) = -\frac{wmg}{vh}, \tag{4.7e}$$

and

$$\frac{\partial F_D}{\partial v}(v, h) = \frac{w}{v} \frac{\partial F_L}{\partial v}(v, h) - \frac{wmg}{v^2} = -\frac{wmg}{v^2} \frac{v^2 - w^2}{v^2 + w^2}. \tag{4.7f}$$

Making use of the results in (4.7), we rewrite the secular equation (4.6) as

$$(p^2 + \omega^2)(p - b) - a = 0, \tag{4.8}$$

where

$$\omega^2 = -\frac{1}{m} \frac{\partial F_L}{\partial h}(v, h) = \frac{g}{h}, \tag{4.9a}$$

$$b = -\frac{1}{m} \frac{\partial F_D}{\partial v}(v, h) = \frac{gw}{v^2} \frac{v^2 - w^2}{v^2 + w^2}, \tag{4.9b}$$

and

$$a = -\frac{1}{m^2} \frac{\partial F_D}{\partial h}(v, h) \frac{\partial F_L}{\partial v}(v, h) = \frac{2g^2 w^3}{hv^2(v^2 + w^2)}. \tag{4.9c}$$

Alternatively, we can write Eq. (4.6) as

$$p^3 - bp^2 + \omega^2 p - g^2 w/hv^2 = 0. \tag{4.10}$$

Since the last term, $-g^2 w/hv^2$, is negative, Eq. (4.10) has at least one root with $\mathrm{Re}\, p > 0$, indicating an instability, i.e., z_1 and $\dot{x}_1$ increasing exponentially with time.

For cases of practical interest in magnetic suspension, usually $v \gg w$. Therefore, to a first approximation, we can neglect a in (4.8), obtaining

$$(p^2 + \omega^2)(p - b) = 0. \tag{4.11}$$

The roots of (4.11) are

$$p = \pm i\omega \tag{4.12}$$

and

$$p = b = \frac{gw}{v^2} + \cdots, \tag{4.13}$$

where "..." indicates terms of higher order in w/v. We can obtain a slightly more accurate expression for the roots (4.12) by writing (4.8) as

$$p^2 = -\omega^2 + a/(p - b). \tag{4.14}$$

Substituting (4.12) into the right-hand side of (4.14), we find

$$p = \pm i\omega - a/2\omega^2 + \cdots = \pm i\omega - 2gw^3/v^4 + \cdots. \tag{4.15}$$

The root $p = b$ represents ustable motion whereas (4.15) represents damped harmonic motion. We shall see in Sec. V that the exact analysis also gives a root approximately at $p = b$ and roots near $p = \pm i\omega$. In the latter roots, however, Rep in (4.15) does not agree with Rep exact.

Typical values of the parameters involved are[1] $w = 4.5$ m/sec (aluminum), $h = 0.1$ m, $v = 134$ m/sec (300 mph). Hence $\omega = 9.9$ sec^{-1}, or $f = \omega/2\pi = 1.6$ Hz, and $b = 2.5 \times 10^{-3}$ sec^{-1}.

From the above we see that the frequency of oscillation is slow (~1.6 Hz) and that the unstable mode has a time constant that is long (~400 sec ≃ 6.7 min) and should be easily controlled at high speeds. This unstable mode basically results from the fact that the drag force is decreasing with increasing velocity.

If one examines the amplitudes of vibration (as will be done in Sec. VII), it will be found that the mode with frequency $p = b$ corresponds to an essentially horizontal type of deviation from equilibrium whereas the $p = \pm i\omega$ modes correspond to vertical oscillations of the system with virtually no horizontal acceleration. In other words, the vertical and horizontal motions are almost completely uncoupled.

V. ANALYSIS OF STABILITY: EXACT EQUATIONS

In this section we again consider the stability of the equilibrium of the long wire (i.e., response to small perturbations in velocity and height) but without making the instantaneous approximations. The equations of motion are [see Eqs. (2.12) and (2.14)]

$$m\ddot{z}_0(t) = -mg - Ib_x(0,\ 2z_0(t))$$
$$- wI\int_0^\infty \frac{\partial b_x}{\partial z}(x_0(t) - x_0(t-\tau),\ z_0(t) + w\tau + z_0(t-\tau))\,d\tau \tag{5.1a}$$

$$m\ddot{x}_0(t) = F_P + Ib_z(0,\ 2z_0(t))$$
$$+ wI\int_0^\infty \frac{\partial b_z}{\partial z}(x_0(t) - x_0(t-\tau),\ z_0(t) + w\tau + z_0(t-\tau))\,d\tau. \tag{5.1b}$$

Once more we let $x_0(t) = vt + x_1(t)$, $z_0(t) = h + z_1(t)$, where $x_1(t)$ and $z_1(t)$ are small. The equilibrium point is found to coincide with that given before, Eq. (4.3) or Eqs. (4.7a) and (4.7b).

Linearizing about that equilibrium, we obtain

$$m\ddot{z}_1(t) = -2I\frac{\partial b_x}{\partial z}(0,\ 2h)z_1(t)$$
$$- wI\int_0^\infty \frac{\partial^2 b_x}{\partial z\,\partial x}(v\tau,\ 2h + w\tau)[x_1(t) - x_1(t-\tau)]\,d\tau$$
$$- wI\int_0^\infty \frac{\partial^2 b_x}{\partial z^2}(v\tau,\ 2h + w\tau)[z_1(t) + z_1(t-\tau)]\,d\tau, \tag{5.2a}$$

$$m\ddot{x}_1(t) = 2I\frac{\partial b_z}{\partial z}(0,\ 2h)z_1(t)$$
$$+ wI\int_0^\infty \frac{\partial^2 b_z}{\partial z\,\partial x}(v\tau,\ 2h + w\tau)[x_1(t) - x_1(t-\tau)]\,d\tau$$
$$+ wI\int_0^\infty \frac{\partial^2 b_z}{\partial z^2}(v\tau,\ 2h + w\tau)[z_1(t) + z_1(t-\tau)]\,d\tau. \tag{5.2b}$$

We assume that for $t < 0$, $x_1(t) = z_1(t) = 0$, and that a perturbation occurs at $t = 0$. Therefore the integrals in Eq. (5.2) involving $x_1(t-\tau)$ and $z_1(t-\tau)$ only extend over the interval $0 < \tau < t$ for $t > 0$.

Let us define the Laplace transforms

$$z(s) = \int_0^\infty e^{-st} z_1(t)\,dt, \tag{5.3a}$$

$$x(s) = \int_0^\infty e^{-st} x_1(t)\,dt. \tag{5.3b}$$

We shall now take the Laplace transform of (5.2). In this equation quantities such as

$$I\int_0^\infty \frac{\partial^2 b_x}{\partial z\,\partial x}(vt,\ 2h + w\tau)x_1(t-\tau)\,d\tau$$
$$= I\int_0^t \frac{\partial^2 b_x}{\partial z\,\partial x}(v\tau,\ 2h + w\tau)x_1(t-\tau)\,d\tau \tag{5.4}$$

appear. This is the convolution of two functions of t, and the Laplace transform of this quantity is therefore (by the convolution theorem[5])

$$F_x^{zx}(s)x(s), \tag{5.5}$$

where

$$F_\alpha^{\beta\gamma}(s) = I\int_0^\infty e^{-st}\frac{\partial^2 b_\alpha}{\partial\beta\,\partial\gamma}(vt,\ 2h + w\tau)\,dt, \qquad \alpha, \beta, \gamma = x, z. \tag{5.6}$$

Similar considerations apply to other terms in (5.2).

Hence, the Laplace transform of (5.2) is

$$m[s^2 z(s) - sz_1(0) - \dot{z}_1(0)]$$
$$= -2I\frac{\partial b_x}{\partial z}(0,\ 2h)z(s) - w[F_x^{zx}(0) - F_x^{zx}(s)]x(s)$$
$$- w[F_x^{zz}(0) + F_x^{zz}(s)]z(s), \tag{5.7a}$$

$$m[s^2 x(s) - sx_1(0) - \dot{x}_1(0)]$$
$$= 2I\frac{\partial b_z}{\partial z}(0,2h)z(s) + w[F_z^{zx}(0) - F_z^{zx}(s)]x(s)$$
$$+ w[F_z^{zz}(0) + F_z^{zz}(s)]z(s), \tag{5.7b}$$

where $F_x^{zx}(0)$ is $F_x^{zx}(s)$ at $s = 0$ and $z_1(0)$ is $z_1(t)$ at $t = 0$, etc.

From (2.13) and (5.6) we find

$$\frac{\partial b_x}{\partial z}(0,\ 2h) = \frac{\mu_0 I}{8\pi h^2}, \tag{5.8a}$$

$$\frac{\partial b_z}{\partial z}(0,\ 2h) = 0. \tag{5.8b}$$

$$F_x^{zx}(s) = -(\mu_0 I^2/2\pi)\int_0^\infty e^{-st}[-2vt/R^4 + 8vt(2h + wt)^2/R^6]\,dt, \tag{5.9a}$$

$$F_x^{zz}(s) = -(\mu_0 I^2/2\pi)\int_0^\infty e^{-st}[-6(2h + wt)/R^4 + 8(2h + wt)^3/R^6]\,dt, \tag{5.9b}$$

$$F_z^{zx}(s) = -(\mu_0 I^2/2\pi)\int_0^\infty e^{-st}[2(2h + wt)/R^4 - 8(vt)^2(2h + wt)/R^6]\,dt, \tag{5.9c}$$

$$F_z^{zz}(s) = -F_x^{zx}(s), \tag{5.9d}$$

where $R = [(vt)^2 + (2h + wt)^2]^{1/2}$. (5.10)

We can rewrite (5.9) in terms of dimensionless integrals as follows: We let

$$\lambda = 2hs/v, \tag{5.11}$$

$$\eta = w/v, \tag{5.12}$$

$$x = vt/2h, \tag{5.13}$$

and

$$r = [x^2 + (1+\eta x)^2]^{1/2}. \tag{5.14}$$

Then

$$F_x^{zx}(s) = -F_z^{zz}(s) = -(\mu_0 I^2/4\pi v h^2) I_x^{zx}(\lambda), \tag{5.15a}$$

$$F_x^{zz}(s) = -(\mu_0 I^2/4\pi v h^2) I_x^{zz}(\lambda), \tag{5.15b}$$

$$F_z^{zx}(s) = -(\mu_0 I^2/4\pi v h^2) I_z^{zx}(\lambda), \tag{5.15c}$$

where

$$I_x^{zx}(\lambda) = \int_0^\infty e^{-\lambda x}[-x/r^4 + 4x(1+nx)^2/r^6]\,dx, \tag{5.16a}$$

$$I_x^{zz}(\lambda) = \int_0^\infty e^{-\lambda x}[-3(1+\eta x)/r^4 + 4(1+\eta x)^3/r^6]\,dx, \tag{5.16b}$$

$$I_z^{zx}(\lambda) = \int_0^\infty e^{-\lambda x}[(1+\eta x)/r^4 - 4x^2(1+\eta x)/r^6]\,dx. \tag{5.16c}$$

Eq. (5.7) can be rewritten as

$$\{s^2 + \omega_0^2 - \omega_1^2[I_x^{zz}(0) + I_x^{zz}(\lambda)]\}z(s) - \omega_1^2[I_x^{zz}(0) - I_x^{zx}(\lambda)]x(s) = sz_1(0) + \dot{z}_1(0), \tag{5.17a}$$

$$-\omega_1^2[I_x^{zx}(0) + I_x^{zx}(\lambda)]z(s) + \{s^2 + \omega_1^2[I_x^{zx}(0) - I_z^{zx}(\lambda)]\}x(s) = sx_1(0) + \dot{x}_1(0), \tag{5.17b}$$

where

$$\omega_0^2 = \mu_0 I^2/4\pi h^2 m, \tag{5.18}$$

and

$$\omega_1^2 = (w/v)\omega_0^2. \tag{5.19}$$

Relating ω defined previously in (4.9a) to ω_0, we see that

$$\omega^2 = \omega_0^2 v^2/(v^2 + w^2). \tag{5.20}$$

The determinant of the coefficients of the left-hand side of (5.17) can be written as

$$\text{determinant} = sD(s), \tag{5.21}$$

where

$$D(s) = (s^2 + \omega_0^2 - \omega_1^2 A)[s - (2h/v)\omega_1^2 B] - (2h/v)\omega_1^4 C = 0, \tag{5.22}$$

$$A = I_x^{zz}(0) + I_x^{zz}(\lambda), \tag{5.23a}$$

$$B = -[I_z^{zx}(0) - I_z^{zx}(\lambda)]/\lambda, \tag{5.23b}$$

and

$$C = [I_x^{zx}(0) + I_x^{zx}(\lambda)][I_x^{zx}(0) - I_x^{zx}(\lambda)]/\lambda. \tag{5.23c}$$

The Laplace transforms are given by

$$z(s) = (\{sz_1(0) + \dot{z}_1(0)]\{s^2 + \omega_1^2[I_z^{zx}(0) - I_z^{zx}(\lambda)]\} + [sx_1(0) + \dot{x}_1(0)]\omega_1^2[I_x^{zx}(0) - I_x^{zx}(\lambda)])/sD(s), \tag{5.24a}$$

$$x(s) = (\{s^2 + \omega_0^2 - \omega_1^2[I_x^{zz}(0) + I_x^{zz}(\lambda)]\}[sx_1(0) + \dot{x}_1(0)] + \omega_1^2[I_x^{zx}(0) + I_x^{zx}(\lambda)][sz_1(0) + \dot{z}_1(0)])/sD(s). \tag{5.24b}$$

The roots of $D(s)$ in the complex s plane are poles of $z(s)$ and $x(s)$. For $\mathrm{Re}\, s < 0$ we must analytically continue (5.24) into this region *after* we have performed the integrations necessary to obtain $I_x^{zz}(\lambda)$, etc. The origin represents a pole in $x(s)$, but not $z(s)$. This is seen by taking the limit as $s \to 0$ in (5.24a) and applying L'Hospital's rule. The extra pole in $x(s)$ at $s = 0$ occurs because the equilibrium conditions [Eq. (4.3)] are insensitive to the origin of x. Therefore if $x_0(t) = vt$, $z_0(t) = h$ represents equilibrium motion and so does $x_0(t) = vt + c$, $z_0(t) = h$, where c is any constant. From the fact that we cannot expand the integrals $I_x^{zz}(\lambda)$, etc., in a Taylor series in s (or λ) to *any* order s^n, we do not expect $x(s)$ and $z(s)$ to be analytic at $s = 0$. Hence, $s = 0$ represents a branch point and the negative real axis is a branch cut.

We now examine the behavior of $D(s)$ for s near b [see Eqs. (4.8)–(4.13)]. The corresponding value of λ is near $2hb/v$ which is typically $\sim 4\times10^{-6}$. Consequently, it is numerically quite accurate to evaluate A, B, and C [Eq. (5.23)] in the limit $\lambda \to +0$. By comparing the integrals necessary for the evaluation of A, B, and C to those already obtained in determining F_L and F_D [Eq. (3.3)], it is straightforward to show that

$$A \simeq 2I_x^{zz}(0) = \eta/(1+\eta^2), \tag{5.25a}$$

$$B \simeq \frac{dI_z^{zx}}{d\lambda}(0) = \frac{1-\eta^2}{2(1+\eta^2)^2}, \tag{5.25b}$$

and

$$C \simeq -2I_x^{zx}(0)\frac{dI_x^{zx}}{d\lambda}(0) = \frac{\eta}{(1+\eta^2)^3}, \tag{5.25c}$$

where $\eta = w/v$.

Rewriting (5.22) in terms of λ, we find

$$D(s) = (v/2h)^3 d(\lambda), \tag{5.26}$$

where

$$d(\lambda) = (\lambda^2 + \lambda_0^2)\left(\lambda - \frac{\eta(1-\eta^2)}{2(1+\eta^2)}\lambda_0\right) - \frac{\eta^3\lambda_0^4}{1+\eta^2} \tag{5.27}$$

and

$$\lambda_0 = 2h\omega/v = 2(gh)^{1/2}/v. \tag{5.28}$$

Typically $\lambda_0 \sim 10^{-2}$ and $\eta \sim \frac{1}{50}$. Actually, for speeds down to $v = w$ ($\eta = 1$), Eq. (5.27) remains quite accurate.

The pole is given by

$$D(s) = 0 \quad \text{or} \quad d(\lambda) = 0. \tag{5.29}$$

In terms of $s = v\lambda/2h$, (5.29) can be rewritten as

$$(s^2 + \omega^2)(s - b) - a = 0, \tag{5.30}$$

where the definitions in (4.9) apply. Hence a pole in the complex s plane occurs at the root of the secular equation of the instantaneous approximation [Eq. (4.8)] which is given approximately by $s = p = b$ for $v \gg w$. This pole on the positive real axis prevents one from applying the final-value theorem to examine the behavior of $z(s)$ and $x(s)$ near $s = 0$ and hence $z_1(t)$ and $x_1(t)$ for $t \to \infty$.[5] This is a source of the error in the work of Bailey and Norwood[2] who concluded the magnetic system should be stable from the results of the final-value theorem. Since there is a pole at $s = b$, there will be a term of the form e^{bt} in $z_1(t)$ and $x_1(t)$ corresponding to an instability.

The other roots of the secular equation (4.8) occur near $p = \pm i\omega - 2gw^3/v^4$. We expect poles in the complex s plane to occur near these roots, although not precisely on them. In fact, the poles occur in the region $\mathrm{Re}s > 0$, whereas the roots $p = \pm i\omega - 2gw^3/v^4$ occur in the region $\mathrm{Re}p < 0$. Let us calculate the position of the poles. We rewrite (5.22) as

$$s^2 + \omega_0^2 - \omega_1^2 A = \frac{2h}{v}\omega_1^4 C \Big/ \left(s - \frac{2h}{v}\omega_1^2 B\right). \tag{5.31}$$

Since the poles in which we are interested occur near $s = \pm i\omega$, the corresponding value of $|\lambda|$ is small ($\sim 10^{-2}$). Therefore it is accurate to evaluate C and B in the limit $\lambda \to +0$. The right-hand side of (5.31) then becomes $a/(s - b)$ which can, in fact, be set equal to zero for the purpose of determining the poles to lowest order. It is not accurate, however, to take $\lambda \to +0$ in A if one wishes to determine the lowest-order contributions to $\mathrm{Re}s$. To demonstrate, we expand A to first order in λ, obtaining

$$A \simeq \eta/(1+\eta^2) + \lambda(1-\eta^2)/2(1+\eta^2)^2. \tag{5.32}$$

(Although A is not analytic about $\lambda = 0$, the first derivative of A at $\lambda = 0$ does exist. Higher-order derivatives, however, do not exist at $\lambda = 0$.)

Substituting (5.32) into (5.31) and setting the right-hand side equal to zero, we find that the poles occur at

$$s \simeq \pm i\omega + b/2 = \pm i\omega + gw/2v^2 + \cdots. \tag{5.33}$$

Since $gw/2v^2 \gg 2gw^3/v^4$ for $\eta = w/v \ll 1$, $\mathrm{Re}s$ is therefore positive. These poles also prevent one from applying the final-value theorem and represent unstable motion.

Thus for the long wire, all three poles occur in the region $\mathrm{Re}s > 0$ for the parameters of interest. For the case of the monopole moving over a thin conducting plate, however, we have found that only the pole at $s = b$ occurs in the region $\mathrm{Re}s > 0$. The remaining two poles occur in the region $\mathrm{Re}s < 0$. In general, the sign of $\mathrm{Re}s$ for these latter poles depends upon the velocity dependence of the steady-state forces (as discussed in Sec. VI). We do not expect that more realistic magnet configurations will possess this additional instability.

Although $\mathrm{Re}p$ (as given by the instantaneous approximation) does not agree with $\mathrm{Re}s$, the frequency determined by the instantaneous approximation does agree with the frequency determined from the Laplace-transform method. This agreement rests upon the requirement that $|\lambda| = 2h|s|/v \ll 1$ or frequencies $\ll v/4\pi h \sim 100$ Hz. Since $f = \omega/2\pi \sim 1.6$ Hz (typically), the instantaneous approximation is well justified for determining the frequency. Similar considerations apply to the other root ($s = b$).

We do not expect any poles other than the ones already discussed (including $s = 0$) to occur in the complex s plane although we have not rigorously proved this statement. We have certainly found the $|\lambda| \ll 1$ poles. We argue that no poles occur for $|\lambda| \gtrsim 1$ since the forces in the problem are not strong enough to cause such high frequencies or accelerations. Likewise we have not rigorously proved that the contribution from the branch cut to $z_1(t)$ and $x_1(t)$ is negligible. However, it is reasonable to expect that for $t \to \infty$, the contribution from the branch cut will not be significant compared with that of the poles.

VI. CORRECTIONS TO INSTANTANEOUS APPROXIMATION

In this section we give a further discussion of the instantaneous approximation when departures from steady motion are not necessarily small. We also determine corrections to this approximation for any general magnetic source and investigate the stability of the system.

First consider a wire whose position coordinates are given by

$$z_0(t) = h + h_1 \sin\gamma t, \tag{6.1a}$$

$$x_0(t) = vt. \tag{6.1b}$$

We do not assume that h_1 is small compared to h; however, we shall consider the frequency γ to be small. Let us calculate the magnetic forces on the wire (per unit length) for the motion given by (6.1).

From (2.12) and (2.14) we find

$$F_z = -Ib_x(0, 2z_0(t)) - wI\int_0^\infty d\tau \frac{\partial b_x}{\partial z}(v\tau, 2z_0(t) + \omega\tau - f(\tau, t)), \tag{6.2a}$$

$$F_x = Ib_z(0, 2z_0(t)) + wI\int_0^\infty d\tau \frac{\partial b_z}{\partial z}(v\tau, 2z_0(t) + w\tau - f(\tau, t)), \tag{6.2b}$$

where

$$f(\tau, t) = 2h_1 \sin\tfrac{1}{2}\gamma\tau \cos(\gamma t - \tfrac{1}{2}\gamma\tau). \tag{6.3}$$

If $f(\tau, t) = 0$, Eq. (6.2) would be the instantaneous approximation for the forces under the motion (6.1). Let us calculate the first-order correction due to $f(\tau, t)$ by expanding (6.2). We find

$$F_z = F_L(v, z_0(t)) + wI\int_0^\infty d\tau \frac{\partial^2 b_x}{\partial z^2}(v\tau, 2z_0(t) + w\tau) f(\tau, t) + \cdots, \tag{6.4a}$$

$$F_x = -F_D(v, z_0(t)) - wI\int_0^\infty d\tau \frac{\partial^2 b_z}{\partial z^2}(v\tau, 2z_0(t) + w\tau) f(\tau, t) + \cdots, \tag{6.4b}$$

where $F_L(v, h)$ and $F_D(v, h)$ are given by (3.3). Furthermore, if we assume that $\gamma z_0(t) \ll 1$, we can expand $f(\tau, t)$ in γ as

$$f(\tau, t) = h_1\gamma\tau \cos\gamma t + \cdots = \dot{z}_0(t)\tau + \cdots. \tag{6.5}$$

Substituting (6.5) into (6.4), we can write the forces as

$$F_z = F_L(v, z_0(t)) + wI\dot{z}_0(t)\frac{\partial}{\partial w}\int_0^\infty d\tau \frac{\partial b_x}{\partial z}(v\tau, 2z_0(t) + w\tau) + \cdots, \tag{6.6a}$$

$$F_x = -F_D(v, z_0(t)) - wI\dot{z}_0(t)\frac{\partial}{\partial w}\int_0^\infty d\tau \frac{\partial b_z}{\partial z}(v\tau, 2z_0(t) + w\tau) + \cdots. \tag{6.6b}$$

From (2.13) or from (2.12), (2.14), and (3.3), we have after taking the appropriate derivatives

$$F_z = F_L(v, z_0(t))\left(1 + \frac{w}{v^2}\dot{z}_0(t)\frac{v^2 - w^2}{v^2 + w^2} + \cdots\right), \tag{6.7a}$$

$$F_x = -F_D(v, z_0(t))\left(1 + \frac{2w\dot{z}_0(t)}{v^2 + w^2} + \cdots\right). \tag{6.7b}$$

Since $\dot{z}_0(t) \ll v$ usually, the corrections to the forces (as given by the instantaneous approximation) due to vertical velocity are quite small. Numerical evaluation of (6.2) for a wide range of parameters also shows that the corrections are small and in reasonable agreement with (6.7) so long as $\gamma z_0(t)/v \ll 1$.

We note that in (6.7a) the sign of the $\dot{z}_0(t)$ term in the lift force (F_z) is positive. This corresponds to negative damping and indicates an instability if the damping associated with the coupling to the horizontal motion is negligible. A simple analysis of the vibration in the vertical direction (keeping a constant horizontal velocity) shows that the motion is of the form $\exp[(\pm i\omega + \frac{1}{2}b)t]$, where ω is given by (4.9a) and b by (4.9b). The rate of the growth of the amplitude of vibration is slow, but it is larger than the rate for decay associated with the coupling to the horizontal motion [see Eq. (4.15)]. Hence, a slow net growth of the amplitude occurs for a long wire.

This result is, of course, in agreement with the findings of Sec. V, (5.33). The expansion of F_z to first order in $\dot{z}_0(t)$ is the equivalent in the tir... domain of expanding A to first order in s (or ... in the frequency domain.

Next let us examine the effects of accelera... the horizontal direction. Consider motio... by

$$x_0(t) = vt, \quad t < 0$$
$$= vt + \tfrac{1}{2}at^2, \quad t > 0$$
$$z_0(t) = h.$$

From (2.12) and (2.14) we find ... to be ($t > 0$)

$$F_z = -Ib_x(0, 2h) - wI\int_0^\infty \frac{\partial b_x}{\partial z}(...$$

$$F_x = Ib_z(0, 2h) + wI\int_0^\infty \frac{\partial b}{\partial z}$$

where

$$v' = v + at, \tag{6.10}$$

$$f'(\tau, t) = -\tfrac{1}{2}a\tau^2, \qquad t > \tau$$

$$= \tfrac{1}{2}a(t^2 - 2t\tau), \quad t < \tau. \tag{6.11}$$

Again, if $f'(\tau, t) = 0$, Eq. (6.9) would give the forces in the instantaneous approximation.

Due to the fact that the magnetic field of a long wire falls off with distance so slowly ($\sim 1/r$), a simple expansion in terms of the acceleration a [or $f'(t, \tau)$] is not an accurate method of determining the corrections to the instantaneous approximation. Nevertheless, we can determine under what conditions the instantaneous approximation is valid.

It is straightforward to show that

$$F_z = F_{L\infty}(1 + (w/v')I_z), \tag{6.12a}$$

$$F_x = -2(w/v')F_{L\infty}I_x, \tag{6.12b}$$

where

$$I_z = \int_0^\infty dx \left(\frac{1}{[x + g(x, s)]^2 + (1 + \eta' x)^2} - \frac{2(1 + \eta' x)^2}{[(x + g(x, s))^2 + (1 + \eta' x)^2]^2} \right). \tag{6.13a}$$

$$I_x = \int_0^\infty dx \frac{[x + g(x, s)](1 + \eta' x)}{\{[x + g(x, s)]^2 + (1 + \eta' x)^2\}^2} \tag{6.13b}$$

$$g(x, s) = -(ah/v'^2)x^2, \qquad x < s$$

$$= (ah/v'^2)(s^2 - 2sx), \quad x > s \tag{6.13c}$$

$$x = v'\tau/2h, \tag{6.13d}$$

$$s = v't/2h, \tag{6.13e}$$

$$\eta' = w/v', \tag{6.13f}$$

and

$$F_{L\infty} = \mu_0 I^2/4\pi h. \tag{6.13g}$$

It is clear that if $ah/v'^2 \ll 1$, then I_z and I_x are given accurately by the values found by setting $g = 0$:

$$I_z \simeq -\eta'/(1 + \eta'^2), \tag{6.14a}$$

$$I_x \simeq \tfrac{1}{2}(1 + \eta'^2). \tag{6.14b}$$

Numerical evaluation of I_z and I_x also shows that the instantaneous approximation for the forces is quite accurate as long as $ah/v'^2 \ll 1$. Under most conditions of interest in magnetic levitation $a < g = 9.8$ m/sec, so that for $v' > w$ and $h = 0.1$ m, the quantity ah/v'^2 is small compared to unity.

Let us now extend this type of analysis to an arbitrary magnetic source. Since any magnetic source can be made up of a set of monopoles q_i at (x_i, y_i, z_i), we write for the scalar potential of the source

$$\Omega'(x, y, z, t) = \sum_i \frac{\mu_0 q_i}{4\pi} \frac{1}{R_i}, \tag{6.15}$$

where

$$R_i = \{[x - x_i(t)]^2 + [y - y_i(t)]^2 + [z - z_i(t)]^2\}^{1/2}, \tag{6.16a}$$

$$x_i(t) = a_i + x_0(t), \tag{6.16b}$$

$$y_i(t) = b_i + y_0(t), \tag{6.16c}$$

and

$$z_i(t) = c_i + z_0(t). \tag{6.16d}$$

The point $(x_0(t), y_0(t), z_0(t))$ represents some fixed point in the magnet such as the center of mass and (a_i, b_i, c_i) represents the position of q_i relative to the fixed point. We restrict our attention to purely translational degrees of freedom. Substituting (6.15) and (6.16) into (2.9), we obtain the magnetic field of the eddy currents:

$$\vec{B}(x, y, z, t) = -\nabla\Omega(x, y, z, t)$$

$$= \sum_i \frac{\mu_0 q_i}{4\pi} \left[\vec{b}(x - x_i(t), y - y_i(t), z + z_i(t)) + w \int_0^\infty \frac{\partial \vec{b}}{\partial z}(x - x_i(t - \tau), y - y_i(t - \tau), z + w\tau + z_i(t - \tau))\, d\tau \right], \tag{6.17}$$

where

$$\vec{b}(x, y, z) = \vec{r}/r^3, \tag{6.18a}$$

and

$$\vec{r} = (x, y, z). \tag{6.18b}$$

The force on the source magnet is

$$\vec{F} = \sum_j q_j \vec{B}(x_j, y_j, z_j). \tag{6.19}$$

If we define

$$a_{ji} = a_j - a_i, \tag{6.20a}$$

$$b_{ji} = b_j - b_i, \tag{6.20b}$$

and

$$c_{ji} = c_j + c_i, \tag{6.20c}$$

then from Eqs. (6.17)–(6.20) we find

$$\vec{F} = \sum_{i,j} \frac{\mu_0 q_i q_j}{4\pi} \times \left[\vec{b}(a_{ji}, b_{ji}, c_{ji} + 2z_0(t)) + w \int_0^\infty \frac{\partial \vec{b}}{\partial z} (a_{ji} + x_0(t) - x_0(t-\tau),\ b_{ji} + y_0(t) - y_0(t-\tau), c_{ji} + w\tau + z_0(t) + z_0(t-\tau)) d\tau \right]. \tag{6.21a}$$

Consider first motion of the form

$$x_0(t) = vt, \tag{6.21b}$$

$$y_0(t) = 0, \tag{6.21c}$$

$$z_0(t) = \text{arbitrary}. \tag{6.21d}$$

From (6.21) the force becomes

$$\vec{F} = \sum_{i,j} \frac{\mu_0 q_i q_j}{4\pi} \left[\vec{b}(a_{ji}, b_{ji}, c_{ji} + 2z_0(t)) + w \int_0^\infty \frac{\partial \vec{b}}{\partial z} (a_{ji} + v\tau, b_{ji}, c_{ji} + w\tau + 2z_0(t) + \Delta(t, \tau)) d\tau \right], \tag{6.22}$$

where

$$\Delta(t, \tau) = z_0(t-\tau) - z_0(t). \tag{6.23}$$

Now, if over the region of integration on τ, where the integrand is large, $\Delta(t, \tau)$ is small, we can expand the second term of (6.22) as

$$\frac{\partial \vec{b}}{\partial z}(a_{ji} + v\tau, b_{ji}, c_{ji} + w\tau + 2z_0(t)) + \frac{\partial^2 \vec{b}}{\partial z^2}(a_{ji} + v\tau, b_{ji}, c_{ji} + w\tau + 2z_0(t))\Delta(t, \tau) + \cdots.$$

If we further expand $\Delta(t, \tau)$ as

$$\Delta(t, \tau) = -\dot{z}_1(t)\tau + \cdots$$

then we can write (6.22) as (after some manipulation)

$$F_z = F_L(v, z_0(t)) - w\dot{z}_0(t) \frac{\partial}{\partial w} \left(\frac{F_L(v, z_0(t)) - F_L(\infty, z_0(t))}{w} \right) + \cdots \tag{6.24a}$$

and

$$-F_x = F_D(v, z_0(t)) - w\dot{z}_0(t) \frac{\partial}{\partial w} \left(\frac{F_D(v, z_0(t))}{w} \right) + \cdots. \tag{6.24b}$$

By symmetry, $F_y = 0$. In (6.24), $F_L(v, h)$ and $F_D(v, h)$ are the steady-state lift and drag forces [e.g., see (3.3) for a long wire and also Ref. 1].

For motion of the form

$$x_0(t) = \text{arbitrary}, \tag{6.25a}$$

$$y_0(t) = 0, \tag{6.25b}$$

and

$$z_0(t) = h, \tag{6.25c}$$

we can show in a similar manner that

$$F_z = F_L(\dot{x}_0(t), h) - \frac{\ddot{x}_0(t) w}{4} \frac{\partial^2}{\partial v \partial w} \times \left[\int_h^\infty dh \left(\frac{F_L(v, h) - F_L(\infty, h)}{w} \right) \right]_{v=\dot{x}_0} + \cdots \tag{6.26a}$$

and

$$-F_x = F_D(x_0(t), h) - \frac{\ddot{x}_0(t) w}{4} \frac{\partial^2}{\partial v \partial w} \times \left[\int_h^\infty dh \left(\frac{F_D(v, h)}{w} \right) \right]_{v=\dot{x}_0} + \cdots. \tag{6.26b}$$

We assume that the appropriate integrals converge. In the case of the long wire, the force falls off as $1/h$ so that (6.26) is not meaningful. However, for two wires (see Ref. 1), Eq. (6.26) can be evaluated. Equations (6.24) and (6.26) are expressions for the force on any general magnetic source moving above a thin conducting plate from which corrections to the instantaneous approximation can be estimated. We note that only a knowledge of the steady-state lift and drag forces as a function of v (or precisely v/w) and h are necessary to estimate the first-order corrections.

Let us examine the coefficient of the $\dot{z}_0(t)$ term in F_z, as this coefficient is crucial in determining whether or not vertical vibrations are stable. For the monopole, dipole, one long wire, and two long wires, we can write[1]

$$F_L(v, h) = F_L(\infty, h)[1 - (1 + v^2/w^2)^{-n}], \qquad (6.27)$$

where $n = \frac{1}{2}$ for the monopole and dipole and $n = 1$ for the long wire (or wires). Likewise, for rectangular coils of dimensions $a \times b$ (b dimension parallel to the velocity), the velocity dependence of the lift force can be fitted approximately by a formula of the form (6.27) if $b/a \geq 1$ for the coils described in Ref. 1 with $n < \frac{1}{2}$ (e.g., if $b = 2a$, $n \simeq \frac{1}{4}$).[6] In general n depends upon a, b, and probably h.

Substituting (6.27) into (6.24a), we find that $[h - z_0(t)]$

$$F_z = F_L(v, z_0(t)) - \frac{\dot{z}_0(t) F_L(\infty, z_0(t))}{w(1 + v^2/w^2)^{n+1}} \left(1 + \frac{v^2}{w^2}(1 - 2n)\right). \qquad (6.28)$$

We see that if $n \leq \frac{1}{2}$, the coefficient of the $\dot{z}_0(t)$ term will be negative and hence the vertical oscillations should be damped. If $n > \frac{1}{2}$, then at high speeds ($v \gg w$) the coefficient will be positive and the system unstable as is the case for long wires. Presumably a coil with $b/a \ll 1$ will also be unstable, but coils for which $b/a \geq 1$ will be stable since $n < \frac{1}{2}$ (stable with respect to vertical perturbations, not horizontal velocity changes).

Finally, let us remark that for the parameters of interest in this paper, the correction terms in (6.24) and (6.26) are generally small. The only reason that the $\dot{z}_0(t)$ terms in F_z assume any importance is that there is essentially no other significant damping in the system. Even with the $\dot{z}_0(t)$ terms included, the growth of the amplitude (or damping in case of stable configurations) is small and can be controlled easily. Hence, from a practical viewpoint, since a control system is necessary to damp out the vertical oscillations, the presence of a small amount of natural damping or growth of the amplitude is not of major concern. In this context, the instantaneous approximation (with or without corrections) can be extremely useful in an analysis of a complicated system.

VII. NUMERICAL SOLUTION OF DYNAMIC EQUATIONS

We have found that the equilibrium of magnets moving over a thin conducting plate is unstable. In most systems, using either the instantaneous approximation or an exact analysis, it is found that the secular equation resulting from the linearized equations of motion has at least one real root in the right half-plane, corresponding to an exponentially growing term, as well as two complex poles located near the imaginary axis representing oscillatory terms with little damping (either positive or negative damping can occur). However, these results on stability do not contain enough information about the motion which results if the magnet is disturbed from its equilibrium. In order to find schemes for stabilizing the equilibrium of levitation systems it is necessary to know whether both the horizontal and vertical motion resulting from perturbations contain terms which correspond to the exponentially growing mode or the highly oscillatory mode, whether the coupling between horizontal and vertical motion is significant, and how accurately the linearized equations describe the motion. In order to answer some of these questions, we used numerical integration techniques to solve for the motion of an infinite wire subjected to various disturbances.

In order to facilitate the numerical analysis of the equations of motion, it is convenient to write them in a somewhat different form than used previously. Furthermore, let us describe the motion of the wire in terms of error coordinates which describe its deviation from steady motion. Using the same coordinate system and notation as in Sec. II, define

$$y(t) = x_0(t) - vt = \text{position error}. \qquad (7.1)$$

Then define

$$y_1(t) = \dot{y}(t) = \dot{x}_0(t) - v = \text{velocity error}, \qquad (7.2)$$

from which it follows that

$$\dot{y}_1(t) = \ddot{x}_0(t) = \text{horizontal acceleration}. \qquad (7.3)$$

Similarly, define

$$y_2(t) = z_0(t) - h = \text{height error} \qquad (7.4)$$

and

$$y_3(t) = \dot{y}_2(t) = \dot{z}_0(t) = \text{vertical velocity}, \qquad (7.5)$$

so that

$$\dot{y}_3(t) = \ddot{z}_0(t) = \text{vertical acceleration}. \qquad (7.6)$$

Thus, the two second-order equations of motion given in (4.1) can be written (in terms of error coordinates) as three coupled first-order differential equations. Continuing, (4.1) can be rewritten as

$$m\dot{y}_3(t) = -mg + F_L(y_1(t) + v, y_2(t) + h, y_3(t)), \qquad (7.7a)$$

$$m\dot{y}_1(t) = F_P - F_D(y_1(t) + v, y_2(t) + h, y_3(t)), \qquad (7.7b)$$

where the dependence of F_L and F_D on $y_3(t)$ is due to the correction term (Sec. VI).

The coupled first-order differential equations given by (7.5) and (7.7) are known as state equations, and $y_1(t)$, $y_2(t)$, and $y_3(t)$ are state variables which describe the motion of the wire above the plane.[7] This system of equations is now in the form required for application of standard numerical integration techniques. Using a predictor-corrector numerical integration routine,[8,9] a computer program was written to obtain responses for the nonlinear equations (7.8) subject to various initial conditions. The response of $y_2(t)$ for initial height [$y_2(t)$] errors of 1 and 2 in. and $y_1(0) = y_3(0) = 0$ are shown in Fig. 2. The system parameters are assumed to be as given previously, namely, $v = 134$ m/sec, $w = 4.5$ m/sec (aluminum), and $h = 0.1$ m. The velocity error for these initial height errors was essentially zero and is not plotted. Thus, we observe that there is negligible coupling between the vertical motion and horizontal motion. It is seen that the vertical response is oscillatory with a period of 0.65 sec. This frequency agrees very well with the frequency of the complex poles found by both the exact analysis and the instantaneous approximation. There is no noticeable growth in the oscillations over the first few periods shown in Fig. 2. However, these oscillations are growing with a time constant of about 600 sec as determined by the response obtained over the first two minutes.

The responses for initial velocity errors with zero initial height errors are shown in Fig. 3. These responses are seen to be almost purely exponential with a time constant of approximately 300 sec, which agrees very well with the approximate value of the real root ($s = b$) found earlier in the linear analysis. Again, it was found that there was essentially no coupling between the horizontal and vertical errors in this case. Furthermore, as one might now expect, it was found that the response to a combination of height and velocity errors produced a response which was the superposition of the individually induced errors. It can be seen by studying the linearized versions of Eq. (7.8) that there is indeed very little coupling between the horizontal and vertical motion as indicated by our numerical results.

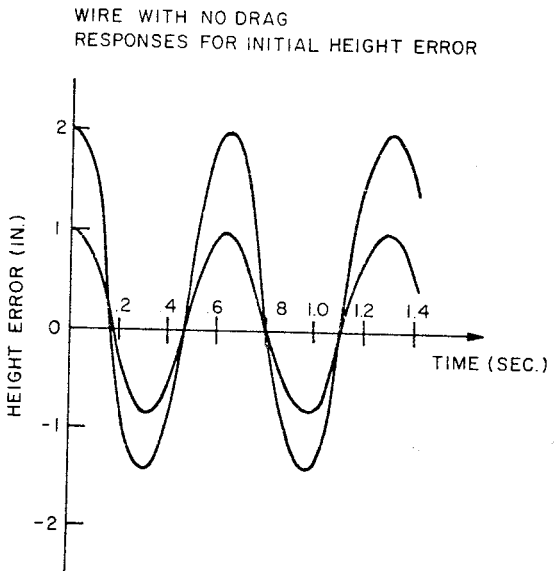

FIG. 2. Vertical motion resulting from initial height error, wire without aerodynamic drag ($v = 134$ m/sec = 300 mph, $w = 4.5$ m/sec, $h = 0.1$ m = 3.9 in.).

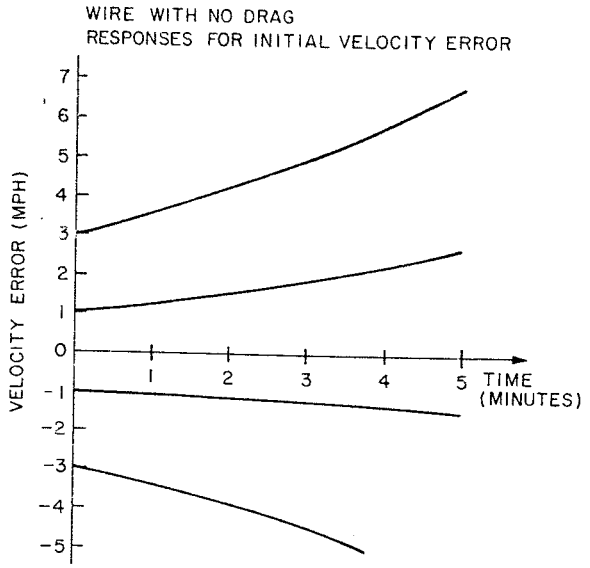

FIG. 3. Velocity error resulting from an initial velocity perturbation, wire without aerodynamic drag (parameters same as Fig. 2).

In summary, our numerical solution of the equations of motion demonstrated that (for the wire with nominal values of height and velocity), (a) unstable vertical oscillatory motion results from initial height errors, but the rate of growth of the oscillations is very small, (b) unstable horizontal motion (i.e., velocity errors growing without bound) results from initial velocity errors, and (c) there is negligible coupling between the vertical and horizontal motion.

In order to study the effect of the first-order correction terms to the forces obtained by the instantaneous approximation on the motion of the wire, the motion resulting from the forces without the corrections was determined numerically. Over the first few cycles shown in Fig. 2 there was no detectable difference in the vertical motion, and over the 5-min period in Fig. 3, there was no de-

tectable difference in the horizontal motion. Thus, since any active control will have to damp out vertical oscillations in a very few cycles, we stress that the instantaneous approximation without correction terms is sufficiently accurate for control system analysis and design.

In order to make the problem more realistic as well as to study the effects of losses on the unstable horizontal motion, let us add aerodynamic drag to the equations of motion (7.7). If this is done, (7.7a) becomes

$$\dot{y}_1(t) = -\frac{\mu_0 I^2 w[y_1(t)+v]}{4\pi m[y_2(t)+h]\{[y_1(t)+v]^2+w^2\}} - \frac{k_a}{m}[y_1(t)+v]^2 + \frac{F_D^0}{m} + \frac{k_a}{m}v^2, \tag{7.8}$$

where k_a is the drag coefficient and $k_a v^2$ is the additional force which must be applied to the vehicle to maintain the nominal velocity v. Because of the negligible coupling between the horizontal and vertical motion, the amount of aerodynamic drag needed to stabilize the horizontal motion can be obtained by linearizing (7.8) and setting $y_2(t)$ to zero. If this is done, it can be shown that the condition for stability of the horizontal motion is

$$k_a > \mu_0 I^2 w/8\pi v h(v^2+w^2) \equiv k_{cr}. \tag{7.9}$$

For the nominal parameter values given earlier in the paper, it can be shown that condition (7.9) implies that the aerodynamic drag must be approximately one-half the nominal magnetic drag for stability. Thus, since the nominal lift-to-magnetic-drag ratio is 30, the lift-to-total-drag ratio must be ≤ 20 to guarantee that the equilibrium is stable.

In order to investigate the effects of aerodynamic drag on the response of the wire to perturbations, numerical results were obtained (using the previously mentioned computer program) for various initial conditions and for various values of k_a. The velocity error responses for $k_a = 1.2$, 10, 25, and 100 times the minimum value needed for stability as given by (7.9) and for an initial velocity error of 3 mph (1% error) are shown in Fig. 4. Indeed the errors do decay to zero as would be expected. However, it is seen that 25 times the minimum drag is needed to cause the velocity error to decay to zero in one minute. This is certainly an unacceptable amount of drag (it implies a lift-to-drag ratio of approximately 5). The response to initial height errors was found to be essentially unaffected by the addition of the aerodynamic drag, which is not unexpected due to the negligible coupling between horizontal and vertical motion. Thus, the addition of sufficient aerodynamic drag to the nonlinear equations of motion of the wire

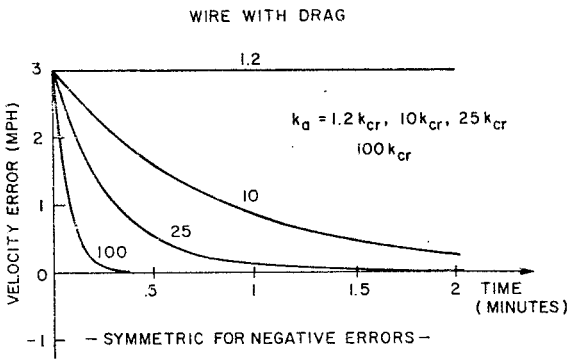

FIG. 4. Velocity error for wire with various amounts of aerodynamic drag (parameters same as Fig. 2.).

does indeed cause the horizontal motion to be stable. For a well-designed vehicle, estimates indicate that approximately twice the aerodynamic drag needed for stability would be present. However, the vertical response to perturbations is unstable and the amount of drag needed to damp out velocity errors quickly enough is prohibitive. Thus feedback control must be utilized to obtain suitable responses of the wire (or any magnet system) to disturbances.

VIII. DISCUSSION OF CONTROL

It is apparent from the results of Sec. VII that some means of control would have to be added to the considered magnetic system in order to obtain suitable transient responses to disturbances. Since it was shown that the linearized equations of motion (Sec. III) provided a very good approximation to the motion of the wire (for the size perturbations of interest) and that the coupling between horizontal and vertical motion is negligible (for the nominal parameter values), let us investigate the linearized equation of motion for the velocity error only, i.e.,

$$\dot{y}_1(t) = -\alpha y_1(t), \tag{8.1}$$

where

$$\alpha = \mu_0 I^2 w(v^2-w^2)/4\pi m h(v^2+w^2)^2 - 2k_a v/m.$$

Let us add a general control function $u(t)$ to this equation and determine what an appropriate choice of $u(t)$ would be to obtain a suitable response of the wire. The equation of motion is then

$$\dot{y}_1(t) = -\alpha y_1(t) + u(t). \tag{8.2}$$

We want to adjust $u(t)$ to keep $y_1(t)$ as close as possible to zero at all times. However, it is apparent from physical reasoning that $u(t)$ must not be allowed to become unbounded since this would re-

quire infinite energy. Let us formulate the problem of choosing $u(t)$ as an optimal control problem. Suppose we choose $u(t)$ to minimize the functional

$$F(y(0), u(t)) = \tfrac{1}{2} \int_0^\infty [\, q_1 y_1^2(t) + q_2 u^2(t)]\, dt, \qquad (8.3)$$

subject to the constraint of (8.2). In (8.3) q_1 and q_2 are positive constant weighting factors which are chosen to achieve acceptable responses. It is apparent that the closer $y_1(t)$ is kept to zero at all times, the smaller is the first term of the integrand. However, very large values of $u(t)$ will not be part of the optimal control since $u^2(t)$ ($\propto$ energy) is included in the integrand. The problem we have formulated is well known in optimal control theory as the linear state regulator.[10] It can be shown that the optimal control is given by

$$u_{opt}(t) = -ky_1(t), \qquad (8.4)$$

where k is the positive solution of the equation

$$-2k\alpha + k^2/q_2^2 - q_1 = 0,$$

which is

$$k = q_2\alpha[1 + (1 + q_1/q_2)^{1/2}]. \qquad (8.5)$$

Note that k is optimal for any arbitrary initial conditions. With this control, the equation of motion (7.2) becomes

$$\dot{y}_1(t) = (-\alpha + k)\, y_1(t). \qquad (8.6)$$

Because of its form which is proportional to $y_1(t)$, $u(t)$ is known as a feedback control. Results similar to (8.6) could be obtained by means other than by determining an optimal linear control. For example, if the propulsive power instead of the propulsive force were assumed constant, the linearized equation of horizontal motion would have the same form as (8.6). In addition, we remember that aerodynamic drag produced an additive term in α in the linearized equations. Thus, it is apparent that a simple feedback controller which varies the propulsive force applied to the wire in proportion to the velocity error will produce a better response, and the prohibitive amount of drag required for an acceptable response can be avoided.

Similarly, one could find a feedback controller which would stabilize the vertical motion and damp out vertical oscillations due to disturbances.

For example, a feedback controller could be used to obtain sufficient damping by varying the current which creates the magnetic field, by controlling the angle of an airfoil, or by controlling the current in smaller trim (or control) coils. However, while the proposed feedback control of the propulsive force applied to a levitated magnet is straightforward in theory and practice, there are a number of practical difficulties associated with the techniques of control of the vertical motion. For example, how easily and quickly can currents be varied if superconducting magnets are used, what geometries would be best for trim coils, etc.? Thus, the feedback control of the vertical motion requires a more detailed study than can be presented here.

IX. CONCLUSIONS

The equilibrium obtained by magnetic systems of levitation is inherently unstable. While the presence of aerodynamic drag helps to stabilize the horizontal motion, it is necessary to incorporate feedback control in the system design in order to produce a stable equilibrium and to obtain sufficiently damped transient responses to disturbances. Although it is necessary to add a first-order correction to the lift force obtained by the instantaneous approximation to study the stability of certain magnet configurations, it is apparent that the instantaneous approximation yields sufficiently accurate force laws for the dynamical analysis of magnetic levitation systems. This is particularly true when feedback control is introduced to obtain a sufficiently damped response.

It was also noted in the case of the long wire that the coupling between the horizontal and vertical motion was negligible at cruise speeds (300 mph). If this fact is in general true for all magnet systems, the design of control systems to produce good transient responses will be simplified. However, this fact needs to be investigated further. Additional analysis is also needed to determine practical means of implementing a feedback controller to damp out vertical oscillations in the inherently underdamped magnetic systems. This problem is certainly more difficult than that of velocity control (assuming decoupling of the horizontal and vertical motion). Also, in order to demonstrate the feasibility of magnetic levitation for high-speed vehicles, further study needs to be made with respect to practical coil geometries as well as means for lateral control, for emergency braking, and for making the transition from low-speed operation (no levitation) to high-speed operation.

ACKNOWLEDGMENTS

The authors would like to thank Dr. John R. Reitz, Dr. R. H. Borcherts, and Professor G. W. Ford for useful discussions.

[1]John. R. Reitz, J. Appl. Phys. 41, 2067 (1970).
[2]Paul B. Bailey and Frederick R. Norwood, J. Appl. Phys. 41, 4890 (1970).
[3]Robert H. Borcherts and John R. Reitz, Transportation Res. 5, No. 3 (1970).
[4]L. C. Davis and John R. Reitz, J. Appl. Phys. 42, xxxx (1971).
[5]W. R. LePage, *Complex Variables and the Laplace Transform for Engineers* (McGraw-Hill, New York, 1961).
[6]John. R. Reitz (private communication).
[7]William R. Perkins and Jose B. Cruz, Jr., *Engineering of Dynamic Systems* (Wiley, New York, 1969), Chap 7.
[8]A. Ralston and H. S. Wilf, *Mathematical Methods for Digital Computers* (Wiley, New York, 1960), pp. 95–109.
[9]*Scientific Subroutine Package*, *Subroutine HPCG* (IBM, White Plains, N. Y., 1968).
[10]Michael Athans and Peter L. Falb, *Optimal Control* (McGraw-Hill, New York, 1966).

FORCE ON A RECTANGULAR COIL MOVING ABOVE A CONDUCTING SLAB*

John R. Reitz and L. C. Davis
Scientific Research Staff, Ford Motor Company, Dearborn, Michigan 48121

Abstract

The force on a rectangular, current-carrying coil moving above and parallel to a conducting plate of arbitrary thickness is investigated. Expressions are developed for the lift and drag forces on the coil as a function of speed. Numerical calculations are made for a very thick plate and for plates with thickness of the order of the skin depth. Thick plate results are compared with experimental measurements of lift and drag on a superconducting coil suspended above a rotating aluminum wheel.

*Work supported in part by the Department of Transportation

FORCE ON A RECTANGULAR COIL MOVING ABOVE A CONDUCTING SLAB*

John R. Reitz and L. C. Davis
Scientific Research Staff, Ford Motor Company, Dearborn, Michigan 48121

Abstract

The force on a rectangular, current-carrying coil moving above and parallel to a conducting plate of arbitrary thickness is investigated. Expressions are developed for the lift and drag forces on the coil as a function of speed. Numerical calculations are made for a very thick plate and for plates with thickness of the order of the skin depth. Thick plate results are compared with experimental measurements of lift and drag on a superconducting coil suspended above a rotating aluminum wheel.

1. Introduction

Considerable interest has been generated during the past few years in the use of magnetic levitation as a support mechanism for tracked vehicles with speeds in excess of 150 mph.[1-7] A number of different magnetic suspension schemes are possible, but one of the more interesting concepts uses d.c. coils or permanent magnets in the vehicle, and a passive, conducting track. Levitation is produced by the induced currents in the track acting back on the vehicle magnets.

The use of high-field-strength, low-weight magnets in the vehicle, which may be realized through the use of superconducting coils, can greatly improve the performance of a magnetic suspension system. In 1966 Powell and Danby[1] proposed a suspension for a high-speed train using superconducting coils in the vehicle and a track of unpowered, closed loops of normal metal. Discrete track loops are not essential,

*Work supported in part by the Department of Transportation

however; one can also produce lift from eddy currents induced in a continuous metallic track or roadbed, and such a track is superior from the point of view of construction cost and rigidity. Early analyses of the continuous guideway concept were made by Coffey et al[2] and Guderjahn et al.[3]

In an earlier paper[5] we calculated the lift and drag forces on rectangular, current-carrying coils moving above a thin, conducting sheet, due to eddy currents induced in the sheet. The results can be summarized as follows:

(1) at high speeds the lift force on the coil approaches the force due to the image of the coil (located below the sheet),

(2) at all speeds the drag force is (w/v) times the lift force, where w is a characteristic velocity which depends on the conductivity and thickness of the plate, and

(3) the speed-dependence of the lift force depends upon coil geometry.

In this report we investigate the forces on rectangular coils moving above a conducting slab of arbitrary thickness. We formulate the general problem and show how it can be solved. Specific calculations are carried out for rectangular coils above an infinitely thick slab, for a sinusoidal current sheet above a slab of arbitrary thickness, and for a rectangular coil above a plate whose thickness is approximately a skin depth. Complete analytic solutions are obtained for certain limiting cases.

2. Formulation of the Problem

A conducting plate of thickness T and conductivity σ divides space into three regions: region 1 (above the plate) contains the moving coil, region 2 is the plate itself, and region 3 (below the plate) contains no magnetic sources or conducting material. Let the upper surface of the plate coincide with the x-y plane (i.e., $z = 0$). The rectangular coil, which is located in a plane parallel to the surface

of the plate, at z = h, moves in the x direction with constant velocity v. The coil is oriented so that one of its sides is parallel to the x direction. The coil carries a constant current, the number of ampere turns being I.

Maxwell's equation for the magnetic field in the plate,

$$\text{curl } \underset{\sim}{B} = \mu_0 \underset{\sim}{j} \tag{1}$$

may be combined with Ohm's law and Faraday's law to yield

$$\text{curl curl } \underset{\sim}{B} = - \mu_0 \sigma \, \partial \underset{\sim}{B}/\partial t \quad . \tag{2}$$

In a coordinate system moving along with the coil $\partial/\partial t$ may be replaced by $v\partial/\partial x$. Furthermore curl curl may be converted to $- \nabla^2$. Therefore, each component of $\underset{\sim}{B}$ in region 2 must satisfy

$$\frac{\partial^2 B}{\partial x^2} + \frac{\partial^2 B}{\partial y^2} + \frac{\partial^2 B}{\partial z^2} = \lambda_1 \frac{\partial B}{\partial x} \tag{3}$$

where $\lambda_1 \equiv \mu_0 \sigma v$. If we take the origin of coordinates at a point on the upper surface of the plate directly below the center of the coil, the symmetry of the problem allows us to write $\underset{\sim}{B}$ in the form (for one Fourier coefficient):

(Region 2)

$$\left.\begin{aligned} B_x &= \cos k_y y \; e^{ik_x x} \left(b_x e^{\alpha z} + c_x e^{-\alpha z}\right) \\ B_y &= \sin k_y y \; e^{ik_x x} \left(b_y e^{\alpha z} + c_y e^{-\alpha z}\right) \\ B_z &= \cos k_y y \; e^{ik_x x} \left(b_z e^{\alpha z} + c_z e^{-\alpha z}\right) . \end{aligned}\right\} \tag{4}$$

This field satisfies (3) provided

$$- k_x^2 - k_y^2 + \alpha^2 = ik_x \lambda_1$$

or

$$\alpha = \pm \left[k^2 + ik_x \lambda_1\right]^{\frac{1}{2}} \quad , \tag{5}$$

where

$$k^2 \equiv k_x^2 + k_y^2 \quad . \tag{6}$$

Thus,

$$\beta \equiv (\alpha/k) = \beta_1 + i\beta_2 \quad , \tag{7}$$

where

$$\left.\begin{aligned} \beta_1 &= 2^{-\frac{1}{2}} \left[(\lambda_1^2 k_x^2/k^4 + 1)^{\frac{1}{2}} + 1\right]^{\frac{1}{2}} \\ \beta_2 &= 2^{-\frac{1}{2}} \left[(\lambda^2 k_x^2/k^4 + 1)^{\frac{1}{2}} - 1\right]^{\frac{1}{2}} \end{aligned}\right\} . \tag{8}$$

Now the coefficients b_x, c_x, etc., are not all independent. We have div $\underset{\sim}{B} = 0$ and $(\text{curl } \underset{\sim}{B})_z = 0$. The last equation comes about because the current in the coil has no z-component, hence the induced eddy currents also have no z-component. When we apply these equations to (4) we obtain

$$b_y = ik_y b_x/k_x \quad , \quad b_z = -ikb_x/(k_x\beta) \quad , \tag{9}$$

$$c_y = ik_y c_x/k_x \quad , \quad c_z = ikc_x/(k_x\beta) \quad . \tag{10}$$

In the region above the plate $\underset{\sim}{B}$ is composed of two contributions:

(Region 1)

$$\left.\begin{aligned} B_x &= B_x^c + a_x \cos k_y y e^{ik_x x} e^{-kz} \\ B_y &= B_y^c + a_y \sin k_y y e^{ik_x x} e^{-kz} \\ B_z &= B_z^c + a_z \cos k_y y e^{ik_x x} e^{-kz} \end{aligned}\right\} . \tag{11}$$

The first term $\underset{\sim}{B}^c$ is the field due to the coil, whereas the term in a is the field due to the eddy currents. Again the coefficients a_x, etc., are not independent:

$$a_y = ik_y a_x/k_x \quad , \quad a_z = ika_x/k_x \quad . \tag{12}$$

Below the plate the field is given by:

(Region 3)

$$\left.\begin{aligned} B_x &= d_x \cos k_y y \, e^{ik_x x} \, e^{kz} \\ B_y &= (ik_y/k_x) d_x \sin k_y \, e^{ik_x x} \, e^{kz} \\ B_z &= -(ik/k_x) \, d_x \cos k_y y \, e^{ik_x x} \, e^{kz} \end{aligned}\right\} \quad (13)$$

The coefficient a_x (hence, also a_y and a_z) may be obtained by applying the boundary conditions, i.e., continuity of the normal and tangential components of the magnetic field, at both the upper and lower surfaces of the plate. If we write $a_x = a_{x1} + ia_{x2}$, etc., the eddy current field may be written:

(Field in Region 1 due to eddy currents)

$$\left.\begin{aligned} B_x &= 2 \cos k_y y \, e^{-kz} \, (a_{x1} \cos k_x x - a_{x2} \sin k_x x) \\ B_y &= 2 \sin k_y y \, e^{-kz} \, (a_{y1} \cos k_x x - a_{y2} \sin k_x x) \\ B_z &= 2 \cos k_y y \, e^{-kz} \, (a_{z1} \cos k_x x - a_{z2} \sin k_x x) \end{aligned}\right\} \quad (14)$$

If the moving magnet is a rectangular coil, the a_{x2} and a_{y1} terms produce the lift force, and the a_{z2} term produces drag.

We now apply the boundary conditions. At $z = -T$,

$$\left.\begin{aligned} b_x \, e^{-\alpha T} + c_x \, e^{\alpha T} &= d_x \, e^{-kT} \\ b_z \, e^{-\alpha T} + c_z \, e^{\alpha T} &= -(ik/k_x) d_x \, e^{-kT} \end{aligned}\right\} \quad (15)$$

The boundary condition on B_y is the same as the first equation in (15). This procedure yields

$$c_x = \frac{(1 - \beta)}{(1 + \beta)} \, b_x \, e^{-2\alpha T} \quad . \quad (16)$$

At $z = 0$,

$$\left.\begin{aligned} a_x - iW_1 &= b_x + c_x \\ a_z + W_2 &= b_z + c_z \end{aligned}\right\} \quad (17)$$

where $-iW_1$ is the (two-dimensional) Fourier transform of B_x^c, and W_2 is the Fourier transform of B_z^c. We also obtain

$$a_y + W_1' = b_y + c_y \tag{18}$$

where W_1' is the Fourier transform of B_y^c, but because of the symmetry of the problem, this is the same equation as the first one in (17). W_1, W_1' and W_2 are real quantities. For all of the coils and current-carrying circuits which we have investigated, we find that

$$\left.\begin{aligned} W_2 &= -(k/k_x)\, W_1 \quad , \\ W_1' &= (k_y/k_x)\, W_1 \quad . \end{aligned}\right\} \tag{19}$$

The calculation of these transforms will be discussed in Section 4.

Solving (17) for a_x [after first using (9), (10), (12), (16) and (19)], we obtain

$$a_x = iW_1 \frac{(1-\beta)}{(1+\beta)} \frac{(1 - e^{-2\beta kT})}{\left[1 - \left(\frac{1-\beta}{1+\beta}\right)^2 e^{-2\beta kT}\right]} \quad , \tag{20}$$

with β given by Eqs. (7) and (8). This equation and Eq. (23) below have been derived independently by Chilton and Coffey.[8]

Before applying Eq. (20) in full generality we first consider certain limiting cases. We return to the general case in Section 6.

3. One Dimensional Current Sources

Let the moving "coil" be replaced by a number of long parallel current-carrying wires (all in the y direction and at $z = h$). Each wire is one of a pair carrying opposite currents so that the symmetry of Section 2 is maintained. We can utilize the results of Section 2 directly by letting

$$\left.\begin{aligned} k_y &= 0 \\ k_x &= k \end{aligned}\right\} \quad . \tag{21}$$

The electromagnetic problem is now a two-dimensional one and the situation is considerably simplified.

Equation (20) for a_x is directly applicable except that $\lambda_1 k_x/k^2$ in Eq. (8) becomes simply λ_1/k.

(a) Sinusoidal Current Sheet

If the moving "coil" is a one dimensional sinusoidal current sheet with

$$I(x')dx' = I_0 \sin(kx')\, dx' \tag{22}$$

at height $z = h$, then there is a single wave vector k inthe problem. The lift force is proportional to a_{x2}; furthermore, from (12), $a_{z2} = a_{x1}$, and the drag is proportional to this coefficient. Thus,

$$\frac{F_L + iF_D}{F_I} = \frac{(\beta - 1)}{(\beta + 1)} \frac{(1 - e^{-2\beta kT})}{\left[1 - \left(\frac{1-\beta}{1+\beta}\right)^2 e^{-2\beta kT}\right]} \quad , \tag{23}$$

where F_L is the lift force, F_D is the drag, and F_I is the image force. The lift-to-drag ratio, F_L/F_D, is plotted in Fig. 1 versus kT for various values of the magnetic Reynold's number S:[9]

$$S \equiv \frac{\lambda_1}{k} = \frac{\mu_0 \sigma v}{k} \quad . \tag{24}$$

We notice that the plate acts like a thin sheet up to thicknesses $T = \delta$ where

$$\delta \equiv (2/\lambda_1 k)^{\frac{1}{2}} \tag{25}$$

is the skin depth. At thicknesses greater than about 1.3 δ the plate gives the full F_L/F_D of a thick plate. (In fact a plate with $T \approx 1.5\ \delta$ appears to give a somewhat superior performance to an infinitely thick one. This occurs because β in Eq. (23) is complex, and thus a sinusoidal modulation is superimposed on what would otherwise be a monotonic behavior versus thickness.)

In the high speed limit (S large) equation (8) reduces to

$$\beta_1 = \beta_2 = (S/2)^{\frac{1}{2}} \quad . \tag{26}$$

For an infinitely thick plate in the high-speed limit

$$\frac{F_L + iF_D}{F_I} = \frac{(S/2)^{\frac{1}{2}}(1 + i) - 1}{(S/2)^{\frac{1}{2}}(1 + i) + 1} \quad . \tag{27}$$

The F_L/F_D ratio:

$$F_L/F_D = (S/2)^{\frac{1}{2}} \quad \begin{matrix}\text{(high-speed limit;} \\ \text{infinitely thick slab)}\end{matrix} \tag{28}$$

(b) Two Parallel Wires

Consider two current-carrying wires (Currents I and -I) separated in the x direction by 2b. The wires are at z = h. The Fourier transforms are

$$\left.\begin{aligned} W_1 &= \frac{\mu_0 I}{2\pi} \sin(kb)\, e^{-h|k|} \quad , \\ W_2 &= \frac{\mu_0 I}{2\pi} \sin(|k|b)\, e^{-h|k|} \quad . \end{aligned}\right\} \tag{29}$$

The lift and drag forces over an infinitely thick plate were calculated analytically by Borcherts and Reitz[6] by expanding the integrands (in the integration over k) in powers of $(\lambda_1 h)^{-\frac{1}{2}}$. We give here only the high-speed limit F_L/F_D for the case where b is substantially greater than h:

$$F_L/F_D = 2(\lambda_1 h/\pi)^{\frac{1}{2}} \quad \begin{matrix}\text{(high-speed limit,} \\ \text{infinitely thick slab)}\end{matrix} \tag{30}$$

4. Rectangular Coil Above an Infinitely Thick Slab

If the conducting slab is very thick, Eq. (20) reduces to

$$a_x = iW_1 \frac{(1 - \beta)}{(1 + \beta)} \quad , \tag{31}$$

where β is given by (7) and (8). From the analysis of Section 3 we expect that the slab will appear infinitely thick if the thickness is more than a few skin depths at all of the relevant wave-numbers. Using (8) we find that

$$a_x = a_{x1} + ia_{x2}, \text{ etc.}; \tag{32}$$

$$\left.\begin{aligned} a_{x1} &= 2W_1 \frac{\beta_2}{(\beta_1 + 1)^2 + \beta_2{}^2} \quad , \\ a_{x2} &= - W_1 \left(1 - \frac{2(\beta_1 + 1)}{(\beta_1+1)^2 + \beta_2{}^2}\right) \quad . \end{aligned}\right\} \tag{33}$$

a_{z1}, a_{z2}, etc., are obtained from (12).

(a) Calculation of W_1 and W_2

The rectangular coil is considered to be made up of two finite-length wire pairs: one pair of length 2b is parallel to the direction of motion, the other pair of length 2a is transverse to the direction of motion. The wires are at height h. The second pair will produce both z and x components of field; the first pair will

produce z and y components of field. Consider the transverse pair; the x-component of field at z = 0 is

$$B_x^{\,w} = \frac{\mu_0 I}{4\pi}\left[\frac{-h}{[(x+b)^2+h^2]}\left(\frac{y+a}{[(y+a)^2+h^2+(x+b)^2]^{\frac{1}{2}}} - \frac{(y-a)}{[(y-a)^2+h^2+(x+b)^2]^{\frac{1}{2}}} \right) \right.$$

$$\left. + \frac{h}{[(x-b)^2+h^2]}\left(\frac{y+a}{[(y+a)^2+h^2+(x-b)^2]^{\frac{1}{2}}} - \frac{(y-a)}{[(y-a)^2+h^2+(x-b)^2]^{\frac{1}{2}}} \right) \right] . \quad (34)$$

The x-y Fourier transform of this gives W_1 since there is no other contribution to B_x. The calculation of the Fourier transform of (34) is straightforward and is given in the appendix; we find

$$W_1 = \frac{\mu_0 I}{\pi^2} \frac{\sin k_x b \sin k_y a \, e^{-kh}}{k_y} . \quad (35)$$

$B_z^{\,w}$ from the transverse wire pair can be written down (an expression similar to (34)), and its transform is found to be

$$W_2^{(1)} = -(k_x/k)W_1 . \quad (36)$$

To this we must add the transform of B_z from the other wire pair, $W_2^{(2)}$. $W_2^{(2)}$ is obtained from $W_2^{(1)}$ by interchanging k_x and k_y. We thus obtain

$$W_2 = -(k/k_x)W_1 \quad (37)$$

as anticipated in Eq. (19).

(b) Calculation of Lift and Drag

We now have to evaluate the eddy current field, Eq. (14) at the wire positions, integrate over the wire lengths, and integrate over dk_x, dk_y. The integration over the wire length is performed immediately, and we obtain

$$F_L = \frac{8\mu_0 I^2}{\pi^2} \int_0^\infty dk_2 \sin^2 k_2 a \int_0^\infty dk_1 \sin^2 k_1 b \, e^{-2kh} \left[\frac{1}{k_2^{\,2}} + \frac{1}{k_1^{\,2}} \right]$$

$$\times \left(1 - \frac{2(\beta_1 + 1)}{(\beta_1+1)^2 + \beta_2^{\,2}} \right) \quad (38)$$

and

$$F_D = \frac{8\mu_0 I^2}{\pi^2} \int_0^\infty dk_2 \sin^2 k_2 a \int_0^\infty dk_1 \sin^2 k_1 b e^{-2kh} \frac{k}{k_1 k_2^2} \frac{2\beta_2}{(\beta_1+1)^2+\beta_2^2} \quad . \qquad (39)$$

In (38) the first term in the brackets comes from the transverse pair of wires and the second term from the longitudinal pair.

The lift and drag forces have been calculated numerically for a few representative cases. The coils considered had the dimensions 2a × 2b and were at height h above the thick slab. b is always taken in the direction of motion. Table I gives results for various ...es in terms of a convenient magnetic Reynold's number:[10] $\lambda_1 h = \mu_0 \sigma v h$. Figure 2 shows data on two 2 × 4" coils over a thick "aluminum" slab. Actually an aluminum alloy with 43% the conductivity of copper was chosen in order to be able to compare with some experimental results. The 2 × 4" coil has its long dimension in the direction of motion. The results of Ford Motor Company experiments carried out by Dr. R. H. Borcherts are also shown in the figure. These measurements were made on a superconducting coil suspended above the rim of a rotating, solid aluminum wheel; the wheel is two feet in diameter, 6 inches wide, and can be rotated to rim speeds of 300 mph. The comparison of lift/drag ratio is an absolute one; for the lift curves, however, the experimental points are normalized to the theoretical curve at 300 mph. Experimental and theoretical values of F_L at 300 mph, for these two coils and several others, agreed on an absolute basis within ± 10%. The comparison between theory and experiment is really quite good.

The 4 × 2" coil (short dimension in the direction of motion) has a lower F_L/F_D ratio at all speeds. It also shows a substantially larger value of peak drag than the 2 × 4" coil, but it does achieve a fixed fraction of its asymptotic lift at a lower speed than the longer coil. These last features were also found to apply to rectangular coils

moving over a thin plate.

Figure 3 shows the lift force and lift/drag ratio of a 1 m × 2 m coil at a height of 0.3 m above a pure aluminum slab. The lift/drag achievable at 300 mph is quite impressive.

5. High Speed Limit

In the high-speed limit, Eqs. (7) and (8) give

$$\beta_1 = \beta_2 = [\lambda_1 k_x / 2k^2]^{1/2} \quad . \tag{40}$$

This approximation has been substituted in Eqs. (39) for the drag; in the lift, Eq. (38), only the leading term (i.e., the image for β_1) is retained. This asymptotic lift/drag ratio for a number of different coils is plotted in Fig. 4 as a function of b/h. It is seen that coils which are long in the direction of motion give the best performance relative to the lift/drag ratio; however, this observation must be made with some caution. Figure 4 gives the asymptotic lift/drag; at a fixed, finite speed, coils with large b/a achieve a smaller fraction of their asymptotic lift than do coils with a smaller b/a, and in some speed ranges these two effects would tend to cancel.

For a fixed b/a ratio, and for coils with b/h in the range 5 to 10, the F_L/F_D ratio varies approximately as $(bh)^{1/4}$.

(a) Force on a Moving Monopole or Dipole

If the dimensions of the coil (2b and 2a) are very small compared to h, the coil looks like a dipole. The forces on a dipole can be calculated analytically in the high-speed limit. We first consider a monopole; later we construct a dipole from two monopoles. The monopole q is placed at a height h above the origin of coordinates in the moving system. The field of q at z = 0 is

$$\left.\begin{aligned} B_x^q &= (qx/4\pi)(h^2+r^2)^{-3/2} \\ B_z^q &= -(qh/4\pi)(h^2+r^2)^{-3/2} \end{aligned}\right\} \tag{41}$$

etc., where $r^2 = x^2 + y^2$.

The x-y Fourier transform of B_z^q is W_2:

$$W_2 = -(q/4\pi^2)\, e^{-kh} \quad . \tag{42}$$

The x-y Fourier transform of B_x^q is $-iW_1$:

$$W_1 = (qk_x/4\pi^2 k)\, e^{-kh} \quad . \tag{43}$$

In this case the lift and drag forces are produced by the coefficients a_{zl} and a_{xl}, respectively, in Eq. (14). The lift force on the monopole in the high-speed limit is the image force

$$F_L = q^2/(16\,\pi h^2) \quad . \tag{44}$$

The drag force is given by

$$F_D = 2q(q/4\pi^2) \int_0^\infty \int_0^\infty (2k_x/\lambda_1)^{\frac{1}{2}}\, e^{-2hk}\, dk_x dk_y$$

$$= (2/\lambda)^{\frac{1}{2}}(q^2/2\pi) \int_0^\infty k^{3/2}\, e^{-2hk}\, dk \int_0^{\pi/2} (\cos\Phi)^{\frac{1}{2}}\, d\Phi \quad . \tag{45}$$

Now

$$\int_0^{\pi/2} (\cos\,\Phi)^{\frac{1}{2}}\, d\Phi = \tfrac{1}{2}\,\Gamma(\tfrac{3}{4})\Gamma(\tfrac{1}{2})/\Gamma(\tfrac{5}{4})$$

$$= 1.200$$

Thus

$$F_D = 1.744\ (\lambda_1 h/\pi)^{\frac{1}{2}}\, F_L \tag{46}$$

A dipole can be constructed of two monopoles (of opposite sign). The dipole result is obtained from the limit when thetwo monopoles are brought to the same position. The Fourier transform W_2 becomes

$$W_2 = -(q/4\pi^2)(e^{-kh_1} - e^{-kh_2}) \quad , \tag{47}$$

etc. The lift force is the image force

$$F_L = 3p^2/(32\,\pi\, h^4) \tag{48}$$

where

$$p \equiv q(h_1 - h_2) \quad . \tag{49}$$

The drag force is

$$F_D = 1.196\,(\lambda_1 h/\pi)^{1/2}\,F_L \quad . \tag{50}$$

The dipole lift/drag ratio is plotted in Fig. 4 along with the other high-speed limit ratios for various coils. The numerical calculations for the coils are seen to extrapolate satisfactorily to the dipole result when the dimensions are made small.

6. Force on a Coil Above a Plate of Arbitrary Thickness

We now return to the plate of arbitrary thickness T. To calculate the forces on a rectangular coil moving over such a plate we modify Eqs. (38) and (39). Equation (20) is written as a real and imaginary component, and the quantities a_{x1}/W_1 and $-a_{x2}/W_1$ replace $2\beta_2/[(\beta_1+1)^2 + \beta_2^2]$ and $[1 - 2(\beta_1+1)/\{(\beta_1+1)^2 + \beta_2^2\}]$, respectively, in Eqs. (39) and (38).

The resulting equations for lift and drag were evaluated numerically for a 1 × 2 meter coil (at h = 0.3 m) moving above conducting aluminum plates 0.6 inches thick and 1 inch thick. The results are plotted in Fig. 3. The 0.6 inch conducting plate acts very much like a "thin" plate over most of the speed range. The F_L/F_D ratio is approximately a linear function of speed and is essentially the same as given by thin-plate analysis.[5] The speed dependence of F_L is also similar to the earlier prediction except that a fixed fraction of the image force is attained at somewhat lower speeds than thin-plate analysis would indicate.

The 1 inch plate is not a thin plate at v = 300 mph; eddy current distribution throughout its thickness is limited by skin depth considerations. By changing coil geometry (increasing b or h) one can

effectively increase the skin depth, and thereby increase the F_L/F_D ratio at 300 mph to a maximum of 75 (the thin-plate value for a 1 inch aluminum plate).

If this type of magnetic suspension is used to support a high-speed vehicle then one would want to design the system for maximum F_L/F_D at cruise speed (maximum speed) subject to a specified conductor thickness in the roadbed or guideway. This means that the skin depth should not limit F_L/F_D at any speed, and the conductor will act like a "thin" plate over the full speed range. This is an important result since it has been found[11] that the dynamical behavior of a moving magnet is easier to analyse in the thin-plate approximation than in the case where the plate has arbitrary thickness.

7. Force on a Coil Above a Ferromagnetic Plate

If the conducting plate is highly permeable, with a large μ/μ_0, then the analysis presented here requires some modification. The quantity λ_1 defined in Eq. (3) becomes

$$\lambda_1 = \mu \sigma v \quad . \tag{51}$$

Thus, for fixed v and σ, λ_1 is increased by the factor μ/μ_0. The boundary conditions at the upper and lower surfaces of the plate are continuity of the normal component of $\underset{\sim}{B}$ and the tangential component of $\underset{\sim}{H}$. When we apply these boundary conditions we find that Eq. (20) is changed to

$$a_x = iW_1 \frac{(1-\beta/\varkappa)}{(1+\beta/\varkappa)} \frac{\left(1 - e^{-2\beta kT}\right)}{\left[1 - \left(\frac{1-\beta/\varkappa}{1+\beta/\varkappa}\right)^2 e^{-2\beta kT}\right]} \quad , \tag{52}$$

where

$$\varkappa \equiv \mu/\mu_0 \quad . \tag{53}$$

The vertical force on the moving coil is attractive at low

speeds but changes to repulsive at sufficiently high speeds.

If the plate is infinitely thick, then at zero velocity,

$$F_L(v = 0) = - F_I(\kappa - 1)/(\kappa + 1) \tag{54}$$

where F_I is the image force defined earlier. If the plate has finite thickness T, then the force at zero velocity is

$$F_L(v=0) = - \gamma \left[F_I - (1-\gamma^2) \sum_{n=1}^{\infty} \gamma^{2(n-1)} F_I'(n) \right] \tag{55}$$

where $\gamma \equiv (\kappa-1)/(\kappa+1)$, F_I is the force between the coil and its image at distance 2h, and $F_I'(n)$ is the force between the coil and its image at distance 2(h+nT). The transition from attraction to repulsion can be pushed to quite high speeds by appropriate choice of parameters.

The attractive force between a moving coil and highly permeable track forms the basis for another magnetic suspension system originally suggested by Graemiger[12] and recently built into a research vehicle by Messerschmitt-Bölkow-Blohm GmbH in Germany. Electromagnets in the vehicle are suspended below the track. This type of suspension is basically unstable so that the currents in the electromagnets must be controlled by an active control system.

8. Acknowledgments

The authors have benefited from discussions with Drs. R. H. Borcherts and D. F. Wilkie of the Ford Motor Company, Drs. F. Chilton and H. T. Coffey of Stanford Research Institute, and Dr. J. T. Harding of the Office of High Speed Ground Transportation, U. S. Department of Transportation.

References

1. J. R. Powell and G. R. Danby, Amer. Soc. Mech. Engrs. Paper 66-WA/RR-5 (1966).
2. H. T. Coffey, F. Chilton and T. W. Barbee, Jr., J. Appl. Phys. 40, 2161 (1969).
3. C. A. Guderjahn, S. L. Wipf, H. J. Fink, R. W. Boom and K. E. MacKenzie, J. Appl. Phys. 40, 2133 (1969).
4. J. R. Powell and G. R. Danby, Cryogenics 11, 192 (1971).
5. John R. Reitz, J. Appl. Phys. 41, 2067 (1970).
6. R. H. Borcherts and J. R. Reitz, Transportation Res. 5 (No. 3, August 1971).
7. C. Guderjahn and S. L. Wipf, Cryogenics 11, 171 (1971).
8. F. Chilton and H. T. Coffey, Int. Helium Soc. Symposium, Washington, D.C. (May 1971).
9. The parameter S also plays the role of an effective speed since this is the only place where v specifically enters the formulas.
10. $\lambda_1 h$ is a convenient dimensionless quantity for discussing the magnetic forces on coils at height h above the conducting plate. An effective speed parameter S, analogous to Eq. (24), can also be defined here: $S = \lambda_1 \ell_{eff} = \mu_0 \sigma v \ell_{eff}$, but ℓ_{eff} depends on h, b, and a.
11. L. C. Davis and D. F. Wilkie, J. Appl. Phys. (Nov. 1971).
12. P. J. Gheary, Magnetic and Electric Suspensions, British Scientific Research Association (Taylor and Francis, London 1964).
13. W. Magnus and F. Oberhettinger, Formulas and Theorems for the Functions of Mathematical Physics, translated by J. Wermer, (Chelsea Publ. Co., New York, 1949), p. 116.
14. Reference 13, p. 120.

Appendix. Fourier Transform of B_x^w

The Fourier transform, W, of Eq. (35) may be written as

$$(2\pi)^2 W = -\frac{\mu_0 I h}{4\pi} \sum_{i=1}^{2} \sum_{j=1}^{2} (-1)^{i+j} \int_{-\infty}^{\infty} \frac{e^{-ik_x x} dx}{[(x-b_j)^2+h^2]}$$

$$\times \int_{-\infty}^{\infty} \frac{e^{-ik_y y} dy (y-a_i)}{\{(x-b_j)^2 + (y-a_i)^2 + h^2\}^{\frac{1}{2}}}$$

$$= -\frac{\mu_0 I h}{4\pi} \sum_{i=1}^{2} \sum_{j=1}^{2} (-1)^{i+j} e^{-ik_y a_i} e^{-ik_x b_j} Q(k_x,k_y) \quad , \tag{A1}$$

where
$$\left.\begin{aligned} a_1 = a \ , \ a_2 = -a \ , \\ b_1 = b \ , \ b_2 = -b \ , \end{aligned}\right\} \tag{A2}$$

and
$$Q(k_x,k_y) = \int_{-\infty}^{\infty} \int_{-\infty}^{\infty} dxdy \frac{e^{-i(k_x x+k_y y)} y}{[x^2+h^2]\{x^2+y^2+h^2\}^{\frac{1}{2}}} \ . \tag{A3}$$

It is easily shown that

$$Q(k_x,k_y) = \text{sgn}\ (k_y)\ Q(|k_x|,|k_y|) \tag{A4}$$

so that we limit the subsequent discussion to $k_x, k_y > 0$.

Now[13]

$$\int_{-\infty}^{\infty} dy \frac{e^{-ik_y y} y}{\{x^2+y^2+h^2\}^{\frac{1}{2}}} = i \frac{\partial}{\partial k_y} \int_{-\infty}^{\infty} \frac{dy\ e^{-ik_y y}}{\{x^2+y^2+h^2\}^{\frac{1}{2}}}$$

$$= -2i(x^2+h^2)^{\frac{1}{2}} K_1(k_y \sqrt{x^2+h^2}) \ . \tag{A5}$$

Thus[14]

$$Q(k_x,k_y) = -(2i/k_y)(2\pi k/h)^{\frac{1}{2}} K_{\frac{1}{2}}(kh) \tag{A6}$$

where

$$k^2 \equiv k_x^2 + k_y^2 \ . \tag{A7}$$

But

$$K_{\frac{1}{2}}(z) = (\pi i/2)e^{i\pi/4} H_{\frac{1}{2}}^{(1)}(iz)$$

$$= (\pi/2z)^{\frac{1}{2}} e^{-z} , \qquad (A8)$$

so that

$$Q(k_x,k_y) = - 2\pi i\, e^{-kh}/(h\, k_y) . \qquad (A9)$$

Returning now to Eq. (A1) and performing the double sum, we find

$$(2\pi)^2 W = - (2i\mu_0 I/k_y)e^{-kh} \sin k_y a \sin k_x b . \qquad (A10)$$

Now $-iW_1$ of Section 2 is actually a Fourier-cosine transform, involving the full range of k_x and real values of k_y. This gives an extra factor of 2, and

$$W_1 = \frac{\mu_0 I}{\pi^2} \frac{\sin k_x b \sin k_y a\, e^{-kh}}{k_y} . \qquad (A11)$$

Table I. Lift and drag forces on rectangular coil (2a × 2b) moving with velocity v at height h above an infinitely thick slab of conductivity σ. (2b is in the direction of motion.) Multiply F_L and F_D by $8\mu_0 I^2/\pi^2$.

	a/h = 1, b/h = 2		a/h = 2, b/h = 1		a/h = 5, b/h = 10	
$\lambda_1 h$	F_L	F_D	F_L	F_D	F_L	F_D
1	.0212	.0332	.0303	.0554		
2	.0481	.0464	.0697	.0782	1.02	.557
4	.0891	.0550	.126	.0910	1.55	.565
8	.140	.0567	.188	.0902	2.09	.517
16	.193	.0523	.243	.0798	2.59	.439
32	.243	.0445	.289	.0655	3.04	.354
64	.286	.0359	.324	.0512	3.41	.276
128	.321	.0276	.350	.0388	3.72	.209
256	.347	.0209	.369	.0288	3.96	.155
512	.367	.0154	.383	.0211	4.14	.114
1024	.381	.0113	.393	.0152	4.28	.0823
∞	.417	0	.417	0	4.61	0

Figure Captions

Fig. 1 Ratio of lift force to drag force on a one-dimensional sinusoidal current sheet moving with velocity v over a conducting plate as a function of the plate thickness T. The effective speed (magnetic Reynold's number) $S = \mu_0 \sigma v / k$.

Fig. 2 Lift force F_L, drag force F_D, and lift/drag ratio on two rectangular coils at height h = 1.66 inches above an infinitely thick, aluminum slab as a function of speed.
2 × 4" coil: —— (theory), O (experiment);
4 × 2" coil: —— (theory), ● (experiment). Ford Motor Company experimental results by R. H. Borcherts on the same coils are also given . (For the 2 × 4" coil the 4" dimension is in the direction of motion.) We are indebted to Dr. Borcherts for permission to quote his results before publication.

Fig. 3 Lift force F_L and the F_L/F_D ratio on a 1 × 2 m coil moving at h = 0.3 m over an aluminum plate as a function of speed. Results are given for a 0.6 inch plate —— , a one inch plate --- , and an infinitely thick plate —— —— . (The 2 m dimension is in the direction of motion. $\sigma^{-1} = 2.8\ \mu\Omega$ cm)

Fig. 4 Lift-to-drag ratio on rectangular coils (2b × 2a) moving over a thick slab in the high-speed limit as a function of b/h. The ordinate is to be multiplied by $[\mu_0 \sigma v h/\pi]^{1/2}$. The dimension 2b is in the direction of motion.

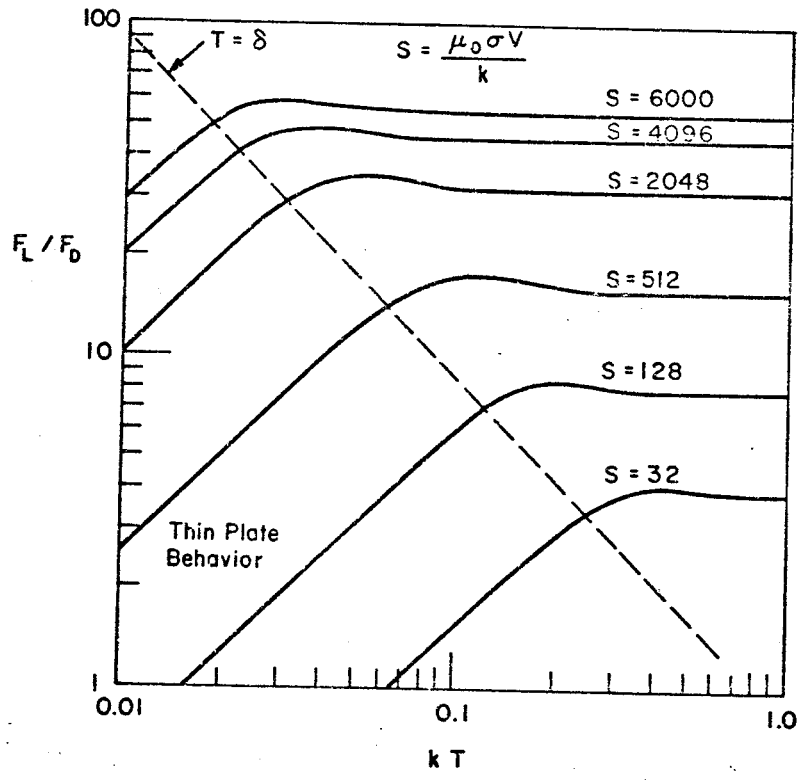
100
10
1
F_L / F_D
T = δ
$S = \frac{\mu_0 \sigma V}{k}$
S = 6000
S = 4096
S = 2048
S = 512
S = 128
S = 32
Thin Plate
Behavior
0.01
0.1
1.0
k T

Fig. 1

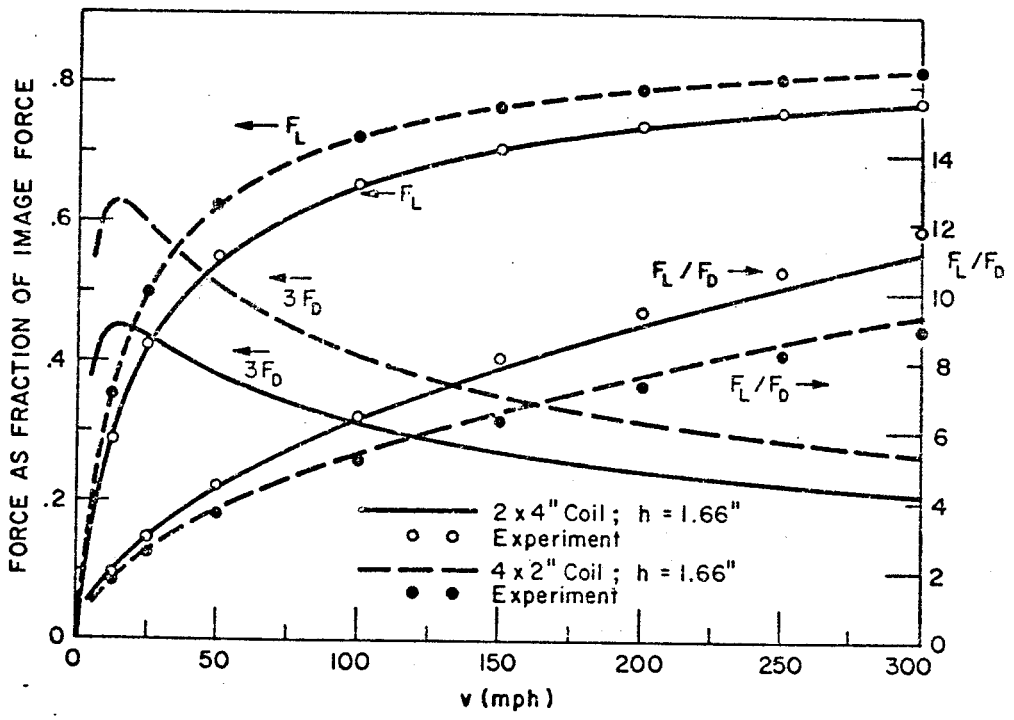
FORCE AS FRACTION OF IMAGE FORCE
.8
.6
.4
.2
0
F_L
F_L
$3F_D$
$3F_D$
F_L/F_D
F_L/F_D
14
12
10
8
6
4
2
0
F_L/F_D
2 x 4" Coil ; h = 1.66"
Experiment
4 x 2" Coil ; h = 1.66"
Experiment
0
50
100
150
200
250
300
v (mph)

Fig. 2

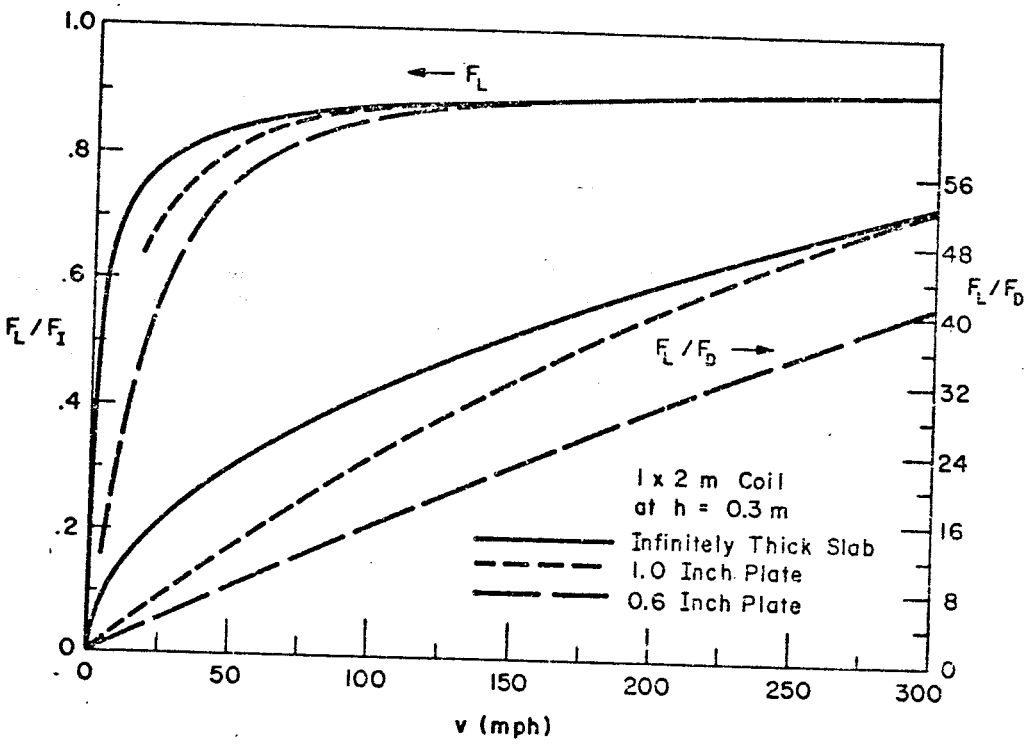
1.0
.8
.6
.4
.2
0
F_L/F_I
F_L
F_L/F_D
56
48
40
32
24
16
8
0
F_L/F_D
1 x 2 m Coil
at h = 0.3 m
Infinitely Thick Slab
1.0 Inch Plate
0.6 Inch Plate
0
50
100
150
200
250
300
v (mph)

Fig. 3

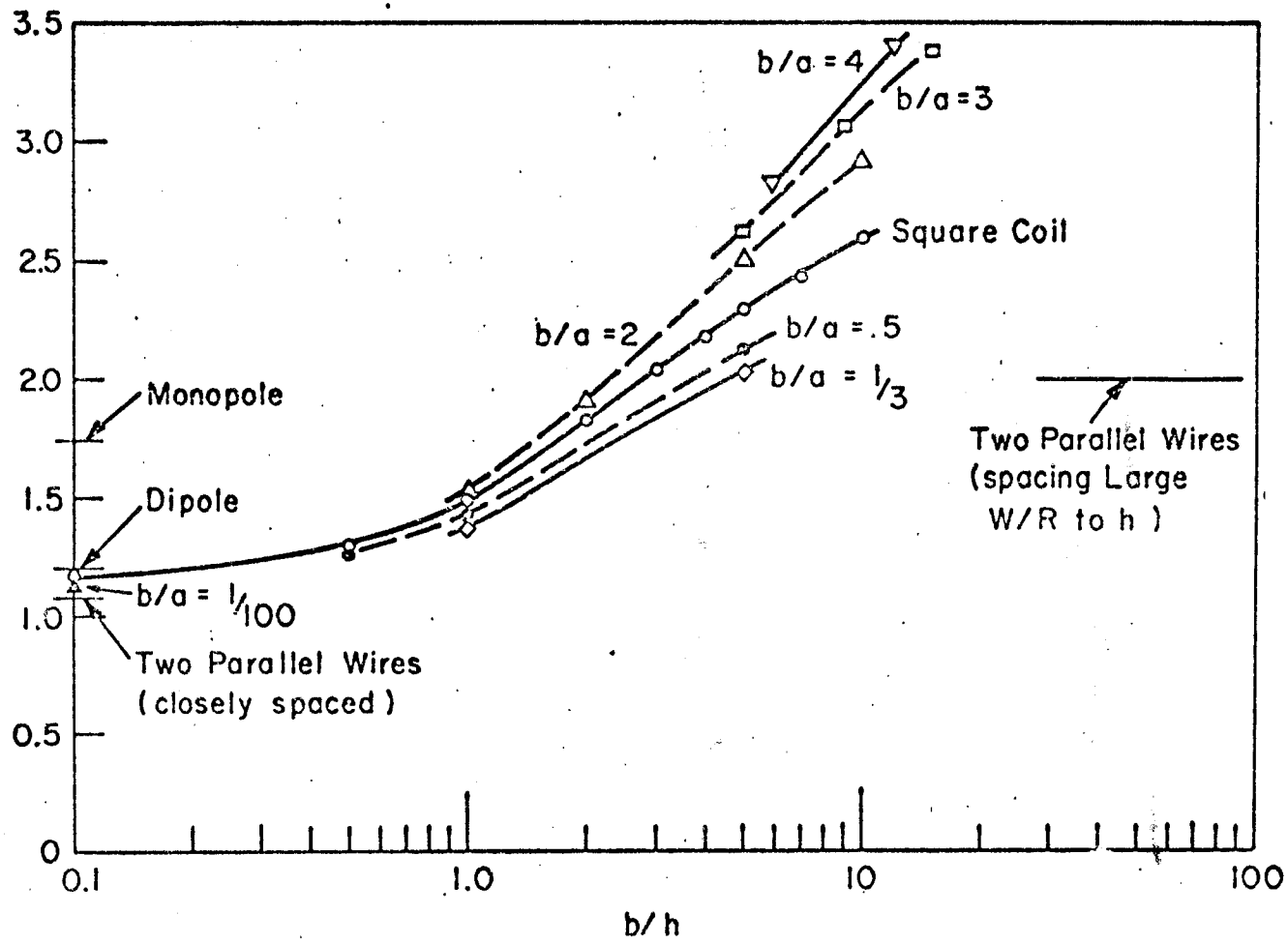
3.5
3.0
2.5
2.0
1.5
1.0
0.5
0
0.1
1.0
10
100
b/h
b/a = 4
b/a = 3
b/a = 2
Square Coil
b/a = .5
b/a = 1/3
Monopole
Dipole
b/a = 1/100
Two Parallel Wires
(closely spaced)
Two Parallel Wires
(spacing Large
W/R to h)

Fig. 4

FORCE ON A COIL MOVING OVER A CONDUCTING SURFACE, INCLUDING EDGE AND CHANNEL EFFECTS*

R. H. Borcherts
Physics Department

and

L. C. Davis
Theoretical Sciences Department

October 20, 1971

*Work supported in part by the Department of Transportation.

FORCE ON A COIL MOVING OVER A CONDUCTING SURFACE, INCLUDING EDGE AND CHANNEL EFFECTS*

R. H. Borcherts and L. C. Davis
Scientific Research Staff, Ford Motor Company, Dearborn, Michigan 48121

ABSTRACT

The lift force F_L and drag force F_D on small conducting coils placed near a large rotating conducting cylinder have been measured as functions of velocity, height and coil geometry. These data are compared with exact theoretical calculations based upon Fourier transforms for coils moving over infinitely wide flat plates. By placing the coil near the edge of the cylinder, the effect of the edge on F_L and F_D and the transverse force F_T were studied. A channel was then cut in the cylinder, and the properties of a U-shaped guideway were examined. Both the edge effects and channel effects were compared with approximate theoretical calculations. Agreement was generally good, substantiating a variety of predictions for the large magnets proposed for the suspension of high speed ground vehicles.

* Work supported in part by the Department of Transportation.

I. INTRODUCTION

One of the proposals for the suspension of high speed ground vehicles involves superconducting coils moving rapidly ($\sim$ 300 mph) over a conducting plate[1-5] or guideway. Superconducting coils are desirable because of their high field strength and low weight. The magnetic field of the moving coil induces eddy currents in the conducting plate (typically aluminum). By Lenz's law, the induced currents generate a magnetic field which opposes the field of the coil, thereby providing a lift force F_L on the coil. The Joule losses of the eddy currents in the plate give rise to a drag force F_D, also on the coil. In addition, if the width of the conducting plate (i.e., in the shape of a strip) is comparable to the width of the coil, an appreciable transverse force F_T may be acting on the coil. Of course, when the coil is exactly centered on the strip, $F_T = 0$. If, on the other hand, the guideway is in the form of a U-shaped channel, a transverse force of the opposite sign occurs. We choose to call this transverse force a guidance force F_G.

A considerable amount of theoretical work has been done to predict F_L and F_D vs. v (v = velocity of magnet) for infinitely wide conducting plates.[1-4, 6-11] Some experimental work on small coils has been reported[1,2,4] which indicated at least qualitative agreement with the predictions of theory. In particular, it has been established at high speeds that F_L tends to saturate (theory predicts that F_L approaches the force due to an image of the coil located an equal distance below the surface of the conducting plate), that $F_D \propto v^{-1}$ if the thickness of the plate is small compared with the skin depth, and that $F_D \propto v^{-\frac{1}{2}}$ if the thickness is large compared with the skin depth.[4] Consequently,

the lift-to-drag ratio (L/D) improves with increasing velocity.

The first objective of the present work is to make a more detailed comparison between theory and experiment for wide conducting plates. Specifically, experimental results are given for: (1) the absolute magnitude of F_L and F_D as a function of velocity, (2) the height dependence of F_L and L/D at 300 mph, and (3) the dependence of L/D at 300 mph on the width and length of the coil (rectangular shaped). These results are compared in Sec. III with the theory of Ref. 10 which gives exact values for F_L and F_D as functions of velocity and height for rectangular coils. The theory is based upon Fourier transform techniques. The actual experimental arrangement (described in Sec. II) consisted of a small superconducting coil placed over a large solid rotating cylinder (24" diameter wheel).

The second objective of this work is to study edge effects. Experimentally the coil was placed close to the edge of the cylinder and F_L, F_D and F_T were measured. Some theoretical work has been done on edge effects where the force on a single monopole moving near the edge of semi-infinite plane sheet has been calculated.[12] A degradation of L/D and an appreciable F_T were found. In Sec. IV, the calculations are extended to find F_L and F_T for a coil in the high-speed limit. A comparison with experiment is made and predictions for full scale magnets are given.

The third objective is to examine the forces on a coil in a U-shaped guideway. After the edge effects were studied, a channel was cut in the cylinder. Measurements were made of the forces on various coils which were placed in the channel as the cylinder was rotated. A theory based upon image magnets is developed in Sec. V to be

compared with the experimental findings at high speed. Predictions of the attainable guidance forces for full scale systems are also made and the conclusions stated in Sec. VI.

II. EXPERIMENTAL

Figure 1 depicts the general experimental set-up of the 24 inch diameter, 6 inch wide solid aluminum wheel, the position of the superconducting coil and the LVDT (linear variable differential transformer) transducers for measuring the lift and drag forces. As depicted, the 3 h.p. variable speed D.C. motor could only drive the wheel to $\sim$ 200 mph. To obtain rim speeds of 300 mph an additional motor of 2 h.p. was employed. Coastdown times from 300 mph were generally in the neighborhood of 4 minutes.

As seen in Figure 1, the lift force on the superconducting magnet is transferred via the stainless steel magnet support tube to the lift transducer. The lift transducer is mounted on a pivotal platform which allows the drag force to be accurately measured. To further reduce possible frictional effects, ball bearings were used in many joints and the only seal between the dewar and the outside air is the loose surgeon glove.

Four coils were used in these experiments and their salient features are listed in Table 1. Because the coils were to be used to measure guidance forces also (where the radius of curvature of the bottom of the channel was reduced), they were made with a $10\frac{1}{2}$ inch radius of curvature while the wheel had a 12 inch radius. For this reason an ambiguity existed in the measurement of the height of the coil above the wheel and the height dependent results presented in Sections III and IV reflects a mean coil position which is 0.030 inch above that part of the leading or trailing edge of the coil. Also included as an

addition in the height position on the experimental results is that due to shrinkage of that length of the tube holding the superconducting coil in the dewar. This was required since reference measurements of the coil height above the wheel were done with the dewar removed. Measurements of the lift and drag forces on the coil were done with the dewar in place and shrinkage of the rod holding the coil therefore increased the clearance. This shrinkage was estimated to be 0.060 inch. For the transverse and channel guidance force measurements a third transducer was placed at the same height as the drag transducer but at right angles to it. Also, in these experiments the lift transformer was suspended from a gimbal arrangement to further reduce friction.

The common vacuum dewar was constructed out of 304 stainless steel with a curved bottom to fit the wheel. While cylindrical for the upper 16 inches, the lower 3 inches of the dewar was rectangular to allow it to nest in the channeled wheel. Since the channel was 5.32 inches wide and the widest coil was 4 inches, this allowed the coil edge to come within 0.66 inch of the side. A similar value was the minimum distance between the wheel and the bottom of the coil.

Accurate positioning of the coil above the center line of the wheel was previously found to be important for precise measurements of the drag force.[4] To improve upon the previous technique, an optical alignment procedure prior to measurement without the dewar in place and with the required drag loads applied was followed. Also, a micropositioning adjustment on the drag force transducer was incorporated to allow adjustments of the coil to be made as the drag force varied during an experiment. These two techniques provided repeatable measurements of the lift and drag forces within $\pm$ 1%. For the recording of the lift and drag force as a function of speed, a multiplexer to the

y axis of an x-y recorder was constructed. The output of the amplifiers of the lift and drag force transducers was sent to the multiplexer and on $\frac{1}{4}$ or $\frac{1}{2}$ second intervals (corresponding to speed changes of 5 mph or less) the lift and drag forces were recorded. The speed signal, sent to the x axis of the recorder, was provided by a d.c. generator mounted at the axle of the 24 inch diameter wheel. Thus the experimental lift and drag force measurements depicted in Figure 2 and generally recorded upon slowing down from 300 mph, became essentially continuous curves.

In the experiments involving measurements of the transverse force (coil near the edge of the wheel) and the guidance force (coil near the side of the channel), care was also taken to see that the coil remained at its designated position in the dewar as the drag and transverse loads were altered. This was done with the micropositioner on the drag force transducer as mentioned above and similarly for the transverse or guidance force transducer. In measurements involving the guidance force where the dewar was fixed in relation to the channel an attraction to the side wall of the dewar was noted (at 4.2°K the 304 stainless steel becomes slightly ferromagnetic). Part of this effect was corrected for by measurements at zero wheel speed. Because of these reasons and the added force measurement, the channel experiments were the most difficult to perform and perhaps have the largest error.

Since the channel was 1.44 inches deep and the pulley ratio between the motor and the wheel were not changed, the maximum speed in the channel was 265 mph instead of the previous 300 mph figure.

III. INFINITELY WIDE CONDUCTING PLATE

In Ref. 10 an exact theory of the lift and drag forces on a flat rectangular coil moving above an infinitely wide conducting plate is given. This theory is based upon a Fourier transform technique and is valid for a plate of arbitrary thickness and permeability μ. In the present work we shall only be concerned with an infinitely thick plate with $\mu = \mu_o$. In this case the lift force is given by[10]

$$F_L = \frac{8\mu_o (NI)^2}{\pi^2} \int_o^\infty dk_2 \sin^2 k_2 a \int_o^\infty dk_1 \sin^2 k_1 b \, e^{-2kh} \left(\frac{1}{k_2^2} + \frac{1}{k_1^2} \right) \times \left(1 - \frac{2(\beta_1 + 1)}{(\beta_1+1)^2 + \beta_2^2} \right) \qquad \text{(III.1)}$$

and the drag force by

$$F_D = \frac{8\mu_o (NI)^2}{\pi^2} \int_o^\infty dk_2 \sin^2 k_2 a \int_o^\infty dk_1 \sin^2 k_1 b \, e^{-2kh} \frac{2\beta_2}{(\beta_1+1)^2 + \beta_2^2} , \qquad \text{(III.2)}$$

where

$$\beta_{1,2} = 2^{-\frac{1}{2}} \left[(\lambda_1^2 k_1^2 / k^4 + 1)^{\frac{1}{2}} \pm 1 \right]^{\frac{1}{2}} , \qquad \text{(III.3)}$$

$$\lambda_1 = \mu_o \sigma v , \qquad \text{(III.4)}$$

and

$$k^2 = k_1^2 + k_2^2 . \qquad \text{(III.5)}$$

The width of the coil is 2a, the length is 2b (parallel to v), and the height above the plate is h. The conductivity of the plate is σ. The number of turns of wire in the coil is N and the current is I. The integrals in (III.1) and (III.2) are evaluated numerically.

In Fig. 2 we show the lift and drag forces on a 2 x 4" coil

at h = 0.91" and 1.66" for velocities up to 300 mph. Both experimental and theoretical results are shown. For convenience, the forces have been normalized to their values at 300 mph. (Note that the scale for F_L is different from that for F_D.) As in all calculations to be compared with the experimental results from the rotating cylinder, the resistivity of the plate was taken to be 4.0 $\mu\Omega$-cm since the 6061-T6 aluminum alloy from which the cylinder was made is reported to have a conductivity 43% that of copper. No measurement of the conductivity was made. We also assume that the cylindrical geometry of the experiment introduces insignificant error. Edge effects are discussed in Sec. V and are seen to be small in the cases considered in Sec. III. A brief discussion of the possible sources of errors is given at the end of this section.

For the 2 × 4" coil in Fig. 2, the lift force at 300 mph was measured to be 3.15 kg at h = 0.91" with I = 32.5 A. For h = 1.66" and I = 59 A, the lift force was 2.37 kg. The calculated values are 3.39 and 2.54 kg, respectively. Likewise, the experimental L/D was found to be 10.5 and 11.85, while the theoretical values are 10.0 and 11.2. We note that for the higher height, the lift force rises to its asymptotic values sooner, the normalized drag peaks higher, and the L/D is larger.[13] A comparison of the 2 × 4" results to that of a 4 × 2" coil is made in Ref. 10 for h = 1.66". In that case, the lift rises faster and L/D is smaller for the 4 × 2" coil.[13] In both cases agreement between theory and experiment is good.

In Fig. 3, the lift force as a function of height at

v = 300 mph and I = 50 A for the four coils is shown. The force vs. height measurements shown in Fig. 3 at 50 A were first obtained at various currents, then, once the square law for currents was experimentally verified, these results were corrected to 50 A. The maximum current used, 70 to 75 A, was in the 2 × 4" coil at a height of 2 inches. The physical properties of the coils are given in Table I. We note that the agreement between theory and experiment in absolute magnitude is better than 10% for the 2 × 4" and 4 × 2" coils and somewhat larger ($\lesssim$ 20%) for the 3 × 4" and 4 × 4" coils. At this high speed the variation of F_L with h is essentially that of the image force.

In Fig. 4, the L/D as a function of height at v = 300 mph is shown for three coils. The agreement between theory and experiment is quite good for the 4 × 2" coil. For both the 2 × 4" and the 4 × 4" coil, the theoretical calculations gave nearly identical L/D as a function of height whereas experimentally a small difference of 5-15%, depending on the height, was found. While this discrepancy is not understood, the general trend that L/D increases with increasing h is evident.[13]

Although agreement between theory and experiment is generally good in Figs. 2-4, there exist some differences. The following are some possible causes: (1) cylindrical geometry of experiment and flat plate geometry of theory, (2) finite width of cylinder (guideway), (3) finite cross-section of the bundle of wires making up the coil (calculations assume all wires concentrated at center of bundle), (4) uncertainties in experimental parameters (height, conductivity of plate, etc.), (5) slight difference in the radius of curvature of coil

and cylinder. We have examined the effects of (1) and (3) on long wires (not coils), and have not found these to be significant. Likewise, particularly for the 2 × 4" coil, the results of Sec. V show that (2) is insignificant. As mentioned in Section II, (5) exists since the coils were formed to the curvature for the guidance experiments. To this end the 4 × 4" coil has "more coil" closer to the wheel than either the 3 × 4" coil or the 2 × 4" coil and consequently, the lift force for the 4 × 4" coil may be somewhat larger than it would be if the coil were of the proper curvature. However, no estimate was made for this error.

IV. EDGE EFFECTS

A. THEORY

The force on a magnet moving over a thin conducting plate of infinite extent has been calculated by Reitz.[3] In the limit of high velocities, the force approaches that given by the image of the magnet below the plate. An equivalent viewpoint is that in the high-speed limit the plate behaves as if it were diamagnetic. That is, the eddy currents induced in the plate generate a magnetic field which exactly cancels the normal component of the field due to the magnet at the surface of the plate. This is also true, at high speeds, for plates of arbitrary thickness and finite extent.

The force on a monopole moving above, and parallel to the edge of a semi-infinite, thin conducting plate has been found.[12] In this section, those results are extended to include a flat coil in the high-speed (diamagnetic) limit.

We consider a rectangular magnet (or coil) of dimensions $2a \times 2b$ (See Fig. 5). The 2b edge is parallel to the edge of the plate and the plane of the coil is parallel to the upper surface of the plate. The lower side of the coil is a distance z_o from the top of the plate. The thickness of the coil (in the vertical direction) is c so that the number of turns of wire is nc where n is the number per meter. The thickness in the horizontal direction of the bundle of wires making up the coil is assumed to be negligibly small. The center of the coil is a horizontal distance $h' + \frac{1}{2}a$ from the edge of the plate and a vertical distance $h = z_o + \frac{1}{2}c$. We let the x-axis coincide with the top edge of the plate, the y-axis is along the surface of the plate perpendicular to the edge, and the z-axis is normal to the plate. The velocity of the magnet is in the x-direction.

It is straightforward to show that the scalar potential associated with the magnet is (I = current)

$$\Omega'(\underset{\sim}{r}) = -\frac{\mu_o In}{4\pi}\left(\int_{S_1}\frac{dS'}{|\underset{\sim}{r}-\underset{\sim}{r}'|} - \int_{S_2}\frac{dS'}{|\underset{\sim}{r}-\underset{\sim}{r}'|}\right) \qquad \text{(IV.1)}$$

where S_1 is the flat surface enclosing the upper side of the magnet and S_2, the lower side. We may think of each increment of area ΔS_i as a monopole of strength $q_i = \pm In\Delta S_i$ (+ for S_2, - for S_1). This sign convention corresponds to the magnetic field near S_2 being directed in the negative z-direction for $I > 0$.

Hence, the scalar potential (IV.1) can be written as

$$\Omega'(\underset{\sim}{r}) = \sum_i \frac{\mu_o q_i}{4\pi R_i} \qquad \text{(IV.2)}$$

where

$$R_i = |\underset{\sim}{r} - \underset{\sim}{r}_i| \quad . \tag{IV.3}$$

The position of q_i is given by $\underset{\sim}{r}_i = (x_i, y_i, z_i)$.

In the high-speed limit, the scalar potential associated with the eddy currents due to a single monopole q_i is[12]

$$\Omega_i(\underset{\sim}{r}) = \frac{\mu_o q_i}{4\pi} \frac{2}{\pi} \left(\frac{1}{R_i'} \tan^{-1} \left\{ (\sigma_i + \tau_i')/(\sigma_i - \tau_i') \right\}^{\frac{1}{2}} - \frac{1}{R_i} \tan^{-1} \left\{ (\sigma_i - \tau_i)/(\sigma_i + \tau_i) \right\}^{\frac{1}{2}} \right) \tag{IV.4}$$

where

$$R_i' = \left\{ (x - x_i)^2 + (y - y_i)^2 + (z + z_i)^2 \right\}^{\frac{1}{2}} \quad , \tag{IV.5a}$$

$$\sigma_i = \left\{ \left[(r + r_i)^2 + (x - x_i)^2 \right] / 4 r r_i \right\}^{\frac{1}{2}} \quad , \tag{IV.5b}$$

$$\tau_i' = \cos \left(\frac{\varphi + \varphi_i'}{2} \right) \quad , \tag{IV.5c}$$

$$\tau_i = \cos \left(\frac{\varphi - \varphi_i'}{2} \right) \quad , \tag{IV.5d}$$

$$r = (y^2 + z^2)^{\frac{1}{2}} \quad , \tag{IV.5e}$$

and

$$\varphi = \tan^{-1}(z/y) \quad . \tag{IV.5f}$$

The quantities r_i and φ_i are found from (IV.5e) and (IV.5f) by replacing y by y_i, z by z_i, etc.

The magnetic field from the eddy currents due to q_i is then

$$\underset{\sim}{B}_i(\underset{\sim}{r}) = - \nabla \Omega_i(\underset{\sim}{r}) \quad . \tag{IV.6}$$

(Expressions for $\nabla \Omega_i$ can be found in Appendix A.)

The total magnetic field of the eddy currents is therefore

$$\underset{\sim}{B}(\underset{\sim}{r}) = \sum_i \underset{\sim}{B}_i(\underset{\sim}{r}) \quad . \tag{IV.7}$$

The force on monopole j is

$$\underset{\sim}{F}_j = q_j \underset{\sim}{B}(\underset{\sim}{r}_j) \quad . \tag{IV.8}$$

Summing over all monopoles gives the total force on the magnet,

$$\underset{\sim}{F} = \sum_j \underset{\sim}{F}_j \quad . \tag{IV.9}$$

In Eqs. (IV.2), (IV.7) and (IV.9), the sums are over all monopoles in S_1 and S_2.

Defining

$$\underset{\sim}{B}_i(\underset{\sim}{r}_j) \equiv \frac{\mu_o q_i}{4\pi} \underset{\sim}{b}_{ji} \quad , \tag{IV.10}$$

we can write

$$\underset{\sim}{F} = \sum_{i,j} \frac{\mu_o q_i q_j}{4\pi} \underset{\sim}{b}_{ji} \quad . \tag{IV.11}$$

Taking all ΔS_i to be equal, $\Delta S = 4ab/N'$, we have

$$\underset{\sim}{F} = \frac{4\mu_o}{\pi} (\ln a\,b)^2 \frac{1}{(N')^2} \sum_{i,j} (\pm)\, \underset{\sim}{b}_{ji} \quad . \tag{IV.12}$$

The number of monopoles in a pole is $N' = NM$, the dimensions of the section of surface occupied by each monopole is $2a/N \times 2b/M$. Numerically, we evaluated (IV.12) as a function of the distance, h', separating the left-hand edge of magnet from the xz plane. To avoid difficulties associated with the indeterminate form of $\underset{\sim}{b}_{ii}$, we chose

to evaluate $\underset{\sim}{B}_i(\underset{\sim}{r}_j)$ at the point $(x_j + .01\ z_o,\ y_j,\ z_j)$, a procedure which was quite convenient but did not introduce any significant error.

We give some typical results in Table II. Absolute accuracy is difficult to obtain due to the nearly complete cancellation of effects due to the separate poles. For example, our calculated value for the lift at $h' = 1m$, which is essentially the same as that for $h' = \infty$, is 93% of the ideal lift of a flat thin coil far from the edge ($h' = \infty$, $c \to 0$, $n \to \infty$, $nc = N$). Exact values of the ideal lift are given by Reitz.[3] We note that the lift is not decreased noticeably for $h' \geq 0$. Since the number of monopoles (10×20 array for each pole) used in the calculation is limited, the results may be somewhat optimistic for $0 < h' < h$.

It is not possible to calculate the lift-to-drag ratio for a semi-infinite sheet in a simple manner. However, to estimate the minimum distance h' required to have negligible degradation of this ratio, we can examine the current distribution in the sheet for the high-speed limit. In Fig. 6, the current distribution in a cross-section containing the center of the coil is shown for two positions of the coil. It is clear that the current distribution is small ($\leq$ 1% of the peak value) at a distance $\gtrsim .2$ meter beyond the edge of the coil. Hence, when $h' = 0.5m$, the presence of the edge at $y = 0$ is of little consequence. Therefore, we expect that since the current distribution is not appreciably altered, the lift-to-drag ratio should be approximately the same as in the infinite-sheet case.[3] For $h' = 0$, on the other hand, the current pattern is definitely altered near $y = 0$ and we would expect a significant increase in the resistive loss of the current flow. Since the power lost in the current flow (Joule

heating) is $F_D v$ (i.e., drag force × velocity of the coil), the drag force should be larger for $h' = 0$ than for $h' = 0.5$ meter. An increased drag force and a slightly decreased lift force combine to give a lower lift-to-drag ratio.

From the range of the current distribution in the sheet beyond the edge of the coil (See Fig. 5), we estimate that a rule-of-thumb value for the minimum h' which can be tolerated without appreciable degradation of the lift-to-drag ratio is $h' \simeq h$, the height of the coil above the sheet.

B. EXPERIMENTAL RESULTS

By placing a coil near the edge of the rotating cylinder, the transverse force (which tends to pull the coil towards the edge) was measured as well as F_L and F_D. In Fig. 7, data are shown for the 2×4" coil (4" parallel to edge) at 300 mph and $h = 1.125$". The closer the coil is to the edge, the stronger is F_T and the weaker is F_L. As noted the ratio $(F_L + F_T)/F_D$ is nearly constant. Although it is not shown, the velocity dependence of this transverse force saturates more quickly than the lift force. For example, at 50 mph the transverse force is 83% of the 300 mph value while the lift force is only 63%.

The theoretical results for a thin semi-infinite plate in the high-speed limit (as calculated in Sec. IV(A) are also shown). The experimental situation is not really the same, however, since eddy currents can flow around the edge and down the end of the cylinder, whereas the eddy currents in the thin plate model are confined to the horizontal plane. While this is a limitation of the thin plate model, it is the only pertinent analytically tractable calculation available. The results are in reasonable agreement with experiment.

V. CHANNEL EFFECTS

A. THEORY

Instead of considering a U-shaped channel directly, it is

simpler to examine the effects of each side separately, adding the resultant forces together for the channel. Although not rigorously correct, this appears to be an adequate approximation for our purposes. Hence, we find the force on a coil moving near a conductor shaped as right-angle corner.

As previously stated, the force on a rectangular coil moving over a thin conducting plate of infinite extent has been calculated by Reitz.[3] At high speeds, the results of his calculation can be summarized as follows. The lift force F_L on the coil approaches the ideal lift force, which is the force due to the image of the coil below the plate. The drag force F_D can be found by equating $F_D v$ (v = velocity of the coil) to the power loss due to Joule heating by the eddy currents induced in the plate. The lift-to-drag ratio is then found to be

$$F_L/F_D = v/w \qquad (V.1)$$

where

$$w = 2/\mu_o \sigma \delta \quad . \qquad (V.2)$$

In Eq. (V.2), σ is the conductivity of the plate and δ is the thickness of the plate. In the event that the skin depth δ_s is smaller than δ, an approximate expression for the lift-to-drag ratio can be found by replacing δ by δ_s in (V.2).

We consider a rectangular coil of dimension $2a \times 2b$ moving in the x-direction with velocity v. The side of the coil with dimension 2b is parallel to the x-direction, which is normal to the drawing Fig. 8. The top surface of the horizontal portion of the conductor coincides with the xy-plane and the right-hand surface of the vertical portion with the xz-plane. The coil is parallel to the xy-plane and is a distance z_o above it. Since the thickness of the coil is negligible,

$z_o = h$. The center of the coil is a horizontal distance y_o from the xz-plane. The x-coordinate of the coil center is taken to be $x = 0$. The thickness of the conductor is δ and is taken to be small.

In the high-speed limit (which is all that is considered in this section), eddy currents flow in such a manner as to completely screen out the field on the side of the conductor opposite to that occupied by the coil (source). In terms of our coordinate system, the magnetic field vanishes in the second, third, and fourth quadrants of the yz-axes for all x. Since the normal component of the field is continuous across the conductor,[13] it must therefore vanish on the xy-plane and on the xz-plane. Hence, the boundary condition on the magnetic field (total field of eddy currents and source) is

$$B_z = 0 \qquad \text{on x-y plane} \tag{V.3}$$

and

$$B_y = 0 \qquad \text{on x-z plane} \tag{V.4}$$

Consequently, the magnetic field due to the eddy currents in the region containing the coil (i.e., $y,z > 0$) is the same as that produced by the set of images shown in Fig. 9. The current in the image coil whose center is at $(0, -y_o, z_o)$ has the same sense as the source, whereas the image coils at $(0, -y_o, -z_o)$ and $(0, y_o, -z_o)$ have current of the opposite sense. It is straightforward to verify that the boundary conditions (V.3) and (V.4) are satisfied.

Let us digress a moment to consider the force of one coil (say coil 1) on another identical coil (coil 2). We place the center of coil 1 at the origin and the center of coil 2 at (0, y, z) and

calculate the force $\underset{\sim}{f}(y,z) = (0, f_y, f_z)$. Reitz has given the mutual inductance for two such coils and has described how to calculate the force $\underset{\sim}{f}$.[3] The expressions for f_y and f_z for coils of dimension a × b with NI ampere-turns of current (and the same sence of current) are given in our notation in Appendix B. (Note that in Appendices B and C and Ref. 3, the dimensions of the coil are a × b, not 2a × 2b as in the main body of this paper and in Ref. 10.)

To return to the problem at hand, we now find the force on the source coil of Fig. 9 due to the three images. The lift force F_L is

$$F_L = F_z = - f_z(0,2z_o) - f_z(-2y_o,2z_o) + f_z(-2y_o,0) . \qquad (V.5)$$

By symmetry, $f_z(-2y_o,0)$ vanishes. The guidance force F_G is

$$F_G = F_y = - f_y(0,2z_o) - f_y(-2y_o,2z_o) + f_y(-2y_o,0) . \qquad (V.6)$$

By symmetry, $f_y(0,2z_o)$ also vanishes. Eqs. (V.5) and (V.6) then give the lift and transverse force on the coil in the high-speed limit. We next find the drag force.

Since we know the magnetic field of the eddy currents in the high-speed limit, we can calculate the eddy current density $\underset{\sim}{i}$ in the conductor ($\underset{\sim}{i} = \delta \underset{\sim}{j}$ where $\underset{\sim}{j}$ is the volume current density). In the region containing the coil, the total magnetic field $\underset{\sim}{B}$ of the eddy currents plus the source is the same as the field from the four coils shown in Fig. 9 (three images and the source). In the remaining regions, $\underset{\sim}{B} = 0$. From Ampere's Circuital Law ($\oint \underset{\sim}{B} \cdot d\ell = \mu_o \int \underset{\sim}{j} \cdot d\underset{\sim}{A}$, where displacement currents are neglected), we find that on the horizontal portion

of the conductor (xy-plane)

$$\mu_o i_x = - B_y \tag{V.7}$$

and

$$\mu_o i_y = B_x \quad , \tag{V.8}$$

and on the vertical portion (xz-plane), we find

$$\mu_o i_x = B_z \tag{V.9}$$

and

$$\mu_o i_z = - B_x \quad . \tag{V.10}$$

To calculate the drag force on the coil, we equate $F_D v$ to the power loss in the conductor

$$F_D v = \text{power} = \frac{1}{\sigma\delta} \int i^2 \, dA \tag{V.11}$$

where the integral is taken over the surface of the conductor bounding the region containing the source coil (i.e., xy-plane, $y > 0$ and xz-plane, $z > 0$).

In Appendix C, we give expressions for the magnetic field $\underset{\sim}{b}(x,y,z)$ at point (x,y,z) due to a coil whose center is at the origin. In terms of $\underset{\sim}{b}(x,y,z)$, the tangential field on the horizontal portion of the conductor is (taking into account the sense of the currents in Fig. 8)

$$B_\alpha(x,y,0) = b_\alpha(x, y - y_o, - z_o) - b_\alpha(x, y - y_o, z_o) + b_\alpha(x, y + y_o, - z_o) - b_\alpha(x, y + y_o, z_o), \quad \alpha = x,y \; . \tag{V.12}$$

By symmetry,

$$b_\alpha(x,y, - z) = - b_\alpha(x,y,z), \quad \alpha = x,y \quad , \tag{V.13}$$

so that the first two terms can be combined and the last two also can be combined in (V.12), giving

$$B_\alpha(x,y,0) = -2[b_\alpha(x, y-y_o, z_o) + b_\alpha(x, y+y_o, z_o)] \quad . \qquad (V.14)$$

In a similar fashion, we find the tangential field on the vertical portion of the conductor to be

$$B_\alpha(x,0,z) = 2[b_\alpha(x,y_o, z-z_o) - b_\alpha(x,y_o, z+z_o)] \ , \quad \alpha = x,z \quad . \ (V.15)$$

Substitution of Eqs. (V.14) and (V.15) into Eqs. (V.7) - (V.10) yields the appropriate value for the eddy current density in the high-speed limit. The drag force is then found from (V.11).[15]

Numerical results for F_L, F_G and F_D are given in Table III for parameters typical of the magnets that are being considered for high speed ground vehicles. The force on a 1m × 2m coil (2m side parallel to v) has been calculated for a height $z_o = h = 0.2$m above the horizontal portion of the conductor as a function of h', the distance between the edge of the coil and the vertical portion of the conductor (i.e., $y_o = h' + \frac{1}{2}a$ in Fig. 7). We notice that in all cases

$$F_D = \frac{w}{v}(F_L + F_G) \quad . \qquad (V.16)$$

Although we have not found a proof of (V.16), we expect that it holds, at least for high speeds, since it has been checked numerically over a wide range of parameters (in the high-speed limit). The fact that F_D is <u>not</u> greater than $(w/v)(F_L + F_G)$ is encouraging with regard to the lift-to-drag ratio of guideways which afford an appreciable guidance force (F_G).

B. EXPERIMENTAL RESULTS

A channel 5.32" wide and 1.44" deep was cut in the cylinder. The forces on coils placed in the channel as the cylinder was rotated were measured. In Fig. 10, the results for the 2 × 4" coil at 265 mph and h = 0.875" and 1.125" are shown. The coil could be moved as much as 1" off center, the edge of the coil thereby being 0.66" from the side of the channel. Over this range, F_L is nearly constant, whereas F_G (which repels the coil from the side panel) increases as the coil is moved off center in such a manner that $(F_L + F_G)/F_D$ is roughly constant. Strictly speaking, this is not the same as (V.16) which would imply that $(F_L + F_{G1} + F_{G2})/F_D$ is constant (as a function of displacement from the center) where $F_G = F_{G1} - F_{G2}$, F_{G1} being due to the near panel and F_{G2} that due to the far panel. However, F_{G2} is small compared with F_{G1} except near the center where they become equal.

Calculated values based upon the theory of Sec. V(A) are also shown. These results are found by calculating F_{G1} and F_{G2} separately and subtracting to find F_G. Likewise, F_L is decreased from its value for an infinitely wide flat plate, $F_{L\infty}$, by ΔF_{L1} and ΔF_{L2}. $\Delta F_{L1,2}$ is the decrease due to the near (far) panel. The lift force is then taken to be $F_L = F_{L\infty} - \Delta F_{L1} - \Delta F_{L2}$. Since ΔF_{G2} and ΔF_{L2} are small in the calculations for Fig. 10, these approximations should be sufficiently accurate for our purposes.

The agreement is not as good as we would have expected. The differences are probably not due to finite speed factors--which could not be calculated accurately. Experimentally, the velocity dependence

of F_L and F_G were essentially identical. More likely, the resolution of the discrepancies lies in the fact that the coil was close to the top of the channel giving rise to an additional lift force.

In Table IV, we make a comparison of the theoretical and experimental values of L/D for coils in the center of the channel at v = 265 mph for several heights. The agreement is good, the small systematic difference probably exists because of the above mentioned effect due to the top of the channel.

VI. SUMMARY

Experimental force data on small superconducting coils placed near a large rotating conducting cylinder have been reported in this paper. F_L and F_D vs. v for various heights and coils have been given, the coils being far from the edges (ends) of the cylinder. Comparison with the theory of Ref. 10 is generally good. Confirmation of the theory then gives us confidence that the predictions for full scale systems[10] are valid.

By moving the coil near an end of the cylinder, experimental data on edge effects were obtained. Likewise, after cutting a channel in the cylinder, guidance forces and the properties of a U-shaped channel were studied. The findings were in reasonable agreement with theoretical calculations. Again, the experiments substantiated our predictions for full scale systems.

Finally, it should be remarked that for a properly designed system with reasonable guidance forces, say 0.5 F_L, (either from separate side panels or from a U-shaped guideway), L/D ~ 30-50 at 300 mph

can be expected.[10] These high values of L/D are obtained without sacrificing much of the potential lift of the system. For comparison, L/D for aerodynamic drag only is estimated to be ~ 20 for well designed vehicles. Consequently, it appears possible to make the magnetic drag (including guidance) smaller than the air drag.

ACKNOWLEDGMENT

The authors would like to acknowledge useful discussions with Dr. J. R. Reitz and Dr. D. F. Wilkie.

APPENDIX A

From Eqs. (IV.4) and (IV.5), it can be shown that (omitting the $\frac{\mu_o q_i}{4\pi}$ factor)

$$\pi \frac{\partial \Omega_i}{\partial z} = -(z+z_i) S_1(i) - y S_5(i) + z S_6(i) + (z-z_i) S_2(i) - y S_7(i) \quad \text{(A1)}$$

and

$$\pi \frac{\partial \Omega_i}{\partial y} = -(y-y_i) S_1(i) + z S_5(i) + y S_6(i) + (y-y_i) S_2(i) + z S_7(i) \quad \text{(A2)}$$

where

$$S_1(i) = \frac{2}{R_i'^3} \tan^{-1} \left\{ (\sigma_i + \tau_i')/(\sigma_i - \tau_i') \right\}^{\frac{1}{2}} , \quad \text{(A3a)}$$

$$S_2(i) = \frac{2}{R_i^3} \tan^{-1} \left\{ (\sigma_i - \tau_i)/(\sigma_i + \tau_i) \right\}^{\frac{1}{2}} , \quad \text{(A3b)}$$

$$S_3(i) = r_i^{\frac{1}{2}} / r^{3/2} , \quad \text{(A3c)}$$

$$S_4(i) = S_3(i) \left\{ (x-x_i)^2 - r^2 + r_i^2 \right\} / \left\{ (x-x_i)^2 + (r_i+r)^2 \right\} , \quad \text{(A3d)}$$

$$S_5(i) = \sin\left(\frac{\varphi+\varphi_i}{2}\right) S_3(i) / R_i'^2 , \quad \text{(A3e)}$$

$$S_6(i) = S_4(i) \left(\frac{\tau_i'}{R_i'^2} + \frac{\tau_i}{R_i^2} \right) , \quad \text{(A3f)}$$

and

$$S_7(i) = \sin\left(\frac{\varphi-\varphi_i}{2}\right) S_3(i) / R_i^2 . \quad \text{(A3g)}$$

APPENDIX B

Force on a rectangular coil of dimensions a × b at (C,y,z) due to an identical coil at origin (b side parallel to x, a side parallel to y):

$$f_z = \frac{\mu_o (NI)^2}{2\pi} \Big\{ -2z\,[z^2 + (y-a)^2]^{-\frac{1}{2}} + 2z\,[z^2 + b^2 + (y-a)^2]^{-\frac{1}{2}}$$

$$-2z\,[z^2 + (y+a)^2]^{-\frac{1}{2}} + 2z\,[z^2 + b^2 + (y+a)^2]^{-\frac{1}{2}}$$

$$+4z\,[z^2 + y^2]^{-\frac{1}{2}} - 4z\,[z^2 + b^2 + y^2]^{-\frac{1}{2}}$$

$$-(y-a)^2/z[(y-a)^2 + z^2]^{\frac{1}{2}} + (y-a)^2 z/(z^2+b^2)[(y-a)^2 + z^2 + b^2]^{\frac{1}{2}}$$

$$-(y+a)^2/z[(y+a)^2 + z^2]^{\frac{1}{2}} + (y+a)^2 z/(z^2+b^2)[(y+a)^2 + z^2 + b^2]^{\frac{1}{2}}$$

$$-2b^2 z/(z^2+y^2)[b^2+z^2+y^2]^{\frac{1}{2}} + b^2 z/[z^2+(y-a)^2][b^2+z^2+(y-a)^2]^{\frac{1}{2}}$$

$$+b^2 z/[z^2+(y+a)^2][b^2+z^2+(y+a)^2]^{\frac{1}{2}} + 2y^2/z[z^2+y^2]^{\frac{1}{2}}$$

$$-2y^2 z/(z^2+b^2)[y^2+z^2+b^2]^{\frac{1}{2}} \Big\},$$

$$f_y = \frac{\mu_o (NI)^2}{2\pi} \Big\{ -(y-a)/[z^2 + (y-a)^2]^{\frac{1}{2}} + (y-a)/[z^2+b^2+(y-a)^2]^{\frac{1}{2}}$$

$$-(y+a)/[z^2 + (y+a)^2]^{\frac{1}{2}} + (y+a)/[z^2+b^2+(y+a)^2]^{\frac{1}{2}}$$

$$+2y/[z^2+y^2]^{\frac{1}{2}} - 2y/[z^2+b^2+y^2]^{\frac{1}{2}}$$

$$-2b^2 y/(z^2+y^2)[b^2+z^2+y^2]^{\frac{1}{2}} + b^2(y-a)/[z^2+(y-a)^2][z^2+(y-a)^2+b^2]^{\frac{1}{2}}$$

$$+b^2(y+a)/[z^2+(y+a)^2][z^2+b^2+(y+a)^2]^{\frac{1}{2}}$$

$$+\ell n\left(\frac{[y-a+\{(y-a)^2+z^2\}^{\frac{1}{2}}][y+a+\{(y+a)^2+z^2\}^{\frac{1}{2}}]}{[y-a+\{(y-a)^2+z^2+b^2\}^{\frac{1}{2}}][y+a+\{(y+a)^2+z^2+b^2\}^{\frac{1}{2}}]}\right)$$

$$+2\ell n\left(\frac{y+\{y^2+z^2+b^2\}^{\frac{1}{2}}}{y+\{y^2+z^2\}^{\frac{1}{2}}}\right)\Big\}$$

APPENDIX C

Magnetic field at (x,y,z) due to a rectangular coil of dimensions a × b at origin (b side parallel to x, a side parallel to y):

$$B_z(x,y,z) = \frac{\mu_o NI}{4\pi}\left\{\frac{-(x-b/2)}{(x-b/2)^2+z^2}\left[\frac{-(y-a/2)}{\{(y-a/2)^2+(x-b/2)^2+z^2\}^{\frac{1}{2}}}+\frac{(y+a/2)}{\{(y+a/2)^2+(x-b/2)^2+z^2\}^{\frac{1}{2}}}\right]\right.$$

$$+\frac{(x+b/2)}{(x+b/2)^2+z^2}\left[\frac{-(y-a/2)}{\{(y-a/2)^2+(x+b/2)^2+z^2\}^{\frac{1}{2}}}+\frac{(y+a/2)}{\{(y+a/2)^2+(x+b/2)^2+z^2\}^{\frac{1}{2}}}\right]$$

$$-\frac{(y-a/2)}{(y-a/2)^2+z^2}\left[\frac{-(x-b/2)}{\{(x-b/2)^2+(y-a/2)^2+z^2\}^{\frac{1}{2}}}+\frac{(x+b/2)}{\{(x+b/2)^2+(y-a/2)^2+z^2\}^{\frac{1}{2}}}\right]$$

$$\left.+\frac{(y+a/2)}{(y+a/2)^2+z^2}\left[\frac{-(x-b/2)}{\{(x-b/2)^2+(y+a/2)^2+z^2\}^{\frac{1}{2}}}+\frac{(x+b/2)}{\{(x+b/2)^2+(y+a/2)^2+z^2\}^{\frac{1}{2}}}\right]\right\},$$

$$B_x(x,y,z) = \frac{\mu_o NIz}{4\pi}\left\{\left[(x-b/2)^2+z^2\right]^{-1}\left[\frac{-(y-a/2)}{\{(y-a/2)^2+(x-b/2)^2+z^2\}^{\frac{1}{2}}}+\frac{(y+a/2)}{\{(y+a/2)^2+(x-b/2)^2+z^2\}^{\frac{1}{2}}}\right]\right.$$

$$\left.-\left[(x+b/2)^2+z^2\right]^{-1}\left[\frac{-(y-a/2)}{\{(y-a/2)^2+(x+b/2)^2+z^2\}^{\frac{1}{2}}}+\frac{(y+b/2)}{\{(y+a/2)^2+(x+b/2)^2+z^2\}^{\frac{1}{2}}}\right]\right\},$$

$$B_y(x,y,z) = \frac{\mu_o NIz}{4\pi}\left\{\left[(y-a/2)^2+z^2\right]^{-1}\left[\frac{-(x-b/2)}{\{(x-b/2)^2+(y-a/2)^2+z^2\}^{\frac{1}{2}}}+\frac{(x+b/2)}{\{(x+b/2)^2+(y-a/2)^2+z^2\}^{\frac{1}{2}}}\right]\right.$$

$$\left.-\left[(y+a/2)^2+z^2\right]^{-1}\left[\frac{-(x-b/2)}{\{(x-b/2)^2+(y+a/2)^2+z^2\}^{\frac{1}{2}}}+\frac{(x+b/2)}{\{(x+b/2)^2+(y+a/2)^2+z^2\}^{\frac{1}{2}}}\right]\right\}.$$

REFERENCES

1. C. A. Guderjahn, S. L. Wipf, H. J. Fink, R. W. Boom, K. E. MacKenzie, D. Williams, and T. Downey, J. Appl. Phys. 40, 2133 (1969).

2. H. T. Coffey, F. Chilton, and T. W. Barbee, Jr., J. Appl. Phys. 40, 2161 (1969); H. T. Coffey, T. W. Barber, Jr., and F. M. Chilton, Low Temperatures and Electric Power (Intern. Inst. of Refrigeration, Commission I, London 1969).

3. J. R. Reitz, J. Appl. Phys. 41, 2067 (1970).

4. R. H. Borcherts and J. R. Reitz, Transportation Res. 5, (No. 3 Aug. 1971).

5. C. A. Guderjahn and S. L. Wipf, Cryogenics 11, 171 (1971).

6. L. Hannakam, Elektrotech. Z. 86, 427 (1965).

7. L. T. Klauder, Jr., Am. J. Phys. 37, 323 (1969).

8. F. Chilton and H. T. Coffey, Int. Helium Soc. Symposium, Washington, D. C. (May 1971).

9. D. C. Burnham, J. Appl. Phys. 42, 3455 (1971).

10. J. R. Reitz and L. C. Davis (to be published).

11. P. L. Richards and M. Tinkam (unpublished).

12. L. C. Davis and J. R. Reitz, J. Appl. Phys. (Sept. 1971).

13. Simplified discussions of L/D given in Refs. 8-11 also predict this feature.

14. The thickness of the conductor is taken to be small enough that the variation of the normal component across it is negligible. In effect, we are treating the eddy currents as current sheets. A more complete discussion of this point of view can be found in Treatise on Electricity and Magnetism, by J. C. Maxwell, (Dover reprint, New York 1954), 3rd ed., Vol. 2, p. 297, and in

Static and Dynamic Electricity, by W. R. Smyth, (McGraw-Hill Book Co., New York 1950), 2nd ed., p. 402.

15. This type of analysis does not work for finding the drag force for the thin semi-infinite plate (Sec. IV) because the eddy currents necessary to produce a complete cancellation of B_z on the surface of the plate diverge at the edge. Hence (V.11) diverges and consequently $F_D \to 0$ as $v \to \infty$ slower than $1/v$.

TABLE I. Physical Properties of Experimental Coils

Nominal Dimensions	a (cm)	b (cm)	N
4 × 2"	4.67	2.12	342
2 × 4"	2.12	4.67	332
3 × 4"	3.39	4.67	325
4 × 4"	4.67	4.67	317

The superconducting wire was single core copper clad Nb-Ti with an overall diameter of 0.015 inch manufactured by Supertechnology Corp., Boston, Massachusetts.

The cross-section of the bundle of wires was 21/64" × 21/64". The width of the coils was 2a and the length (parallel to the direction of motion) was 2b. a and b were measured from the center of the coil to the center of the bundle. The height h was also always measured from the mid-plane of the coil to the top surface of the conducting cylinder. The number of turns of wire was N. Currents were not persistent unless noted to the contrary.

Table II. Force on a flat coil above a diamagnetic semi-infinite sheet ($2a = 1m$, $2b = 2m$, $c = .025m$, $z_o = .2m$, $N = 10$, $M = 20$). The center of the coil is a horizontal distance $h' + \frac{1}{2}a$ from the edge of the sheet.

h'(m)	FZ	FY
-1.0	2.59×10^{-4}	-2.39×10^{-5}
-0.5	9.87×10^{-4}	-5.71×10^{-4}
0	2.98×10^{-3}	-6.50×10^{-4}
0.1	3.19×10^{-3}	-3.05×10^{-4}
0.2	3.19×10^{-3}	-1.19×10^{-4}
0.3	3.16×10^{-3}	-4.89×10^{-5}
0.4	3.14×10^{-3}	-2.21×10^{-5}
0.5	3.13×10^{-3}	-1.10×10^{-5}
1.0	3.12×10^{-3}	-8.06×10^{-7}

$$F_z = \frac{4\mu_o}{\pi} (I n a b)^2 FZ$$

$$F_y = \frac{4\mu_o}{\pi} (I n a b)^2 FY$$

TABLE III. Force on a coil moving above a conductor shaped as a right-angle corner in the high-speed limit. All forces are to be multiplied by $\mu_o(NI)^2/2\pi$ where NI is the number of ampere-turns. (2a = 1m, 2b = 2m, z_o = h = 0.2m, $h' = y_o - \frac{1}{2}a$).

h'(m)	F_L	F_G	F_D
0.1	8.35	6.80	15.15 w/v
0.2	9.35	1.92	11.27 w/v
0.3	9.98	0.707	10.69 w/v
0.4	10.31	0.306	10.62 w/v
0.5	10.48	0.149	10.63 w/v
0.75	10.64	0.034	10.67 w/v
1.0	10.68	0.011	10.69 w/v

TABLE IV. Lift-to-Drag Ratio at 265 mph for Coils at the Center of the Channel.

h (inches)	2 × 4"		3 × 4"		4 × 4"	
	Exp.	Theory	Exp.	Theory	Exp.	Theory
.875	9.40	8.91	8.62	8.35	7.5	6.73
1.0	9.30	8.87	8.60	8.14	7.23	6.29
1.125	9.07	8.74	8.47	7.82	6.97	6.02

FIGURE CAPTIONS

Fig. 1. Sketch of experimental system.

Fig. 2. Lift and drag forces on a 2 × 4" coil as functions of velocity at two different heights above a solid aluminum wheel. (The 4" dimension is parallel to the direction of motion.) Note scale for drag force is different from that for the lift force. At 300 mph, the experimental (theoretical) value of the lift-to-drag ratio is 11.85 (11.2) at h = 1.66" and 10.5 (10.0) at h = 0.91".

Fig. 3. Lift force vs. height at 300 mph and I = 50 A for various coils. The number of turns for each coil is given in Table I.

Fig. 4. Lift-to-drag ratio vs. height at 300 mph for various coils.

Fig. 5. Coordinate system for a coil of finite thickness above a semi-infinite sheet.

Fig. 6. Current distribution in a semi-infinite sheet due to a coil above it in the diamagnetic limit. Results are shown for two positions of the coil. A cross-section through the center of the coil is taken.

Fig. 7. Transverse force, lift force and $(F_L + F_T)/10\ F_D$ at 300 mph for the 2 × 4" coil as functions of the displacement of the coil from the edge of the wheel.

Fig. 8. Coordinate system for coil above a conductor shaped as a right-angle corner.

Fig. 9. Position of coil and images.

Fig. 10. Guidance force and $(F_L + F_G)/10\ F_D$ at 265 mph in a channel for the 2 × 4" coil as functions of the displacement of the coil from the center.

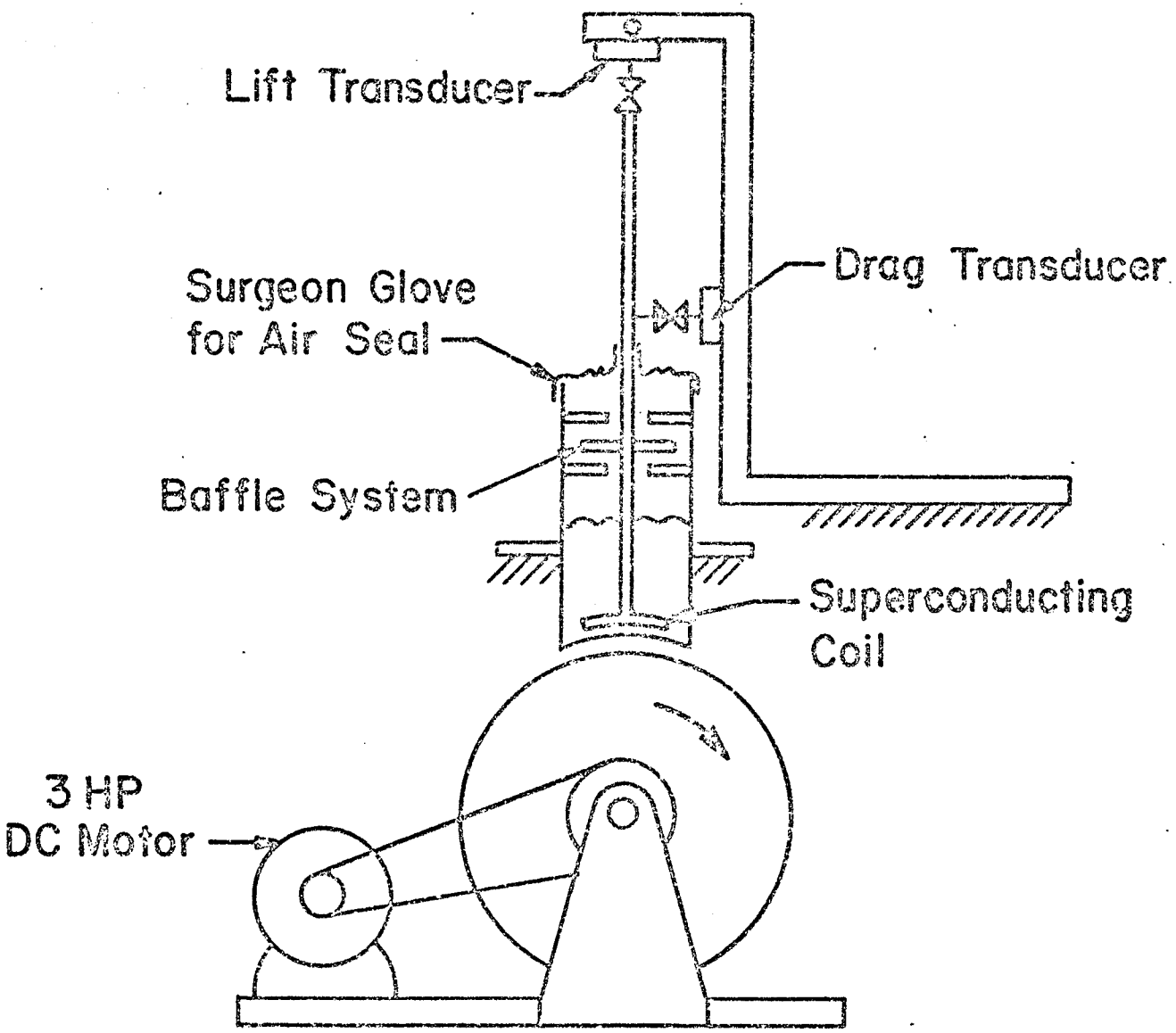
Lift Transducer
Drag Transducer
Surgeon Glove
for Air Seal
Baffle System
Superconducting
Coil
3 HP
DC Motor

FIG. 1

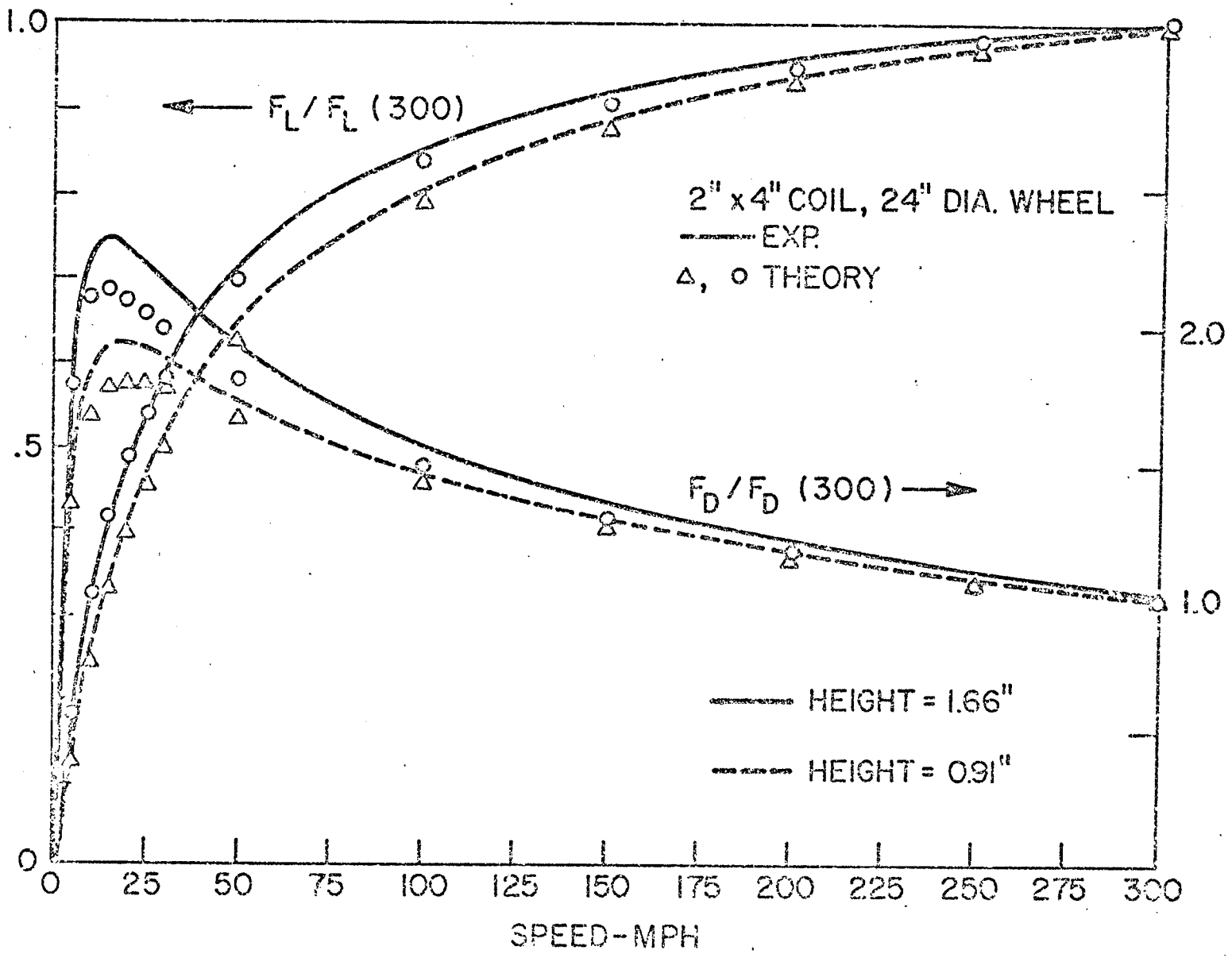
1.0
.5
0
F_L / F_L (300)
2" x 4" COIL, 24" DIA. WHEEL
EXP.
△, ○ THEORY
2.0
F_D / F_D (300)
1.0
HEIGHT = 1.66"
HEIGHT = 0.91"
0
25
50
75
100
125
150
175
200
225
250
275
300
SPEED - MPH

FIG. 2

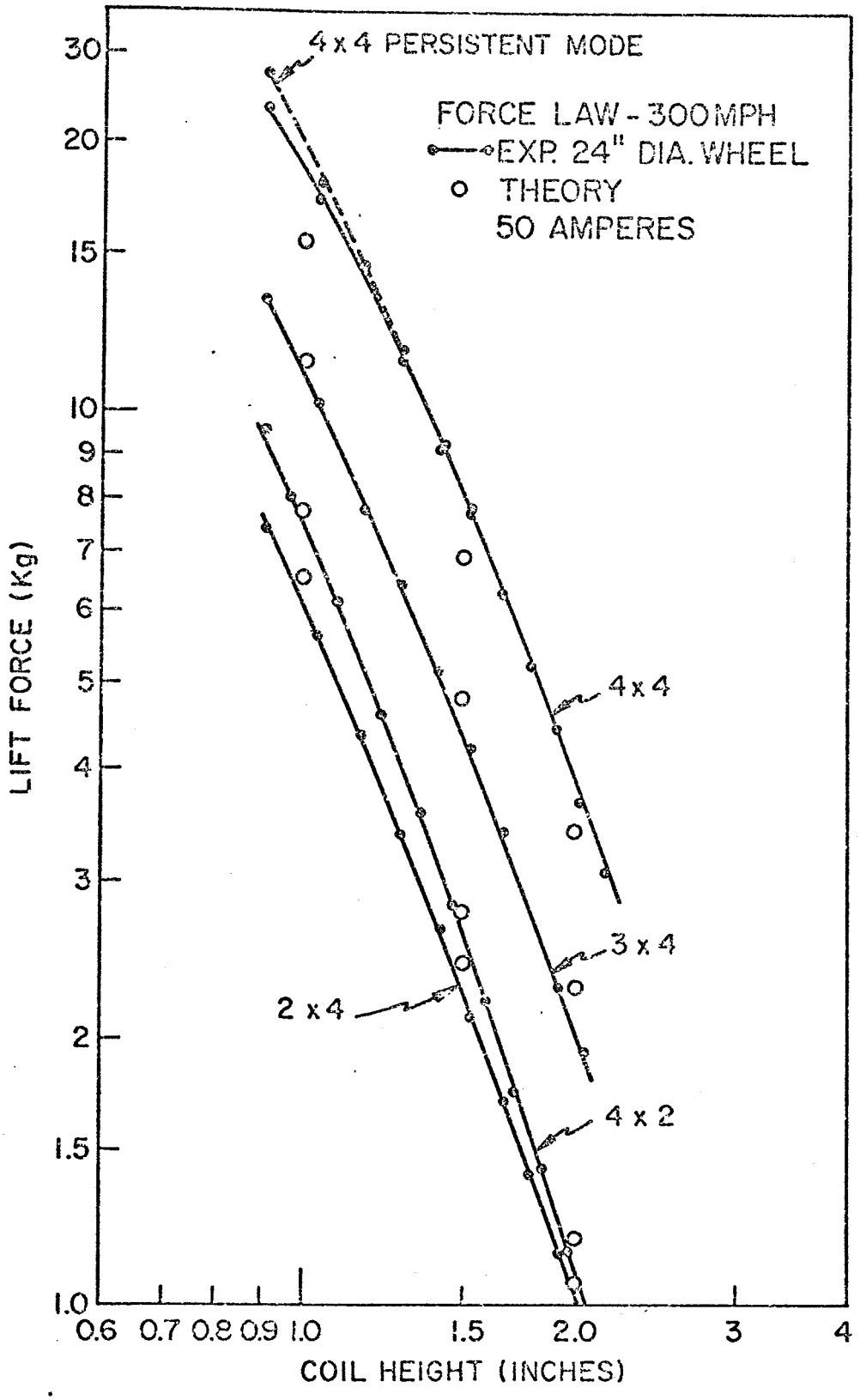
4 x 4 PERSISTENT MODE
FORCE LAW - 300 MPH
EXP. 24" DIA. WHEEL
THEORY
50 AMPERES
4 x 4
3 x 4
2 x 4
4 x 2
LIFT FORCE (Kg)
COIL HEIGHT (INCHES)
30
20
15
10
9
8
7
6
5
4
3
2
1.5
1.0
0.6
0.7
0.8
0.9
1.0
1.5
2.0
3
4

FIG. 3

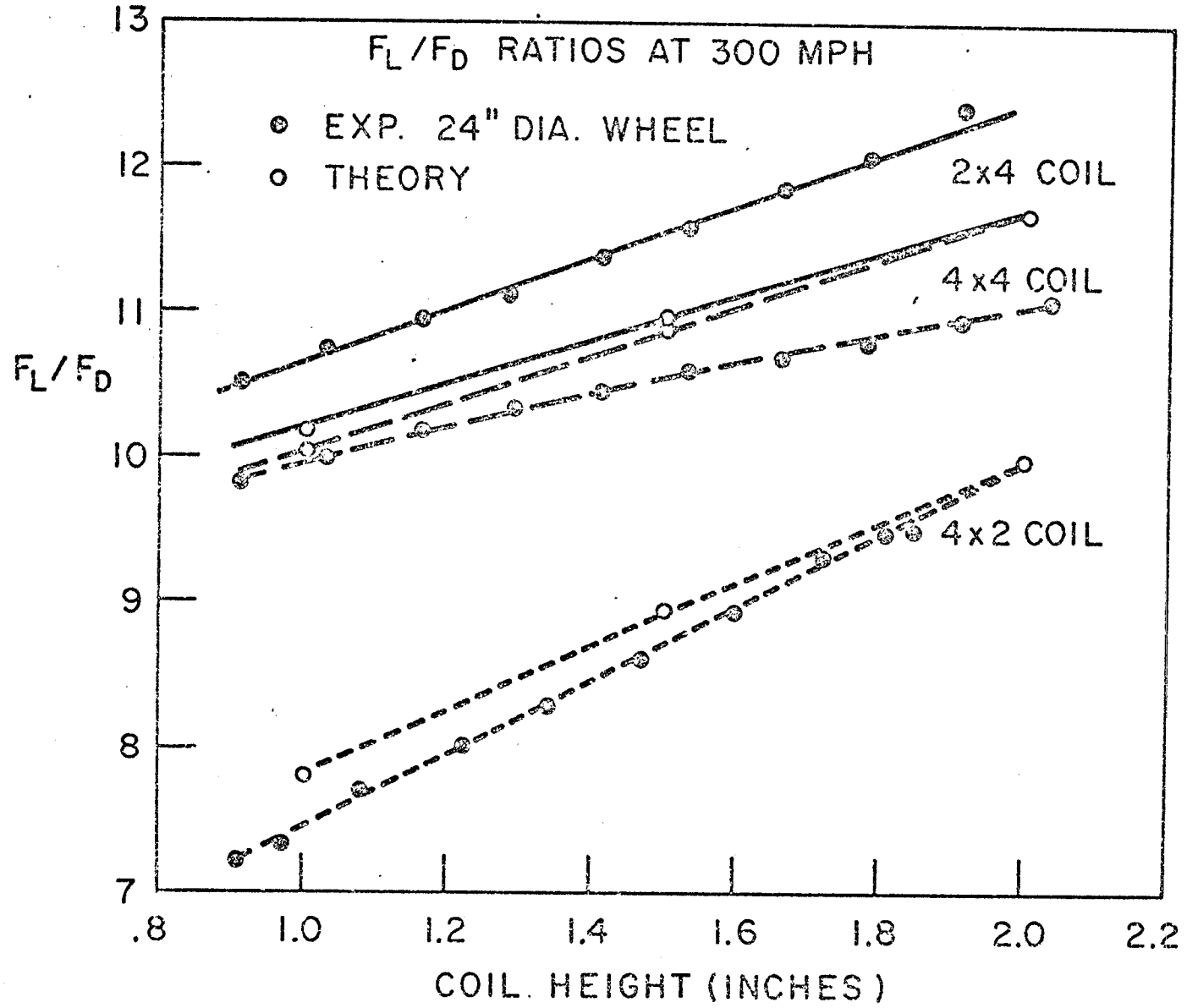
F_L/F_D RATIOS AT 300 MPH
EXP. 24" DIA. WHEEL
THEORY
2x4 COIL
4x4 COIL
4x2 COIL
F_L/F_D
13
12
11
10
9
8
7
.8
1.0
1.2
1.4
1.6
1.8
2.0
2.2
COIL HEIGHT (INCHES)

FIG. 4

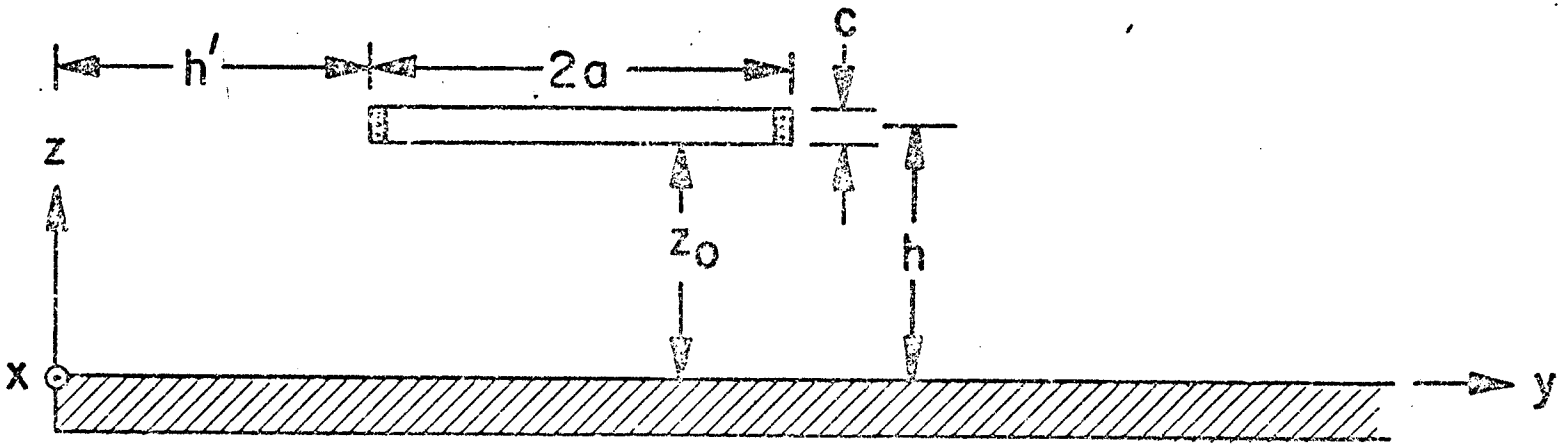

FIG. 5

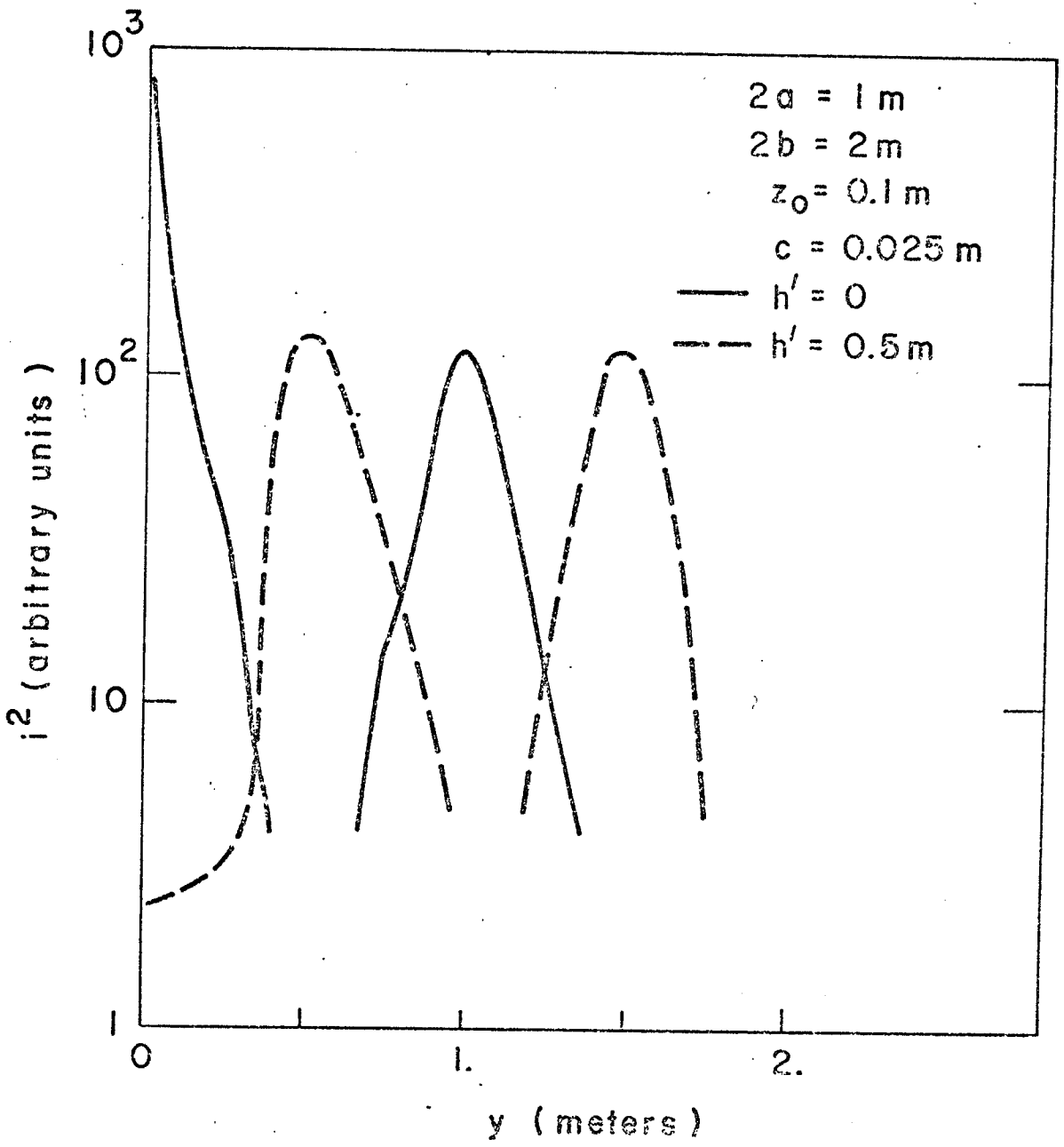
10^3
10^2
10
1
i^2 (arbitrary units)
0
1.
2.
y (meters)
2a = 1 m
2b = 2 m
z_o = 0.1 m
c = 0.025 m
h′ = 0
h′ = 0.5 m

FIG. 6

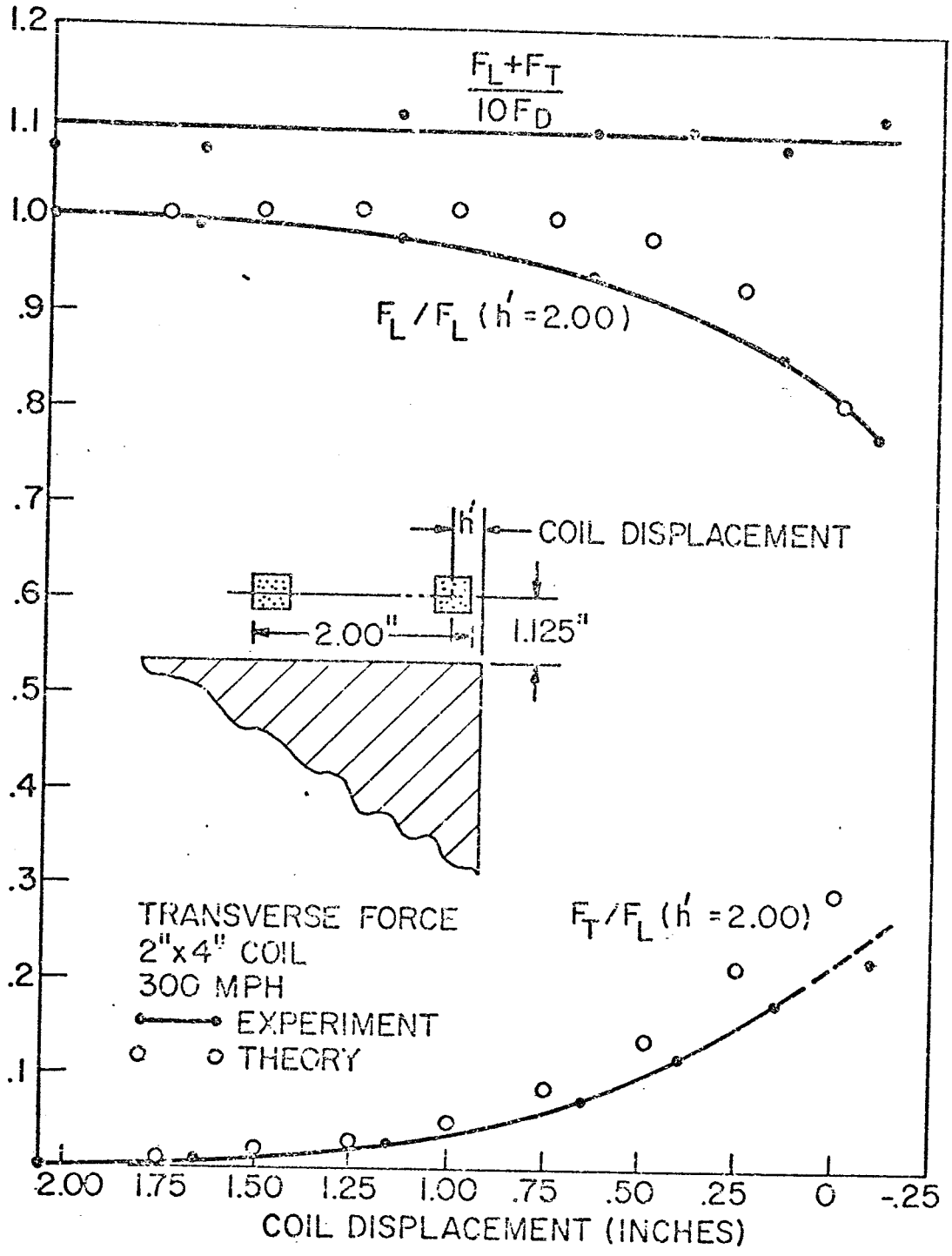
1.2
1.1
1.0
.9
.8
.7
.6
.5
.4
.3
.2
.1
$\frac{F_L+F_T}{10F_D}$
$F_L/F_L\ (h'=2.00)$
h'
COIL DISPLACEMENT
2.00"
1.125"
TRANSVERSE FORCE
2"x4" COIL
300 MPH
EXPERIMENT
THEORY
$F_T/F_L\ (h'=2.00)$
2.00 1.75 1.50 1.25 1.00 .75 .50 .25 0 -.25
COIL DISPLACEMENT (INCHES)

FIG. 7

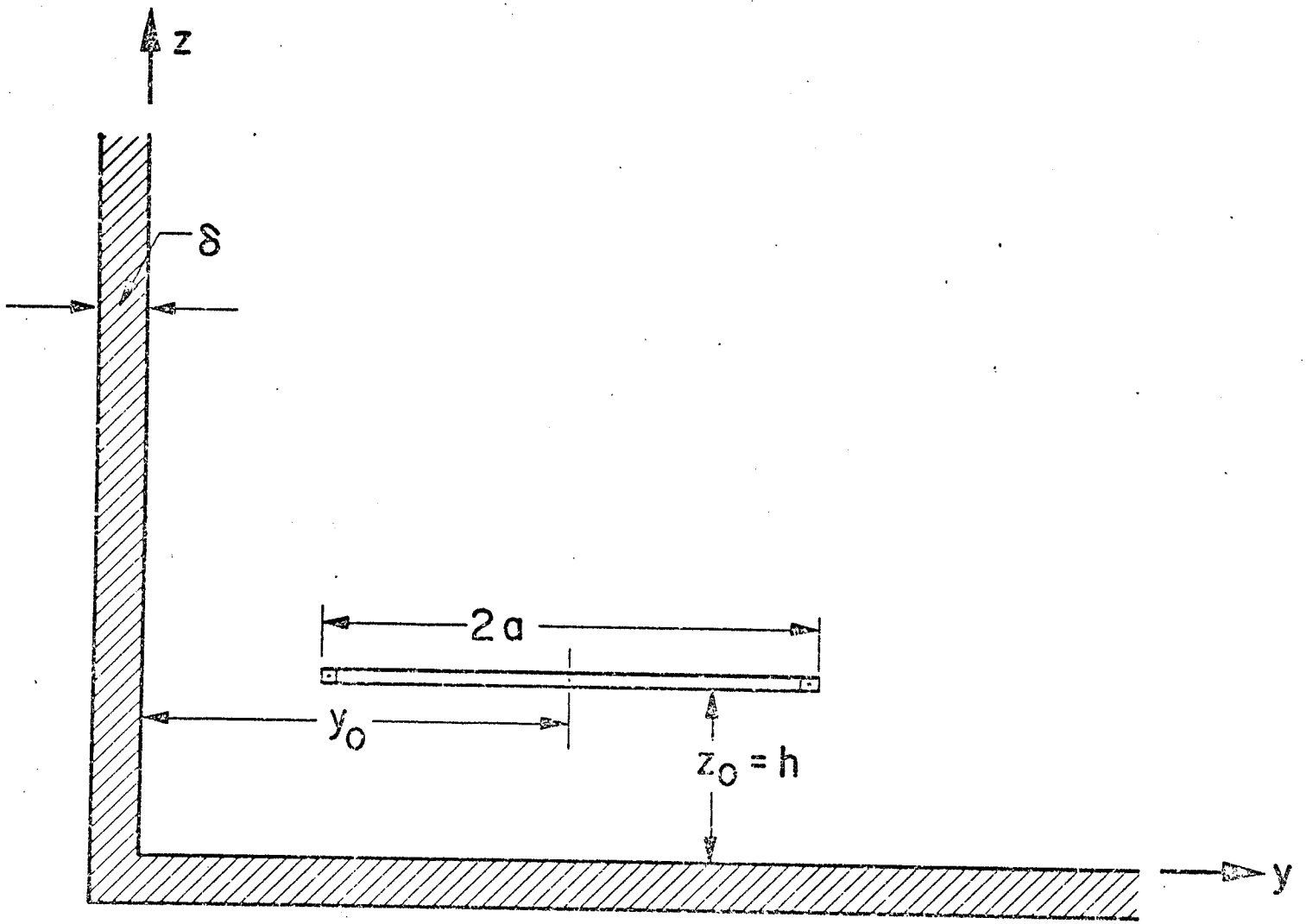

FIG. 8

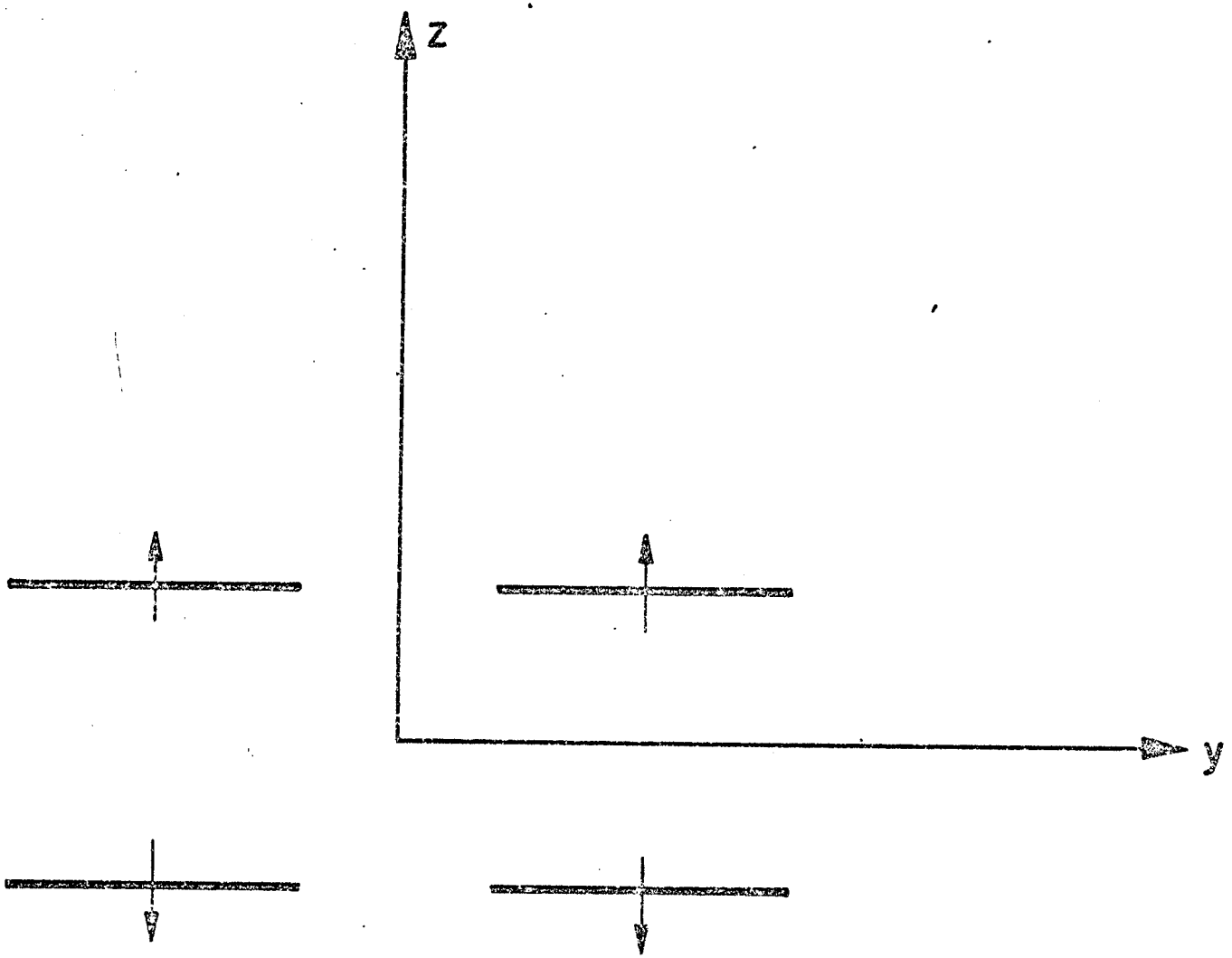

Fig. 9

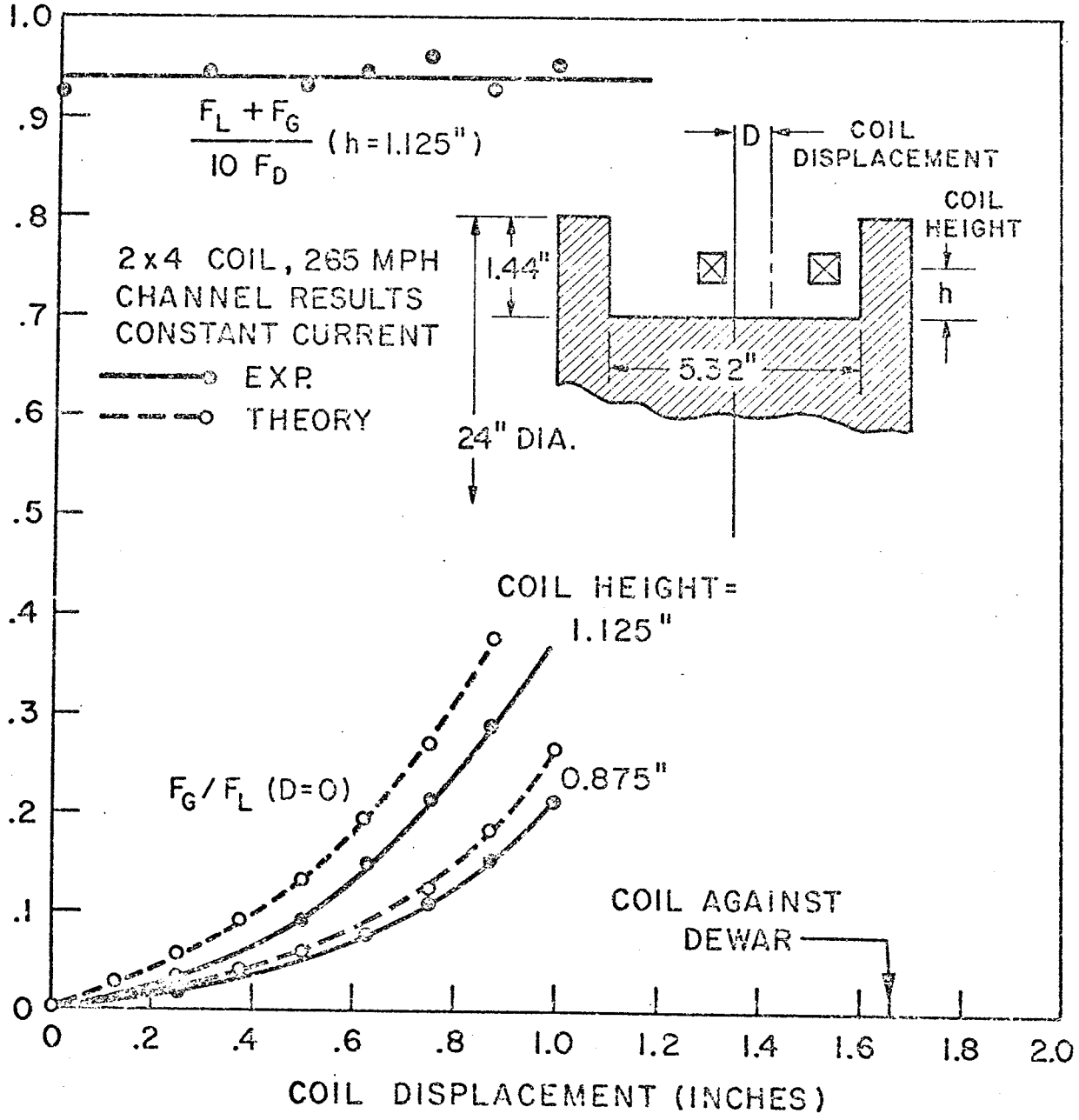
1.0
.9
.8
.7
.6
.5
.4
.3
.2
.1
0
$\frac{F_L + F_G}{10\ F_D}$ (h=1.125")
2x4 COIL, 265 MPH
CHANNEL RESULTS
CONSTANT CURRENT
EXP.
THEORY
D
COIL DISPLACEMENT
COIL HEIGHT
h
1.44"
5.32"
24" DIA.
COIL HEIGHT= 1.125"
0.875"
F_G/F_L (D=0)
COIL AGAINST DEWAR
0
.2
.4
.6
.8
1.0
1.2
1.4
1.6
1.8
2.0
COIL DISPLACEMENT (INCHES)

FIG. 10

DYNAMICS, CONTROL AND RIDE QUALITY OF A MAGNETICALLY LEVITATED HIGH SPEED GROUND VEHICLE

Dennis F. Wilkie
Control Systems Department

March 2, 1972

SCIENTIFIC RESEARCH STAFF

PUBLICATION PREPRINT

Ford

DYNAMICS, CONTROL AND RIDE QUALITY OF A MAGNETICALLY LEVITATED HIGH SPEED GROUND VEHICLE*

Dennis F. Wilkie
Scientific Research Staff, Ford Motor Company, Dearborn, Michigan 48121

ABSTRACT

Magnetic means of suspending vehicles have been proposed for use in high speed ground transportation systems (> 250 mph). However, the motion of such suspension (levitation) systems using magnetic repulsion forces when they are perturbed from equilibrium is oscillatory with a frequency of the order of 1 Hz and a very long damping time. Thus, some means of adding damping to the suspension is required. One means of obtaining the desired damping is by feedback control of the magnet currents. In this paper, the ride characteristics and control current requirements for a magnetically levitated vehicle are determined. The random roadbed roughness is characterized by its power spectral density, and ride quality is analyzed in terms of the power spectral density of the vertical acceleration. Alternative control strategies using feedback proportional to vehicle-track clearance, vertical velocity, and acceleration are considered. It is found that good ride quality can be obtained over a track equivalent to a moderately good highway with a high clearance (> .2m) magnetic suspension. The dynamics of a vehicle in alternative guideways which supply lateral guidance as well as lift forces are analyzed. It is seen that a guideway configuration which provides orthogonal surfaces for guidance and levitation forces leads to inherently more stable vehicle motion and allows the use of simple independent control strategies on all lift and guidance magnets.

---

*Work supported in part by the U.S. Department of Transportation.

I. INTRODUCTION

There is currently considerable interest in the development of a high speed ground transportation (HSGT) system to operate in densely traveled corridors and which can offer an attractive alternative to either conventional aircraft or vertical or short takeoff and landing aircraft (VTOL/STOL) in the range of 200 to 1000 miles. In order for a ground based system to be competitive with aircraft in this range, it is necessary that the vehicles in the HSGT system be capable of cruise speeds from 300 mph to 500 mph. There are a number of reasons why speeds in this range cannot be achieved using conventional steel wheel - steel rail railroad type technology. Some of the problems with conventional rail technology at these speeds are a lack of sufficient friction to propel the vehicle through the wheels, wheel wear, track wear and maintenance, and poor ride quality resulting from the suspension characteristics and track misalignment. Thus, innovative means of suspending and guiding vehicles in such a high speed system must be developed. The alternatives that have been proposed for vehicle support in high speed ground systems are air cushions[1] and magnetic support schemes.[1-7] While there are many schemes for magnetically suspending vehicles using magnetic repulsive forces or attractive forces, permanent magnets, conventional electro-magnets, superconducting magnets, etc., one of the most promising approaches to magnetic levitation supports the vehicle with the repulsive force exerted on magnets traveling over a conducting roadbed by the eddy currents induced in the roadbed. One of the main advantages of such a scheme is that large levitation heights (i.e., magnet to track clearances) of the order of .1m to .3m can easily

be obtained with high field strength magnets, and the ride of the vehicle is then potentially less sensitive to track irregularities than in alternative schemes where the magnet to track clearance is of the order of a few centimeters. Since the construction and maintenance of a very accurate roadbed is quite expensive, and since roadbed construction and operating costs are a substantial percentage of the capital investment and operating costs in such a system, the advantage of tolerating roadbed inaccuracies and changes over time is indeed great.

The characteristics of the motion of a levitated magnet when it is perturbed from steady motion at velocity v and height h above a conducting plane have been investigated by Fink and Hobrecht[8] and by Davis and Wilkie.[9] Davis and Wilkie[9] demonstrated that the force laws obtained by Reitz[5] for steady motion of a magnet over a conducting plane can be used to determine the perturbed motion to a good approximation. They found that the motion resulting from a vertical perturbation is an essentially undamped vertical oscillation with a frequency of the order of 1 Hz, and that an exponentially growing velocity error results from a perturbation in the direction of motion if air drag is not included in the analysis. These motions were found to be essentially decoupled. The small amount of damping of the vertical motion can be either positive or negative (i.e., decaying or growing oscillations) depending on the magnet geometry. However, in either case the transient response to perturbations is unacceptable for use in a passenger carrying vehicle. Thus, the need for a means of feedback control of the motion of levitated magnets to obtain

stability and ride characteristics suitable for carrying passengers at high speeds was indicated.

An initial study of the control currents required to obtain suitable dynamic responses of levitated coils was made.[10] It was found that currents of the order of 5% of the equilibrium current required for levitation are sufficient to produce a well damped response to a vertical perturbation. However, that study did not determine the ride quality obtained with a magnetically levitated vehicle which is continually subjected to the random disturbances caused by guideway irregularities.

In Section II of this paper, the ride characteristics are determined for a magnetically levitated coil with feedback control of the suspension parameters. The coil is assumed to be traveling over a roadbed for which the roughness is specified in terms of the power spectral density of the variation of the height of the track from a nominal reference, and the ride of the vehicle is characterized by the power spectral density of the vertical acceleration. Alternative control strategies using vehicle to track clearance, vertical velocity, and vertical acceleration feedback are considered, and their theoretical or practical rationale are briefly discussed. It is found that a ride comparable to that of a jet aircraft on a calm day can be obtained over a moderately rough track with a high clearance (.3m) magnetic suspension. The advantages of a high clearance suspension system are made clear in this context, and it is found that it is essential that the absolute vertical velocity of the vehicle be used for control as opposed to the relative vertical velocity between the vehicle and the track. Further,

it is found that there is little to be gained in terms of ride quality by using acceleration feedback, and the required control current increases significantly in that case.

All of the dynamics and control studies that have been conducted to date for both magnetic levitation systems[8-10] and tracked air cushion vehicle systems[11-13] have considered only the translational motion in a plane of a point mass under the influence of the lift and drag forces on the magnet. This analysis is probably sufficient for an analysis of ride quality as in Section II of this paper. However, in determining a track (guideway) configuration to provide guidance as well as levitation, it is important to consider the dynamic interactions between the various translational, roll and pitch modes. In Section III, the dynamics of a vehicle for five alternative guideway configurations are discussed and the dynamics of two basic configurations are analyzed in some detail. It is shown that a u-channel or box beam type of guideway results in the greatest decoupling of dynamic modes and thus affords the opportunity of the simplest vehicle control schemes. It is seen that with such a guideway, simple-independent feedback control of individual levitation and guidance magnet currents will achieve good vehicle dynamics with a u-channel or box beam guideway, whereas other guideway configurations would require the implementation of more complex schemes of vehicle guidance and control to achieve acceptable dynamics. Finally, areas where further work is needed with respect to vehicle dynamics and control are discussed.

II. RIDE QUALITY

In this section, the ride quality of a levitated coil (with feedback current control) which is subjected to random track disturbances is discussed. In order to do this, the force laws for such a levitated coil are first reviewed.

A. Equations of Motion

The forces exerted on a coil carrying a current I and in steady motion at velocity v and height h above a thin conducting plate† were determined by Reitz[5] using image techniques. These forces consist of a lift force F_L in the vertical direction and a drag force F_D in a direction tending to stop the coil. The forces were shown to be well approximated by

$$F_L = \eta F_I \tag{1}$$

and

$$F_D = w/v\, F_L \tag{2}$$

where F_I is the ideal lift force on the coil due to an image coil located a distance h below the conducting plane and carrying an equal current I but with the opposite direction as shown in Fig. 1, η is a finite velocity factor which approaches 1 at high velocities, and w is a constant which depends on the parameters of the conducting plane.

---

† The thin plate assumption refers to the fact that eddy currents are assumed to be distributed uniformly throughout its thickness. Depending on coil geometries and speeds, the plate can be as thick as 1.5 inches.

The image force F_I is given by

$$F_I = - I^2 \frac{dM}{d\hat{z}} \tag{3}$$

where M is the mutual inductance between the coil and its image located a distance $\hat{z} = 2z$ below it, and which (for a rectangular coil) is given by

$$M(\hat{z}) = \frac{\mu_o N^2}{2\pi} \left\{ 2a \sinh^{-1}\left(\frac{a}{\hat{z}}\right) - 2a \sinh^{-1}\left(\frac{a}{\sqrt{b^2+\hat{z}^2}}\right) + 2b \sinh^{-1}\left(\frac{b}{\hat{z}}\right) - 2b \sinh^{-1}\left(\frac{b}{\sqrt{a^2+\hat{z}^2}}\right) + 4\sqrt{a^2+b^2+\hat{z}^2} - 4\sqrt{a^2+\hat{z}^2} - 4\sqrt{b^2+\hat{z}^2} + 4\hat{z} \right\} \tag{4}$$

where

N = number of turns in the coil

a = width of coil (normal to x direction)

b = length of coil (in direction of motion)

μ_o = permeability of free space ($4\pi \times 10^{-7}$ wb/Amp m).

The finite velocity factor η is given by

$$\eta = 1 - \frac{1}{(1+v^2/w^2)^n} \tag{5}$$

where n is determined by numerically fitting data calculated for a given coil, and

$$w = 2/\mu_o \sigma \delta \quad , \tag{6}$$

where σ is the conductivity of the conducting plate and δ its thickness. For a 1m × 2m coil levitated at .3m above a 1 cm thick aluminum plate, $n \approx .33$ and $w = 4.5$ m/sec. It has been demonstrated by

Davis and Wilkie[9] that these force laws for steady motion describe the motion of a coil when subjected to perturbations sufficiently well if the steady velocity v in the x direction and height h above the plane are replaced by the instantaneous velocity $\dot{x}(t)$ and the instantaneous height $z(t)$. This is referred to as the instantaneous approximation. As discussed in the introduction, it was shown[9] that coupling between the horizontal and vertical motion of a coil subject to the force laws in (1) and (2) is negligible. The motion resulting from a vertical perturbation is an essentially undamped vertical oscillatory motion for which some means of feedback control must be used. (It should be noted that the force laws resulting from the instantaneous approximation do not reflect as much damping of the system as is actually present. However, this additional damping can be shown to be quite small[9] and is not included here.) Because of the small degree of coupling present between horizontal and vertical modes, the ride quality of a coil subjected to track roughness will be analyzed as simply a vertical translational motion with the velocity in the x direction assumed constant at the value v.

First, the relationship between the perturbed motion of the coil and the track irregularity is derived, assuming that the irregularity is known as a deterministic waveform, $H(t)$. The following variables are defined with reference to Fig. 2.

Define:

$z(t)$ = absolute vertical position of coil center at time t

(absolute denotes with respect to track reference)

$H(t)$ = absolute track height at time t

$e(t) = z(t) - h$ = deviation of absolute position from equilibrium

$c(t) = z(t) - H(t)$ = clearance between coil and track

$\hat{z}(t) = 2c(t)$.

The equation of motion in the z direction is obtained from (1) and (3) to be

$$m\ddot{z}(t) = -I^2 \eta \frac{dM}{d\hat{z}} - mg \qquad (7)$$

where $\ddot{z}(t)$ denotes $d^2z(t)/dt^2$ and $M(\hat{z})$ is given by (4). It is assumed that deviations from equilibrium are relatively small and thus that the linearized form of (7) can be used for analysis. Denoting the equilibrium values of $\hat{z}$ and I as $\hat{z}_e$ and I_e, the linearized form of (7) is

$$m\ddot{z}(t) = -I_e^2 \left.\frac{d^2M}{d\hat{z}^2}\right|_e (\hat{z} - \hat{z}_e) - 2I_e \left.\frac{dM}{d\hat{z}}\right|_e (I - I_e) \quad .^{\dagger} \qquad (8)$$

Assuming $I = i_c + I_e$ where i_c is the control current that will be used for feedback control of the motion ($i_c \ll I_e$) and rewriting (8) in terms of the above defined variables, it follows that

$$\ddot{z}(t) = -\frac{2I_e^2}{m} \left.\frac{d^2M}{d\hat{z}^2}\right|_e (z(t) - H(t) - h) - \frac{2I_e}{m} \left.\frac{dM}{d\hat{z}}\right|_e \cdot i_c \quad . \qquad (9)$$

At this point, it is assumed that the control current i_c is given by

$$i_c = k_1 \dot{z}(t) - k_2(z(t) - h - H(t)) \quad , \qquad (10)$$

that is, currents proportional to absolute vertical velocity and relative position deviation from equilibrium are used for control.

---

† Here, η was assumed to be a constant ≈ 1, which is valid at high speeds.

Other control strategies utilizing relative velocity (between coil and track) as well as acceleration feedback will be discussed. However, the derivation of the relation between track roughness and the ride disturbance with those strategies would proceed essentially the same from this point. It will be seen from later results that the control represented by (10) is probably the best choice when ride quality and control current constraints are considered. Thus, proceeding with the analysis, substituting (10) into (9) and remembering that $\ddot{e}(t) = \ddot{z}(t)$, it follows that

$$\ddot{e}(t) + \beta \dot{e}(t) + \hat{\omega}_o^2 e(t) = \hat{\omega}_o^2 H(t) \tag{11}$$

where

$$\beta \equiv \frac{2k_1 I_e}{m} \left.\frac{dM}{d\hat{z}}\right|_e$$

$$\omega_o^2 \equiv \frac{2I_e^2}{m} \left.\frac{dM}{d\hat{z}}\right|_e$$

and

$$\hat{\omega}_o^2 = \omega_o^2 - \frac{2k_2 I_e}{m} \left.\frac{dM}{d\hat{z}}\right|_e \quad .$$

For either a sinusoidal steady state analysis or a power spectral density (psd) analysis of the vertical response, the Fourier transform of (11) is needed. Thus, denoting

$$E(j\omega) = F[e(t)] = \int_{-\infty}^{\infty} f(t)\, e^{-j\omega t}\, dt \quad , \tag{12}$$

the transform of (11) is found to be

$$E(j\omega) = \frac{\hat{\omega}_o^2 H(j\omega)}{\hat{\omega}_o^2 - \omega^2 + j\omega\beta} \equiv T_e(j\omega) H(j\omega) \quad . \tag{13}$$

Furthermore, it follows that

$$\ddot{E}(j\omega) = F[\ddot{e}(t)] = \frac{-\omega^2 \hat{\omega}_o^2 H(j\omega)}{\hat{\omega}_o^2 - \omega^2 + j\omega\beta} \quad . \tag{14}$$

B. Characterization of Track Irregularities

At this point, it is necessary to discuss how H(t) (or H(jω)), the track disturbance, is to be characterized. There are two approaches that have been taken toward characterizing track disturbances and analyzing ride quality, (i) a deterministic frequency response approach[11,12] and (ii) a power spectral density approach.[13,16,17] In the deterministic approach, H(t) is chosen as a sinusoidal function of the form

$$H(t) = F(\lambda) \sin\left(\frac{2\pi x}{\lambda}\right) = F(\lambda) \sin \frac{2\pi v}{\lambda} t \quad , \tag{15}$$

and $F(\lambda)$ is usually assumed to be linearly proportional to λ. The frequency response of the vertical acceleration, $\ddot{E}(j\omega)$, is then easily obtained from (14) since $H(j\omega) = F\left(\frac{2\pi v}{\omega}\right)$. Apparently, this approach was favored in the past[11] due to the fact that available experimental data relating to human vibration tolerances were expressed in terms of the objectionable amplitude at a discrete sinusoidal frequency. However, it is apparent that track irregularities will not occur as single frequency disturbances. Rather, by their random nature they will generate an essentially continuous frequency spectrum. Furthermore, it is difficult to relate irregularities as given by (15) to specifications regarding track construction and maintenance tolerances and also to experimental track roughness measurements.

The second approach to characterizing ride quality is to specify the power spectral density (psd) of the track roughness and determine the resulting psd of the vertical acceleration of a given vehicle. However, until recently, no specification of ride quality in terms of the vertical acceleration psd was available. In a recent document[14] concerning the Urban Tracked Air Cushion Vehicle, such a psd specification was given, and this psd specification was apparently based on experimental measurements. (This ride appears to be equivalent to the ride of a jet aircraft on a relatively calm day.) Furthermore, experimental measurements of the disturbance psd for various surfaces as highways, airport runways, and railroads are available from various sources.[14] Thus, in this paper the random track disturbances will be characterized by a power spectral density as will the vertical acceleration response to disturbances.

C. Vehicle Responses - Power Spectral Density

If $P_{HH}(\omega)$ is the power spectral density of the random track disturbance $H(t)$, then it follows from (13) [see e.g., ref. 15] that the vertical acceleration psd, $P_{\ddot{e}\ddot{e}}(\omega)$, is given by

$$P_{\ddot{e}\ddot{e}}(\omega) = T_{\ddot{e}}(j\omega)\, T_{\ddot{e}}(-j\omega)\, P_{HH}(\omega) \quad , \tag{15}$$

and thus

$$P_{\ddot{e}\ddot{e}}(\omega) = \frac{\omega^4 \hat{\omega}_o^4 P_{HH}(\omega)}{(\hat{\omega}_o^2 - \omega^2)^2 + \omega^2 \beta^2} \quad . \tag{16}$$

From this and the relationships between $e(t)$, $z(t)$, $\Delta c(t)$ and i_c, it can be shown that the power spectral density of the change in clearance $P_{\Delta c \Delta c}(\omega)$, and of the control current, $P_{i_c i_c}(\omega)$, are given by

$$P_{\Delta c \Delta c}(\omega) = \left[\frac{\omega^4 + \omega^2 \beta^2}{(\hat{\omega}_o^2 - \omega^2)^2 + \omega^2 \beta^2} \right] P_{HH}(\omega) \tag{17}$$

and

$$P_{i_c i_c}(\omega) = \omega^2 \left[\frac{k_2^2 \omega^2 + (k_2 \beta + k_1 \hat{\omega}_o^2)^2}{(\hat{\omega}_o^2 - \omega^2)^2 + \omega^2 \beta^2} \right] P_{HH}(\omega) \quad . \tag{18}$$

Examples of power spectral density measurements for various surfaces are given in Fig. 3 (from reference 13). The abscissa for this plot is the wavelength $\lambda = 2\pi/\Omega$, Ω = wavenumber. Ω is related to ω by $\omega = v\Omega$. For purposes of analysis, $P_{HH}(\Omega)$ can be represented quite well as

$$P_{HH}(\Omega) = A/\Omega^2 \quad . \tag{19}$$

The plot of $P_{HH}(\Omega)$ for $A = 5 \times 10^{-6}$ ft. is shown in Fig. 3 and corresponds approximately to the measurements for a good runway. Measurements and analyses given in other references[16,17] have also indicated that taking $P_{HH}(\Omega) \alpha \Omega^{-2}$ is a good assumption, and ref. 17 verifies that $A = 5 \times 10^{-6}$ ft. would correspond to a very good runway--in fact to new construction.

The mean squared track height deviation $\overline{H^2}$ is related to the power spectral density by[17]

$$\overline{H^2} = \int_{\Omega_1}^{\infty} P_{HH}(\Omega) \, d\Omega \tag{20}$$

where Ω_1 corresponds to the longest wavelength over which the track mean squared deviation is specified and measured, say L. (Note that the factor of $\frac{1}{\pi}$ which often appears in (20) has essentially been absorbed in $P_{HH}(\Omega)$.) Then $\Omega_1 = 2\pi/L$, and for the power spectral density of (19), it follows that

$$\overline{H^2} = \frac{AL}{2\pi} \quad . \tag{21}$$

Thus, the parameter A can be related to the mean squared deviation of a roadbed specified or measured for a given distance. For example, if $\sqrt{\overline{H^2}}$ is 5 mm in 100 m, then $A = 1.57 \times 10^{-6}$ m $= 5.16 \times 10^{-6}$ ft. This corresponds, as mentioned earlier, to a newly constructed airport runway. Obviously, it represents a very smooth roadbed.

Furthermore, the psd $P_{HH}(\omega)$ corresponding to (19) can be found to be

$$P_{HH}(\omega) = \frac{Av}{\omega^2} \quad ,$$

since it is necessary that

$$P_{HH}(\Omega)\, d\Omega = P_{HH}(\omega)\, d\omega \quad .$$

Thus, $P_{HH}(\omega)$ will be assumed to have the form of (19), and the corresponding power spectral densities for $P_{\ddot{e}\ddot{e}}(\omega)$, $P_{\Delta c \Delta c}(\omega)$, and $P_{i_c i_c}(\omega)$ are

$$P_{\ddot{e}\ddot{e}}(\omega) = \frac{Av\,\omega^2 \hat{\omega}_o^4}{(\hat{\omega}_o^2 - \omega^2)^2 + \omega^2 \beta^2} \quad , \tag{22}$$

$$P_{\Delta c \Delta c}(\omega) = \frac{(\omega^2 + \beta^2)\, Av}{(\hat{\omega}_o^2 - \omega^2)^2 + \omega^2 \beta^2} \quad , \tag{23}$$

and

$$P_{i_c i_c}(\omega) = Av \frac{\left[k_2^2 \omega^2 + (k_2 \beta + k_1 \hat{\omega}_o^2)^2 \right]}{(\hat{\omega}_o^2 - \omega^2)^2 + \omega^2 \beta^2} \quad . \tag{24}$$

The mean-squared values of the vertical acceleration, change in clearance, and control current can be determined from the power spectral

densities since

$$\overline{\ddot{e}^2} = \int_0^\infty P_{\ddot{e}\,\ddot{e}}(\omega)\, d\omega \quad . \tag{25}$$

Substituting (22) - (24) into (25) and either performing the integration or using tables of such integrals[14] results in the following mean squared values,

$$\overline{\ddot{e}^2} = \frac{\pi A v \hat{\omega}_o^4}{2\beta} \quad , \tag{26a}$$

$$\overline{\Delta c^2} = \frac{\pi A v(\hat{\omega}_o^2 + \beta^2)}{2\beta \hat{\omega}_o^2} \quad , \tag{26b}$$

and

$$\overline{i_c^2} = \frac{\pi A v\left[k_2^2 \hat{\omega}_o^2 + (k_2\beta + k_1 \hat{\omega}_o^2)^2\right]}{2\beta \hat{\omega}_o^2} \quad . \tag{26c}$$

It is important to note that both the power spectral densities and mean-squared values of the variables $\ddot{e}$, Δc, and i_c depend linearly on A, and thus the results for tracks of varying roughness are obtained by multiplying those obtained for a given value of A by the appropriate factor. The mean-squared values of $\ddot{e}$, Δc, and i_c also depend linearly on the velocity v for the assumed track irregularity psd.

Relationships for the power spectral densities and mean-square values of $\ddot{e}$, Δc, and i_c for the cases of relative velocity/relative position feedback as well as relative position/absolute velocity/absolute acceleration feedback are given in Appendix I. It should be noted that the expressions (22) - (24) and (26a) - (26c) depend only on the damping β, and natural frequency $\hat{\omega}_o$ and not on the type of suspension used to obtain those characteristics. Thus, ride

quality per se is independent of the type of suspension used (e.g., air cushion, magnetic levitation, etc.). However, the change in clearance $\overline{\Delta c^2}$ associated with a given choice of β and $\hat{\omega}_o$ places a constraint on the clearance that a system must maintain, and this is an important factor in determining whether a given suspension can be used. $\overline{i_c^2}$ determines the control current required for a given vertical acceleration psd when using a magnetic levitation scheme.

Consider now the choice of control strategy for obtaining an acceptable ride with a levitated vehicle. It is apparent that absolute vertical velocity would be difficult to measure directly. However, various practical schemes for measuring the relative distance between the vehicle and the track can be proposed. Thus, one control approach is to design a compensation circuit such that any given damping can be obtained using only relative position feedback. This corresponds to pole placement[18] in modern control theory, or the design of a lead/lag network using classical techniques.[19] Assuming one of these methods is used to obtain relative position/relative velocity feedback control, the vertical acceleration power spectral densities shown in Fig. 4 are obtained. These curves are obtained using $A = 5 \times 10^{-6}$ ft., $v = 300$ mph, and the expressions in Appendix I. It is apparent that an acceptable ride quality cannot be obtained by varying the damping $\delta = \beta/2\hat{\omega}_o$. As the damping is lowered, the high frequency response improves but the low frequency peak eventually shifts above the specification curve. It is easy to show analytically that the psd curves approach a constant at high frequencies which depends only on the damping, and thus shifting

the natural frequency (by relative position feedback) cannot help to achieve ride quality in the critical region above 6 Hz. Furthermore, it can be shown that the control current required with this control scheme is infinite, and thus any practical attempt to implement the scheme would require a low pass filter to limit the control current to frequencies below about 50 Hz. It appears that an acceptable ride quality cannot be obtained with this relatively good track using relative position/relative velocity feedback control because the vehicle must use a smoother reference at high frequencies to obtain damping. This essentially implies that some means of sensing absolute vertical velocity must be incorporated into the control system. One means of doing this indirectly would be to mount accelerometers on the vehicle and to obtain absolute velocity by integrating the accelerometer output signals. It should be noted at this point that Hullender et al.[13] stated the ride quality control problem for a tracked air cushion vehicle (TACV) as an optimal control problem in which the suspension characteristics were chosen to minimize a linear sum of the mean squared vertical acceleration and the mean squared change in clearance. Using Weiner-Hopf theory and assuming the power spectral density in (19), they obtained an optimal suspension transfer function. This suspension is shown in Appendix II to be equivalent to that obtained using absolute velocity and relative position feedback.

Using absolute velocity and relative position feedback control, power spectral densities as shown in Figs. 5 and 6 are obtained. Figure 5 is for the case of absolute velocity feedback alone, while relative

position feedback is used in addition to absolute velocity feedback to obtain the results in Fig. 6. The natural frequency in Fig. 5 of 1.175 Hz corresponds to that of a 1m × 2m coil at .3m height, and the position feedback is used to shift the natural frequency to .6 Hz in Fig. 6. The rms values of acceleration ($\ddot{z}$) and control current (i_c) and the peak value† of the change in clearance (Δc) associated with the power spectra of Figs. 5 and 6 are given in Tables 1 and 2 respectively.

TABLE 1. Ride Characteristics for Roadbed with A = 5×10^{-6} feet

δ	$\ddot{z}_{rms}$	Δc_{peak}†	$i_{c_{rms}}$ (% of I_e)
.707	.031 g	.535 in.	2.13%
1.24	.022 g	.644 in.	3.02%

(ABSOLUTE VELOCITY FEEDBACK)

TABLE 2. Ride Characteristics for Roadbed with A = 5×10^{-6} feet

δ	$\ddot{z}_{rms}$	Δc_{peak}†	$i_{c_{rms}}$
.443	.014 g	.720 in.	3.14%
.707	.011 g	.748 in.	3.44%
2.68	.005 g	1.20 in.	5.96%

(ABSOLUTE VELOCITY/RELATIVE POSITION FEEDBACK)

It is seen from Fig. 5 that an acceptable ride can be achieved over a track with roughness parameter A = 5×10^{-6} ft. with velocity feedback alone. As this feedback is increased (δ increasing) it is seen in Fig. 5 that the peak of the psd curve is lowered but the high frequency falloff of the psd curve is quite insensitive above 6 Hz to

†Note that this value is $\sqrt{2}\ \Delta c_{rms}$ which is not exactly a peak value for the change in clearance. Essentially it represents the two sigma level for Δc.

increased damping. Since the region around 6 Hz is the critical region in meeting the ride quality specification with velocity feedback only, it is apparent that increasing the damping does not allow the vehicle to ride over a rougher track. (Recall from (26a) that the vertical acceleration psd is directly proportional to A.) However, it is seen from Fig. 6 that the addition of position feedback which shifts the coil natural frequency to a lower value provides the potential for obtaining an acceptable ride over a much rougher track with a high clearance system. With $\delta = 1.11$ and $f_o = .6$ Hz (a curve not shown in Fig. 6) acceptable ride quality can be obtained over a track about 16 times rougher ($A = 80 \times 10^{-6}$ ft.) with corresponding rms values of $\ddot{z} = .036$ g, $i_{c_{rms}} = 16\%$ and $\Delta c_{peak} = 3.4$ in. Such a track roughness would correspond to a moderate to rough highway. The advantage of a high clearance system is apparent from the required Δc. While a levitation scheme using ferromagnetic forces of attraction and having a nominal magnet-track clearance of .6 in. could be used to achieve the ride corresponding to the $\delta = .707$ curve of Fig. 5, it could not achieve an acceptable ride over a rougher track due to the clearance problem. However, maintaining a track to the specification that $A = 5 \times 10^{-6}$ ft. is probably not reasonable.

There are at least two reasons to investigate the possible advantage to be gained by using acceleration feedback in addition to position and velocity feedback. First, from the point of view of theory, the control problem could be cast in the form of an optimal state regulator control problem in which the feedback is chosen to

minimize the integral of squared terms proportional to vertical acceleration, vertical velocity, and vertical position error with a constraint on control energy. Then the optimal feedback controller would include a term proportional to vertical acceleration as well as vertical position and velocity. Second, from a practical point of view, we have proposed using accelerometers to generate a signal which can be integrated to obtain absolute velocity. Thus, since a signal proportional to vertical acceleration will be readily available, we should consider the potential advantages of using it.

Since acceptable ride quality can be obtained over fairly rough tracks using position and velocity feedback, a potential advantage of using acceleration feedback will exist only if comparable acceleration psd's can be obtained with lower control currents. In Fig. 7, typical acceleration psd's are shown for various degrees of acceleration feedback. (Recall that the power spectral densities for this case are given in Appendix I.) The velocity feedback is held constant for the curves at that needed to achieve $\delta = .707$ with acceleration feedback zero, position feedback is zero, and k_3/k_1 is the ratio of acceleration feedback gain to velocity feedback gain. (Note that the ratio k_3/k_1 has units of sec. but is multiplied by β with units sec.^{-1} in the psd equations of Appendix II.) It is seen that the high frequency falloff of the psd plots is the aspect most sensitive to increasing amounts of acceleration feedback. Thus, the peak of the curves in the range of .5 Hz to 1 Hz becomes the limiting factor on how rough a track can be tolerated for a given set of parameters. The values of $\ddot{z}_{rms}$, $i_{c_{rms}}$ and Δc peak for these curves are given in Table 3.

TABLE 3

k_3/k_1	(g's) $\ddot{z}_{rms}$	(in.) Δc_{peak}	(% of I_e) $i_{c_{rms}}$
.1	.031 g	.621	3.51%
.5	.031 g	.885	9.71%
2.0	.031 g	1.51	33.8%

(1m × 2m coil at .3m, A = 5×10^{-6} ft.)

With k_3/k_1 = .5, a track about 2.5 times rougher (A = 12.5×10^{-6} ft.) could be tolerated, but the corresponding control current would be about 15.4% of I_e. As was pointed out above, a track almost 16 times rougher could be tolerated with this same percentage of control current using only relative position/absolute velocity feedback.

Similar curves to those in Fig. 7, but with position feedback added, are shown in Fig. 8, and the corresponding values of $\ddot{z}_{rms}$, $i_{c_{rms}}$, and Δc peak are given in Table 4.

TABLE 4

k_3/k_1	(g's) $\ddot{z}_{rms}$	(in.) Δc_{peak}	(% of I_e) $i_{c_{rms}}$
.1	.011 g	.812	4.22%
.5	.011 g	1.03	6.6%
2.0	.011 g	1.59	12.9%

Thus, while an 8 times rougher track could be tolerated with k_3/k_1 = .5, the control current required would be 18% of I_e.

An extensive parametric study in which the feedback control terms for acceleration, velocity, and relative position were varied indicates that good ride quality over a given track roughness can always

be achieved with absolute velocity/relative position feedback with lower control currents than when acceleration feedback is added.

In summary, the best feedback control strategy to obtain acceptable ride quality with a magnetically levitated vehicle over a track with random roughness characteristics appears to be a linear combination of the absolute vertical velocity of the vehicle with the relative vehicle to track clearance. If relative instead of absolute velocity is used, the ride quality is not acceptable. If a term proportional to vertical acceleration is added, the control current required to achieve acceptable ride quality over a track of given roughness is greater than that required with absolute velocity/relative position control. It was found that an acceptable ride can be obtained over a track with roughness about equivalent to a moderate highway ($A = 80 \times 10^{-6}$ ft.) when a high clearance suspension system is used. The control current in that case would be 16% of the equilibrium current and the peak value of the dynamic stroke required would be 3.4 inches. However, a suspension system which is limited to a clearance of less than an inch is limited to a smooth track and/or a secondary suspension.

Further reductions in control current may be achievable by using passive coils tuned to the natural frequency and placed below the levitation coils. Finally, if the levitation magnets used in such a system as considered here are superconducting magnets, alternate means of implementing the feedback control other than by directly controlling the levitation magnet currents may be required to avoid excessive heat

losses due to alternating currents, current leads, etc. However, the fundamental dynamics will be the same with such a control strategy, and a well designed system should probably not require control currents to be excessively larger than those calculated here.

III. GUIDEWAY DYNAMICS

The discussion of dynamics and ride quality thus far has only been concerned with the motion of a magnetically levitated vehicle in a vertical plane. However, it is apparent that some means of lateral guidance will be required for a levitated vehicle, and that this guidance should be achieved by non-contact means just as in the case of support. One obvious means of obtaining this lateral guidance is to use magnets working against vertical conducting surfaces to obtain lateral forces. Alternately, a guideway configuration could be chosen such that both levitation and lateral guidance forces are inherently present. Several guideway configurations that might be considered are shown in Fig. 9. A vehicle would ride "in" guideways (a) and (d) but "over" guideways (b), (c) and (e). The fundamental difference between the various configurations is that separate magnets are used to obtain guidance using surfaces orthogonal to the roadbed in the u-channel, box-beam and inverted T, whereas both lift and lateral guidance forces are obtained with each magnet in the vee and the inverted vee guideways. It will be seen in the following analyses that the mode coupling inherent in the vee and inverted vee is undesirable, and a vehicle using this support-guidance scheme would be more difficult to control. (This is inherently true of any guideway design chosen to obtain both lift and guidance forces with the same magnets.)

The inherent dynamic characteristics of guideway configurations (a) - (c) will essentially be the same. That is, mode-coupling should be the same, similar control strategies would be used, etc. The factors influencing a choice between these guideways would be construction costs, ease of maintenance, lateral forces that can be sustained, etc. The same remarks apply to the similarity of guideways (d) and (e). Thus, since the present stage of investigation is concerned only with the fundamental dynamic characteristics of a magnetically levitated vehicle and with an investigation of control requirements, the dynamics of a vehicle in a u-channel guideway and over an inverted vee guideway will be studied as representative of this set of five guideway proposals. It is evident that other guideway configurations would have characteristics similar to one of these configurations also. For example, a half-cylindrical trough would have characteristics similar to the vee guideway.

A. U-Channel Guideway

A representative vehicle in a u-channel guideway with four levitation magnets and four guidance magnets is shown in Fig. 10, and a set of coordinate axes is shown with origin at the vehicle center of gravity. In general, an analysis of the motion of such a levitated vehicle would require that inertial and body axes be defined and that Euler angles be used to relate rotations about the body axes to motion in the inertial coordinate system. This leads to a set of 12 simultaneous, non-linear, first-order differential equations which must be solved numerically for given sets of parameters and initial conditions. However, it is clear from the results of Section II that feedback control

of the vehicle dynamics will be required to obtain acceptable ride quality, and thus that excursions of the vehicle from equilibrium due to perturbations will be small. For relatively small excursions from equilibrium, Euler angles are not required and the motion is described well to a first order approximation as the sum of translations of the center of gravity and rotations about a fixed set of axes with origin at the center of gravity. While this simplifies the equations of motion, an analytical study of the dynamic characteristics would still be difficult. Thus, because of the first order analysis being made and because of the essential decoupling of modes noted previously for a magnet over a plane, effects of coupling and rotation which are obviously small will be neglected.

Consider then the u-channel guideway with coordinate axes as shown in Fig. 10. It follows from the above assumptions that translations and rotations in the xy, yz, and xz planes are decoupled and can be analyzed independently. The motion in the xz plane is analyzed here, but only the results are discussed for motion in the other planes. In Fig. 11, a vehicle is shown with the forces acting on it for a general displacement. Define x_c and z_c as the xz plane coordinates of the center of mass and h as the equilibrium magnet to track clearance. Aerodynamic drag forces are not included in this analysis since the shape of the vehicle strongly affects the nature of these forces in a complex manner and because the fundamental suspension dynamics are being studied. However, these forces will be very important in the final design of any vehicle. The equations of motion for the vehicle are

$$m\ddot{x}_c = F_P(\dot{x}_c) - F_{D1}(\dot{x}_c,\theta,z_c) - F_{D2}(\dot{x}_c,\theta,z_c) \tag{27a}$$

$$m\ddot{z}_c = F_{L1}(\dot{x}_c,\theta,z_c) + F_{L2}(\dot{x}_c,\theta,z_c) - mg \tag{27b}$$

$$\begin{aligned} I\ddot{\theta} = {} & F_{L2}\cdot(B\cos\theta + C\sin\theta) - F_{L1}(B\cos\theta - C\sin\theta) \\ & + F_{D1}\cdot(C\cos\theta + B\sin\theta) + F_{D2}\cdot(C\cos\theta - B\sin\theta) \\ & - F_P\cdot(C\cos\theta) \quad , \end{aligned} \tag{27c}$$

where

m = vehicle mass

I = moment of Inertia about y axis

B, C = dimensions defined in Fig. 11

and $F_L(\dot{x}_c,\theta,z_c)$ and $F_D(\dot{x}_c,\theta,z_c)$ are the lift and drag forces on the magnets as a function of their height and velocity. (The effects on lift and drag forces of magnet rotation can be neglected.) These would be obtained from (1) - (6) for rectangular coil magnets. The propulsive force $F_P(\dot{x}_c)$ is assumed to produce constant propulsive power. The equilibrium point for Eqs. (27) is

$$\begin{aligned} \dot{x}_c &= V \quad , \quad x_c = vt \\ z_c &= 0 \\ \theta &= 0 \quad . \end{aligned} \tag{28}$$

In order to have the equilibrium point at the origin and to simplify the notation, let

$$\begin{aligned} \dot{\xi}_1(t) &= \dot{x}_c(t) - v \\ \xi_2(t) &= z_c(t) \\ \xi_3(t) &= \theta(t) \quad . \end{aligned} \tag{29}$$

With this substitution, the linearized forms of Eqs. (27) are

$$\underset{\sim}{\ddot{\xi}} = \begin{bmatrix} \ddot{\xi}_1 \\ \ddot{\xi}_2 \\ \ddot{\xi}_3 \end{bmatrix} = \begin{bmatrix} \frac{-2w}{m} F_L^{\,v} & \frac{-2w}{mv} F_L^{\,h} & 0 \\ \frac{2}{m} F_L^{\,v} & \frac{2}{m} F_L^{\,h} & 0 \\ \frac{2cw}{Iv} F_L^{\,v} & \frac{2cw}{Iv} F_L^{\,h} & \frac{2B^2}{I} F_L^{\,h} + \frac{mgc}{I} \end{bmatrix} \begin{bmatrix} \dot{\xi}_1 \\ \xi_2 \\ \xi_3 \end{bmatrix}, \quad (30)$$

where $F_L^{\,v} \equiv \frac{\partial F_L}{\partial v}$ and $F_L^{\,h} \equiv \frac{\partial F_L}{\partial h}$.

These equations can be written in the simplified matrix form

$$\underline{\ddot{\xi}} = A \begin{bmatrix} \dot{\xi}_1 \\ \xi_2 \\ \xi_3 \end{bmatrix} = [a_{ij}] \begin{bmatrix} \dot{\xi}_1 \\ \xi_2 \\ \xi_3 \end{bmatrix} \quad (31)$$

where the elements a_{ij} of A are suitably defined. It should be noted that the equilibrium is independent of the origin for $x_c(t)$, and that is why the right hand sides of (30) and (31) are written in terms of $\dot{\xi}_1(t)$ rather than $\xi_1(t)$.

Taking the Laplace Transform of (31) and assuming all initial conditions are zero except $\dot{\xi}_1(0)$, $\xi_2(0)$, and $\xi_3(0)$, it follows from (31) that

$$\begin{bmatrix} s^2 - a_{11}s & -a_{12} & 0 \\ -a_{21}s & s^2 - a_{22} & 0 \\ -a_{31}s & -a_{32} & s^2 - a_{33} \end{bmatrix} \underline{\xi}(s) = \begin{bmatrix} \dot{\xi}_1(0) \\ s\xi_2(0) \\ s\xi_3(0) \end{bmatrix} \quad (32)$$

or

$$F(S)\,\underline{\xi}(S) = \begin{bmatrix} \dot{\xi}_1(0) \\ S\xi_2(0) \\ S\xi_3(0) \end{bmatrix} \quad . \tag{33}$$

Inverting F(S) in (33) yields the responses to initial perturbations as

$$\xi_1(S) = \frac{(S^2 - a_{22})\,\dot{\xi}_1(0)}{S^2(S^2 - a_{11}S - a_{22})} + \frac{a_{12}\,\xi_2(0)}{S(S^2 - a_{11}S - a_{22})} \quad , \tag{34a}$$

$$\xi_2(S) = \frac{a_{21}\,\dot{\xi}_1(0)}{S(S^2 - a_{11}S - a_{22})} + \frac{(S - a_{11})\,\xi_2(0)}{S^2 - a_{11}S - a_{22}} \quad , \tag{34b}$$

$$\xi_3(S) = \frac{a_{31}S\,\dot{\xi}_1(0)}{(S^2 - a_{33})(S^2 - a_{11}S - a_{22})} + \frac{a_{32}S\,\xi_2(0)}{(S^2 - a_{33})(S^2 - a_{11}S - a_{22})}$$

$$+ \frac{\xi_3(0)}{S^2 - a_{33}} \quad . \tag{34c}$$

These responses are characterized by the roots of the equations

$$S^2 - a_{33} = 0 \tag{35a}$$

$$S^2 - a_{11}S - a_{22} = 0 \quad , \tag{35b}$$

which are

$$S_{1,2} = \pm \sqrt{a_{33}} \quad , \quad S_{3,4} = \frac{a_{11}}{2} \pm \sqrt{\frac{a_{11}^2}{4} + a_{22}} \quad . \tag{36}$$

Assuming typical vehicle and magnet parameters, e.g., 1m × 2m coils levitated at h = .3m, and B >> C, then a_{11}, a_{22} and a_{33} can be calculated. For these values $a_{22} \gg a_{11}^2/4$, $a_{33} \approx 12\, a_{22}$, and a_{11}, a_{22}, and a_{33} are all negative. The numerical values for the roots are

$$S_{1,2} = \pm j\ 25.5, \quad S_{3,4} = -4.31 \times 10^{-5} \pm j\ 7.38 \quad (\text{sec}^{-1}) \quad (37)$$

which represent undamped and slightly damped oscillatory modes. Note that these numbers depend only on the form of the magnetic forces and not on the vehicle geometry or mass. The motion resulting from initial perturbations as implied by (34) and (37) can then be summarized as follows:

I. A pure initial rotation ($\xi_3(0) > 0$) will produce an undamped oscillatory rotation about the center of mass with no height or velocity perturbations. The frequency of oscillation is f = 4.06 Hz if a uniformly distributed vehicle mass is assumed.

II. An initial height or velocity error ($\dot{\xi}_1(0) > 0$ or $\xi_2(0) > 0$) will couple to an undamped rotation about the center of mass.

III. The oscillatory modes in the height and velocity are slightly damped, but the time constant is very long--388 min. The frequency is 1.175 Hz.

Recall that there is some damping of the oscillation about the center of mass and of the height and velocity oscillatory motion which does not appear in this analysis due to the instantaneous approximation and the linearization. However, this will add an insufficient amount of damping to the motion, and feedback control will be required.

It is important to determine whether a simple feedback control scheme which is independent for each magnet will achieve sufficient damping of the height, velocity and rotational motion. If this will not work, an interacting control scheme which requires some means of measuring rotations about the center of mass will be required, but this added complexity should be avoided if possible.

Assume that an independent control is implemented for each magnet. Then the vertical velocity, v_z, of a magnet as shown in Fig. 12 will be used for feedback control. It is apparent that this will add damping to the oscillatory translational motion in the vertical direction. Consider the rotational contribution to v_z. First,

$$\varphi = \varphi_o + \theta \tag{38}$$

where φ_o is the value of φ when the vehicle is level and θ is the rotation angle as in Fig. 11. Then the rotational velocity v_T is

$$v_T = - a \omega = - A \dot{\theta} \tag{39}$$

and thus the rotational component of v_z is

$$v_z^r = - A \dot{\theta} \cos\varphi = - A \dot{\theta} (\cos\varphi_o \cos\theta - \sin\varphi_o \sin\theta) \quad . \tag{40}$$

The total vertical velocity is then

$$v_z = \dot{z}_c - A \dot{\theta} (\cos\varphi_o \cos\theta - \sin\varphi_o \sin\theta) \quad , \tag{41}$$

which for small values of θ is approximately

$$v_z = \dot{z}_c - A \dot{\theta} \cos\varphi_o \quad . \tag{42}$$

The control currents in the magnets are then assumed to be proportional to the total vertical velocity

$$i_{c_1} = -kv_z^{\,1} = -k(\dot{z} - A\dot{\theta}\cos\varphi_o) \tag{43a}$$

and

$$i_{c_2} = -kv_z^{\,2} = -k(\dot{z} + A\dot{\theta}\cos\varphi_o) \quad . \tag{43b}$$

There are various alternative ways of obtaining the vertical velocities, $v_z^{\,i}$, for the individual magnets which will not be discussed here. Using these control currents, the matrix F(S) of (33) now becomes

$$F(S) = \begin{bmatrix} S^2 - a_{11}S & -a_{12} - \frac{2w}{mv}F_L^{\,I}kS & 0 \\ -a_{21}S & S^2 + \frac{2}{m}kF_L^{\,I}S - a_{22} & 0 \\ -a_{31} & +\frac{2w}{mv}kF_L^{\,I}S - a_{32} & S^2 + \frac{2k}{m}F_L^{\,I}A\cos\varphi_o S - a_{33} \end{bmatrix}, \tag{44}$$

where $F_L^{\,I} \equiv \frac{\partial F_L}{\partial I}$.

The poles of $F^{-1}(S)$ characterize the response of the controlled vehicle. These poles are the solutions of the characteristic equation

$$S^2\left(S^2 + \frac{2k}{m}F_L^{\,I}A\cos\varphi_o\, S - a_{33}\right)\left[S^2 - \left(a_{11} - \frac{2k}{m}F_L^{\,I} + \frac{2w}{mv}kF_L^{\,I}a_{21}\right)S - \left(a_{22} + a_{11}\frac{2k}{m}F_L^{\,I}\right)\right] = 0 \quad . \tag{45}$$

It is apparent that damping has been added to both the rotational oscillatory motion associated previously with the frequency $\sqrt{-a_{33}}$ as

well as to the vertical and horizontal oscillatory motion associated previously with the frequency $\sqrt{-a_{22}}$. Thus, this relatively simple non-interacting magnet control scheme should work.

Analysis of the vehicle motions in the xy and yz planes yields similar results, namely that oscillatory rotations and translations result from perturbations. Similarly, it can be shown that simple individual magnet control can be used to add damping to all oscillatory modes. This will be seen to be a definite advantage of guideway configurations having orthogonal surfaces for obtaining levitation and guidance forces.

B. Inverted Vee Guideway

The basic dynamics of the inverted vee guideway are analyzed in this section. A schematic view of a vehicle over such a guideway is shown in Fig. 13, where four magnets produce both levitation and guidance forces. (For simplicity, the vehicle is drawn rectangular.) The coordinate system for analyzing the motion is fixed at the equilibrium position of the center of gravity of the vehicle as shown. Similar assumptions as made in the analysis of a vehicle in the u-channel apply. Further, it is apparent that motion in the x-z plane should be similar to that encountered with the u-channel guideway and will not be discussed further. However, it is also apparent that the fundamental difference between the motions of the two guideways is the inherent coupling between the translational and rotational motion in the y-z plane. Thus, the y-z plane motion is that analyzed here. The forces in Fig. 13 are referred to as F_{N1} and F_{N2}, i.e., normal forces, since they produce both lift and guidance components.

Since a fairly detailed derivation of the equations of motion for a vehicle in the u-channel was given earlier and since the geometrical details become quite involved with even this simple geometry, the derivation of the linearized equations of motion is omitted. The resulting equations of motion are

$$\begin{bmatrix} \ddot{y}_c \\ \ddot{z}_c \\ \ddot{\theta} \end{bmatrix} = \begin{bmatrix} a_{11} & 0 & a_{13} \\ 0 & a_{22} & 0 \\ a_{31} & 0 & a_{33} \end{bmatrix} \begin{bmatrix} y_c \\ z_c \\ \theta \end{bmatrix} , \qquad (46)$$

where

y_c, z_c = y-z plane coordinates of the center of gravity

θ = angle of rotation about the center of gravity (clockwise positive)

and

$$a_{11} = \frac{2}{m} \cos^2 \theta_o \frac{\partial F_n}{\partial h} = \frac{2}{m} \cos^2 \theta_o F_n{}^h$$

$$a_{13} = \frac{2}{m} F_n{}^h \cos \theta_o (A \sin \theta_o + B \cos \theta_o)$$

$$a_{22} = \frac{2}{m} \sin^2 \theta_o F_n{}^h$$

$$a_{31} = \frac{2}{I_{cm}} F_n{}^h \cos \theta_o \, [A \sin \theta_o + B \cos \theta_o]$$

$$a_{33} = \frac{2}{I_{cm}} F_n{}^h \, (A \sin \theta_o + B \cos \theta_o)^2 + mg B - mg A \cot \theta_o \, .$$

I_{cm} = moment of inertia about an axis through the center of mass.

Thus, the vertical translational motion is seen to be totally decoupled from the horizontal translation and rotation. This vertical motion is oscillatory and undamped with a frequency of oscillation of $\sqrt{-a_{22}}$, is seen to approach the frequency of a magnet levitated over a plane as $\theta_o \to \pi/2$. Analyzing the coupled y_c, θ motions using Laplace Transform techniques shows the square of the roots of the characteristic equation to be

$$S_{1,2}^2 = \frac{a_{11} + a_{33}}{2} \pm \sqrt{\frac{(a_{11} + a_{33})^2}{2} - (a_{11} a_{33} - a_{13} a_{31})} \quad . \tag{47}$$

For parameter values of interest, $S_{1,2}^2$ are always negative, implying undamped-oscillatory natural modes for $\theta(t)$ and $y_c(t)$. Further analysis is nearly impossible without choosing vehicle dimensions and a value for θ_o. Assuming values as shown in Fig. 14 as well as a uniformly distributed mass, it can be shown that the responses $y_c(t)$ and $\theta(t)$ resulting from any initial perturbations $y_c(0)$, $\theta(0)$ are given by

$$y_c(t) = .4\, y_c(0) \cos(5.9\, t) + .6\, y_c(0) \cos(.362\, t)$$
$$+ 2.21\, \theta(0) \cos(5.9\, t) - 2.21\, \theta(0) \cos(.362\, t) \quad , \tag{48}$$

and

$$\theta(t) = .109\, y_c(0) \cos(5.9\, t) - .109\, y_c(0) \cos(.362\, t)$$
$$+ .6\, \theta(0) \cos(5.9\, t) + .4\, \theta(0) \cos(.362\, t) \quad . \tag{49}$$

Thus, the responses have components at .94 Hz which are in phase and at .058 Hz which are out of phase. These two fundamental components

can be represented as motions of the type shown in Fig. 15. Such coupling between modes is certainly undesirable for the vehicle dynamics. Control strategies could be formulated to damp the motion and decouple the modes, but these would require sensing angles and rates of rotation. Furthermore, simple non-interacting controllers for the individual magnets would not be sufficient. Thus, there is apparently little to be gained in choosing a guideway geometry with which lift and guidance forces can be obtained from the levitation magnets, since such guideways will always contain undesirable coupling between dynamic modes.

CONCLUSIONS

The response of a magnetically levitated vehicle subjected to random guideway irregularities was studied by analyzing the power spectral density of the vertical vehicle accelerations induced by a typical guideway irregularity power spectrum. It was found that the control current should contain terms proportional to the absolute vertical velocity of the vehicle and the relative vehicle to track clearance to obtain acceptable ride quality. High clearance levitation schemes (clearance $\sim$ 10") can obtain good ride quality over a roadbed equivalent to a fair highway with control currents of the order of 16% of the levitation current. However, a low clearance system would be limited to a very accurate track when considering constraints of ride quality and clearance. The vertical acceleration power spectral density specified for the urban tracked air cushion vehicle[14] was used

as a basis for judging the ride quality. While this psd specification may be somewhat open to question, it was clear from the analyses that absolute vertical velocity feedback as opposed to vehicle-track relative velocity feedback must be used to obtain an acceptable ride for any reasonable ride quality specification. Minor improvements in the ride quality can be achieved with the addition of acceleration feedback, but the required increase in control current is not worth the gain.

The dynamics of alternative guideways for supplying lateral guidance as well as lift forces were analyzed. It was seen that a guideway configuration which provides orthogonal surfaces for guidance and levitation leads to an inherently more stable vehicle and allows the use of simple independent control strategies on all lift and guidance magnets. On the other hand, the dynamic mode coupling present with any guideway configuration in which both lift and guidance forces are obtained with a single magnet would necessitate complicated interactive control schemes as well as sensors to measure vehicle roll angles. Thus, a u-channel or box beam type of guideway is recommended for magnetic levitation systems. However, it should be noted that the vehicle was treated as a rigid body in this analysis and that a flexible vehicle might require the implementation of a more complicated interactive control scheme.

ACKNOWLEDGMENT

The author gratefully acknowledges many helpful discussions with Drs. J. R. Reitz, R. H. Borcherts, and L. C. Davis.

REFERENCES

1. Survey of Technology for High Speed Ground Transport, Pt. 1, U. S. Department of Commerce, Washington, D. C., June, 1965, p. v-180.
2. J. R. Powell and G. R. Danby, "High Speed Transport by Magnetically Suspended Trains", ASME Winter Annual Meeting, New York, Railroad Div., 66-WA/RR-5, Nov. 1966.
3. G. R. Polgreen, "Guided Land Transport", Proc. Institute Mechanical Engineers, Pt. 3G, (London), vol. 181, 1966-67, pp. 145-150.
4. H. T. Coffey, F. Chilton, and T. W. Barbee, Jr., "Suspension and Guidance of Vehicles by Superconducting Magnets", (abs.) J. Appl. Phys., vol. 40, 1969, p. 2161.
5. John R. Reitz, "Forces on Moving Magnets Due to Eddy Currents", J. Appl. Phys., vol. 41, No. 5, April 1970, pp. 2067-2071.
6. Robert H. Borcherts and John R. Reitz, "High Speed Transportation via Magnetically-Supported Vehicles. A Study of Magnetic Forces", Transportation Research, vol. 5, 1971, pp. 197-209.
7. R. H. Borcherts and L. C. Davis, "Force on a Coil Moving Over a Conducting Surface, Including Edge and Channel Effects", J. Appl. Phys., May 1972.
8. H. J. Fink and C. E. Hobrecht, "Instability of Vehicles Levitated by Eddy Current Repulsion - Case of an Infinitely Long Current Loop", J. Appl. Phys., vol. 42, No. 9, August 1971, pp. 3446-3450.

9. L. C. Davis and Dennis F. Wilkie, "Analysis of the Motion of Magnetic Levitation Systems: Implications for High Speed Vehicles", J. Appl. Phys., vol. 42, No. 12, November 1971, pp. 4779-4793.

10. Dennis F. Wilkie, "A Study of the Control of Magnetically Levitated Vehicles", Proc. Ninth Annual Allerton Conference on Circuit and System Theory, University of Illinois, Urbana, Illinois, October, 1971, and Ford Motor Company, Scientific Research Staff Technical Report SR-71-104, August 1971.

11. "Technical Extracts: Tracked Air Cushion Vehicle System Study and Analysis Report", TRW Systems Group Report 06818-6008-R000, U. S. Department of Transportation Contract C-353-66 NEG, October, 1967.

12. "Tracked Air Cushion Research Vehicle: Vehicle/Guideway Dynamic Analysis", Grumman Corporation Report PMT-B4-R71-07, U. S. Department of Transportation Contract No. DOT-FR-00005, March 1971.

13. David A. Hullender, David N. Wormley and Herbert H. Richardson, "A Preliminary Study of Actively Controlled Air Cushion Vehicle Suspensions", Massachusetts Institute of Technology, Electronic Projects Laboratory Report EPL-70-76110-11 for U. S. Department of Transportation Contract C-85-65.

14. "Performance Specification and Engineering Design Requirements for Urban Tracked Air Cushion Vehicle", Research Funding Proposal, U. S. Department of Transportation, May 1971.

15. G. C. Newton, L. A. Gould, and J. F. Kaiser, Analytical Design of Linear Feedback Controls, John Wiley and Sons, Inc., New York, 1957.

16. J. S. Mixson and R. Steiner, "Optimization of a Simple Dynamic Model of a Railroad Car Under Random and Sinusoidal Inputs", A.S.M.E. Winter Annual Meeting, Los Angeles, California, November 1969.

17. John C. Houbolt, "Runway Roughness Studies in the Aeronautical Field", Proc. Amer. Soc. Civil Engr., J. Air Transp. Div., vol. 89, No. AT-1, March 1961.

18. J. B. Pearson and C. Y. Ding, "Compensator Design for Multivariable Linear Systems", I.E.E.E. Trans. Aut. Cont., vol. AC-14, No. 2, April 1969, pp. 130-134.

19. B. C. Kuo, Automatic Control Systems, Prentice Hall, Inc., Englewood Cliffs, New Jersey, 1967.

APPENDIX I

For the case of relative position/relative velocity damping, the power spectral densities of the vertical acceleration and control current are

$$P_{\ddot{e}\ddot{e}}(\omega) = \frac{\omega^4(\hat{\omega}_o^4 + \omega^2\beta^2)P_{HH}(\omega)}{(\hat{\omega}_o^2 - \omega^2)^2 + \omega^2\beta^2} \tag{I.1}$$

$$P_{i_c i_c}(\omega) = \frac{\omega^4(k_2^2 + \omega^2 k_1^2)\,P_{HH}(\omega)}{(\hat{\omega}_o^2 - \omega^2)^2 + \omega^2\beta^2} \tag{I.2}$$

where k_1 and k_2 are the feedback gains defined by

$$i_c(t) = k_1(\dot{z}(t) - \dot{H}(t)) - k_2(z(t) - h - H(t)) \quad .$$

For the case of relative position/absolute velocity/absolute acceleration control, the power spectral densities of the acceleration, change in clearance, and control current are

$$P_{\ddot{e}\ddot{e}}(\omega) = \frac{\omega^4\hat{\omega}_o^4\,P_{HH}(\omega)}{(1+\beta k_3/k_1)^2[(\tilde{\omega}_o^2 - \omega^2)^2 + \omega^2\tilde{\beta}^2]} \tag{I.3}$$

$$P_{\Delta c\Delta c}(\omega) = \frac{\omega^2(\omega^2 + \tilde{\beta}^2)\,P_{HH}(\omega)}{(\tilde{\omega}_o^2 - \omega^2)^2 + \omega^2\tilde{\beta}^2} \tag{I.4}$$

and

$$P_{i_c i_c}(\omega) = \frac{\omega^2[\omega^2(k_2 + k_3\hat{\omega}_o^2) + (k_2\beta + k_1\hat{\omega}_o^2)^2}{(1+\beta k_3/k_1)[(\tilde{\omega}_o^2 - \omega^2)^2 + \omega^2\tilde{\beta}^2]} \tag{I.5}$$

where $\hat{\omega}_o$ and β are as defined after (11) in the paper, and

$$\tilde{\omega}_o^2 = \frac{\hat{\omega}_o^2}{1 + \beta k_3/k_1} \quad , \tag{I.6}$$

$$\tilde{\beta} = \frac{\beta}{1 + \beta k_3/k_1} \quad . \tag{I.7}$$

The control current in this case has the form

$$i_c(t) = k_1 \dot{z}(t) - k_2(z(t) - h - H(t)) + k_3 \ddot{z}(t) \quad .$$

APPENDIX II

Hullender, Wormley, and Richardson[13] determined the optimal suspension which would minimize a performance index I where

$$I = \overline{(\Delta \ddot{z}^2)^2} + \rho \overline{(\Delta c)^2} \qquad \text{(II.1)}$$

where $\Delta \ddot{z}$ = absolute vertical acceleration induced by track irregularity

and Δc = change in relative clearance between vehicle and track from equilibrium.

ρ = variable parameter--relative influence between terms in the performance index.

The coordinates of the vehicle and track are defined as follows:

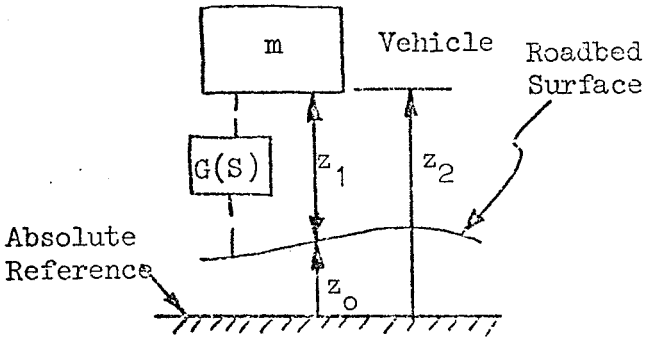

$$z_2 - z_o = z_1$$

$$\Delta z_2 - \Delta z_o = \Delta C$$

The transfer function G(S) relating the change in force $\Delta F(S)$ to the change in vehicle--roadbed clearance, i.e., $\Delta c(S)$, was found in [13] to be (Note that this depends on the assumed track psd.)

$$\Delta F(S) = G(S)\Delta c = \frac{-ma^2 S}{(S+\sqrt{2}a)} \Delta C. \qquad \text{(II.2)}$$

It was stated that this transfer function is the same as that for the following series spring-damper combination:

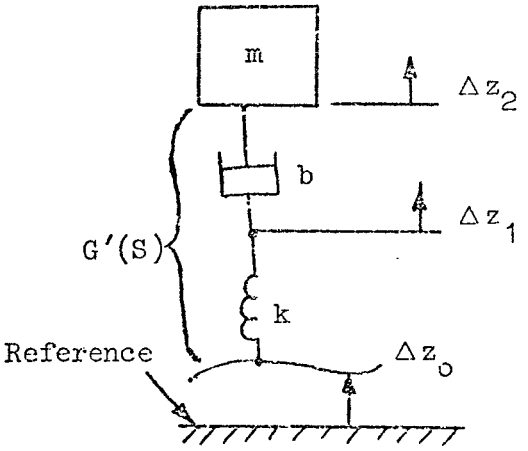

if we choose $k = ma^2$ and $b = ma/\sqrt{2}$.

We proceed to show the following,

(i) The transfer function G'(S) has the form of G(S).

(ii) The change in force, ΔF, resulting from track irregularities when using this series spring damper is equivalent to relative position and absolute velocity feedback.

Assigning an intermediate variable Δz_1, as shown, the equation of motion of m can be written as the following two equations:

$$\Delta F = m\Delta\ddot{z}_2 = -b(\Delta\dot{z}_2 - \Delta\dot{z}_1) \qquad \text{(II.3a)}$$

and

$$0 = b(\Delta\dot{z}_2 - \Delta\dot{z}_1) - k(\Delta z_1 - \Delta z_o) \quad . \qquad \text{(II.3b)}$$

Let us assume that the solutions for Δz_1 and Δz_2 are of the form

$$\Delta z_1 = \Delta z_1^{\,o}\, e^{pt}$$

$$\Delta z_2 = \Delta z_2^{\,o}\, e^{pt} \quad .$$

Then $\Delta \dot{z}_1 = p \Delta z_1^{\,o}\, e^{pt} = p \Delta z_1$

and $\Delta \dot{z}_2 = p \Delta z_2$.

Assuming this, (II.3b) becomes

$$0 = b p \Delta z_2 - b p \Delta z_1 - k \Delta z_1 + k \Delta z_o$$

or

$$(b p + k) \Delta z_1 = b p \Delta z_2 + k \Delta z_o$$

$$\Delta z_1 = \frac{p}{(p + k/b)} \Delta z_2 + \frac{k}{b} \cdot \frac{\Delta z_o}{(p + k/b)} \quad . \qquad \text{(II.4)}$$

Substituting (II.4) into (II.3a),

$$\Delta F = - b p \Delta z_2 + b p \left[\frac{p \Delta z_2 + (k/b) \Delta z_o}{(p + k/b)} \right]$$

or

$$\Delta F = \frac{- kp(\Delta z_2 - \Delta z_o)}{(p + k/b)} \quad ,$$

so that

$$\Delta F = \frac{- kp \Delta c}{(p + k/b)} \quad . \qquad \text{(II.5)}$$

If the Laplace Transform technique was used--p would be replaced by S and everything else would be the same. Thus, the series spring-damper does represent the transfer function obtained in reference 13.

But now

$$\Delta F = \frac{-kp\Delta c}{p+k/b} = -k\Delta c\,\frac{[p+k/b-k/b]}{p+k/b}$$

and

$$\Delta F = -k\Delta c\left[1-\frac{k/b}{p+k/b}\right]$$

and

$$\Delta F = -k\Delta c + \frac{k^2}{b}\cdot\frac{\Delta c}{(p+k/b)} \quad . \tag{II.6}$$

But $\Delta F = m\Delta\ddot{z}_2 = mp^2\Delta z_2$, which from (II.5) implies

$$mp\Delta z_2 = \frac{-kp\Delta c}{p+k/b}$$

or

$$\frac{mk}{b}p\Delta z_2 = -\frac{k^2}{b}\cdot\frac{\Delta c}{(p+k/b)} \quad . \tag{II.7}$$

Substituting (II.7) for the second term in (II.6) gives

$$\Delta F = -k\Delta c - \frac{mk}{b}p\Delta z_2$$

or

$$\Delta F = -k\Delta c - \frac{mk}{b}\Delta\dot{z}_2 \quad . \tag{II.8}$$

Thus, the force is obtained as a linear combination of relative position change and absolute velocity.

It is interesting to note that this is also equivalent to the following spring and damper combination:

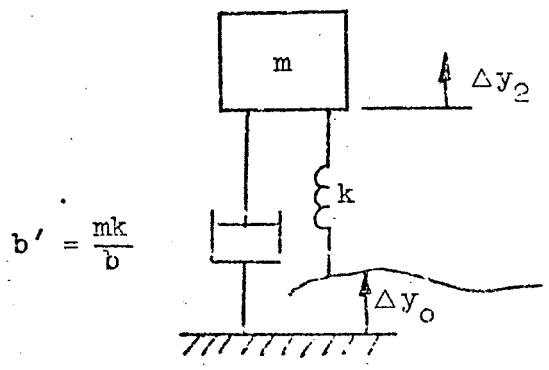

FIGURE CAPTIONS

Figure 1. A magnetically levitated coil over a conducting plane with its image coil.

Figure 2. Definition of variables for analyzing the perturbed motion of a coil.

Figure 3. Typical power spectral density measurements for various surfaces.

Figure 4. Vertical acceleration power spectrum for a vehicle with relative position/relative velocity control. ($A = 5 \times 10^{-6}$ ft, $v = 300$ mph).

Figure 5. Vertical acceleration power spectrum for a vehicle with absolute vertical velocity feedback. ($A = 5 \times 10^{-6}$ ft, $v = 300$ mph).

Figure 6. Vertical acceleration power spectrum for vehicle with relative position/absolute velocity control. ($A = 5 \times 10^{-6}$ ft, $v = 300$ mph).

Figure 7. Vertical acceleration power spectrum for vehicle with relative position/acceleration feedback control. ($A = 5 \times 10^{-6}$ ft, $v = 300$ mph).

Figure 8. Vertical acceleration power spectrum for vehicle with relative position/absolute velocity/acceleration feedback control. ($A = 5 \times 10^{-6}$ ft, $v = 300$ mph).

Figure 9. Alternative guideway configurations.

Figure 10. A typical vehicle in a u-channel guideway.

Figure 11. Vehicle perturbed from steady motion in longitudinal plane.

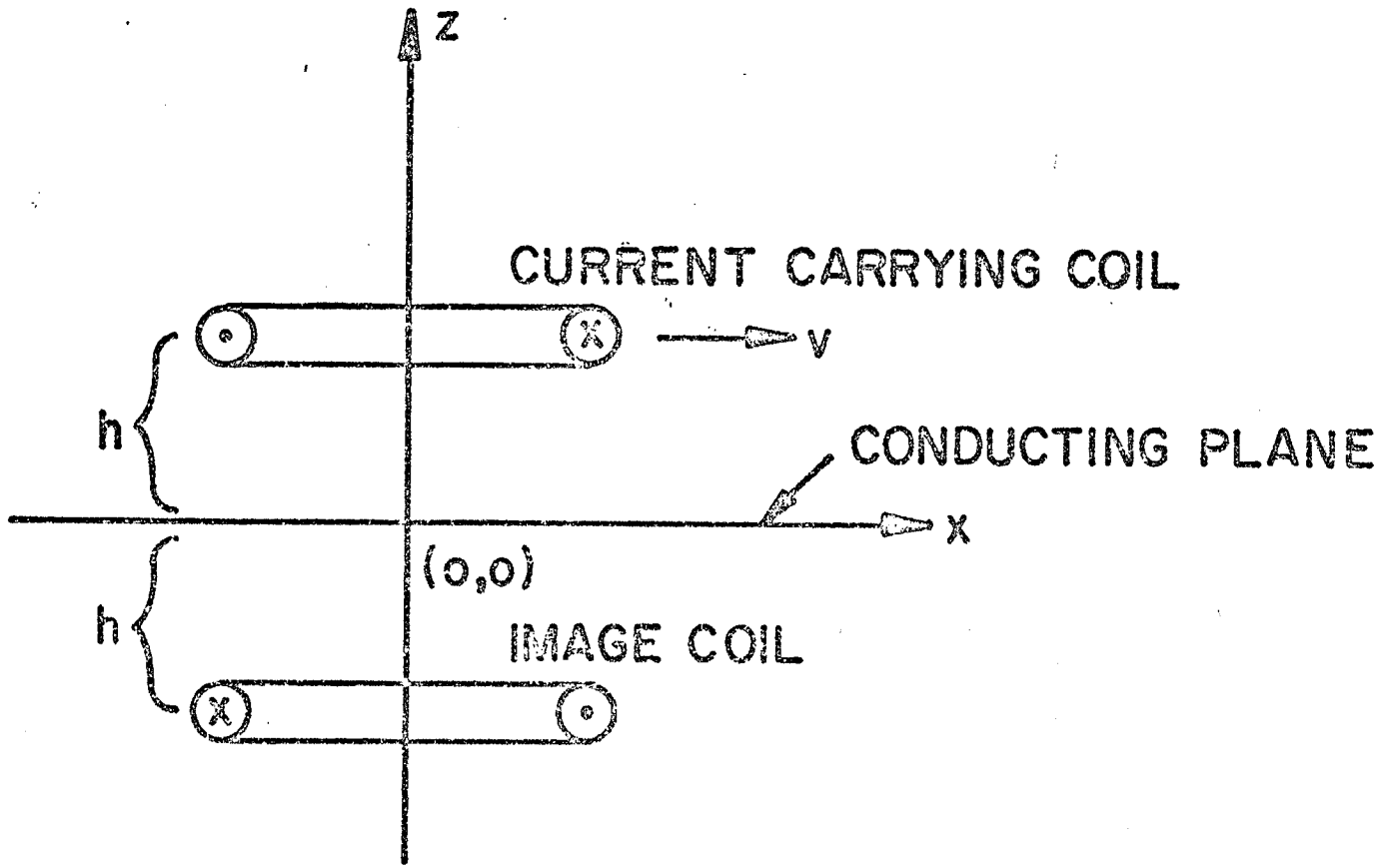
z
CURRENT CARRYING COIL
v
h
CONDUCTING PLANE
x
(o,o)
h
IMAGE COIL

FIG. I

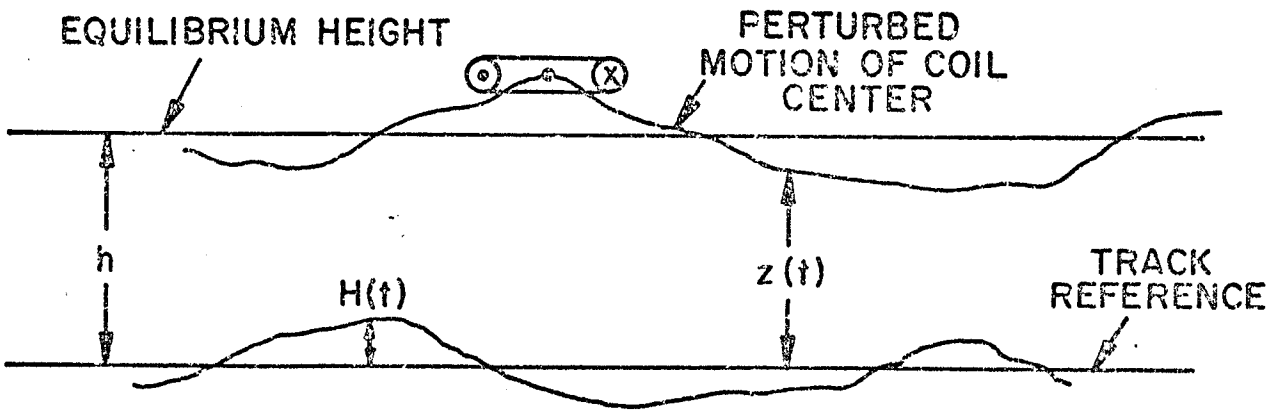
EQUILIBRIUM HEIGHT
PERTURBED
MOTION OF COIL
CENTER
h
H(t)
z(t)
TRACK
REFERENCE

FIG. 2

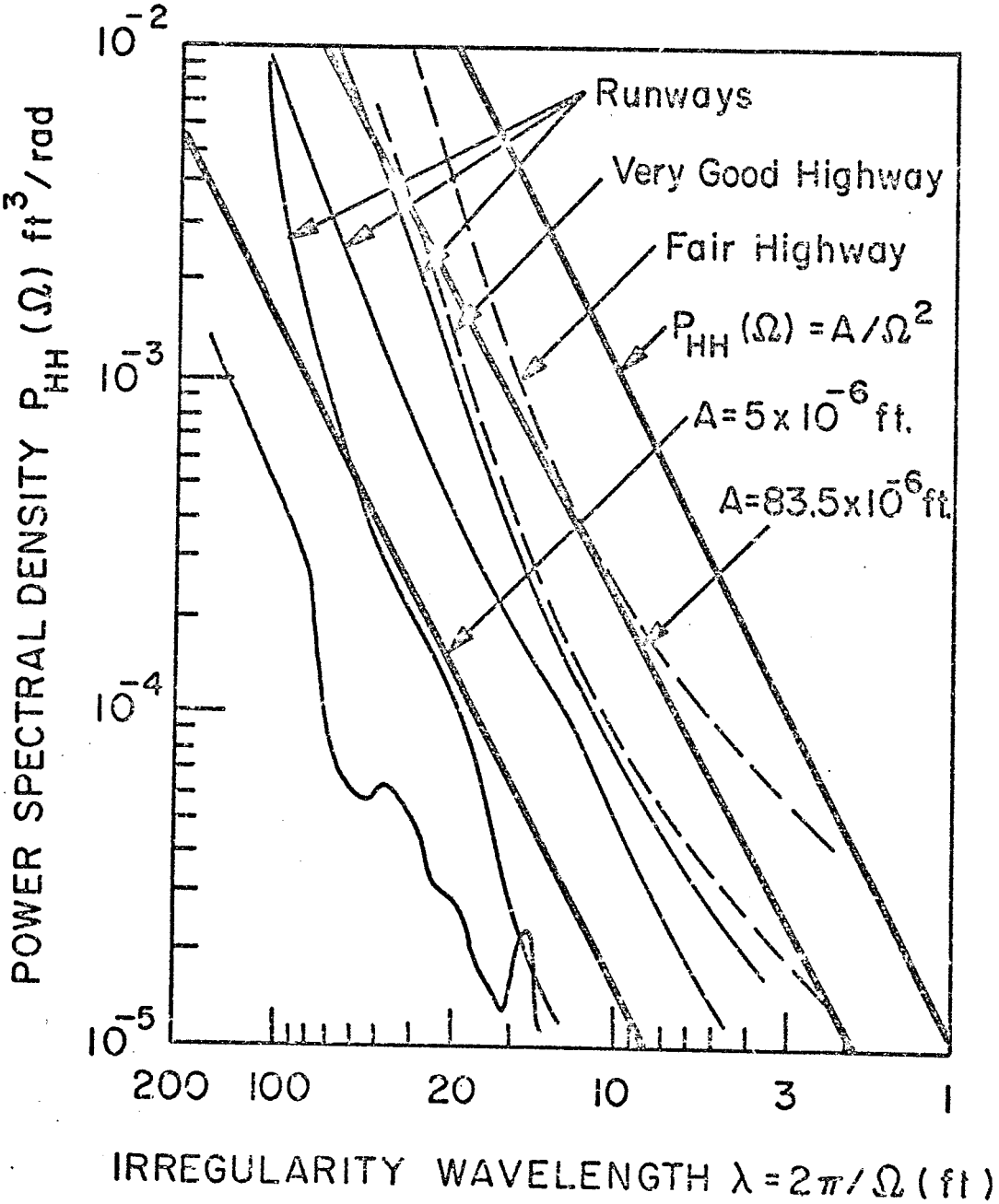
10^{-2}
10^{-3}
10^{-4}
10^{-5}
POWER SPECTRAL DENSITY $P_{HH}(\Omega)$ ft^3/rad
Runways
Very Good Highway
Fair Highway
$P_{HH}(\Omega) = A/\Omega^2$
$A = 5 \times 10^{-6}$ ft.
$A = 83.5 \times 10^{-6}$ ft.
200
100
20
10
3
1
IRREGULARITY WAVELENGTH $\lambda = 2\pi/\Omega$ (ft)

FIG. 3

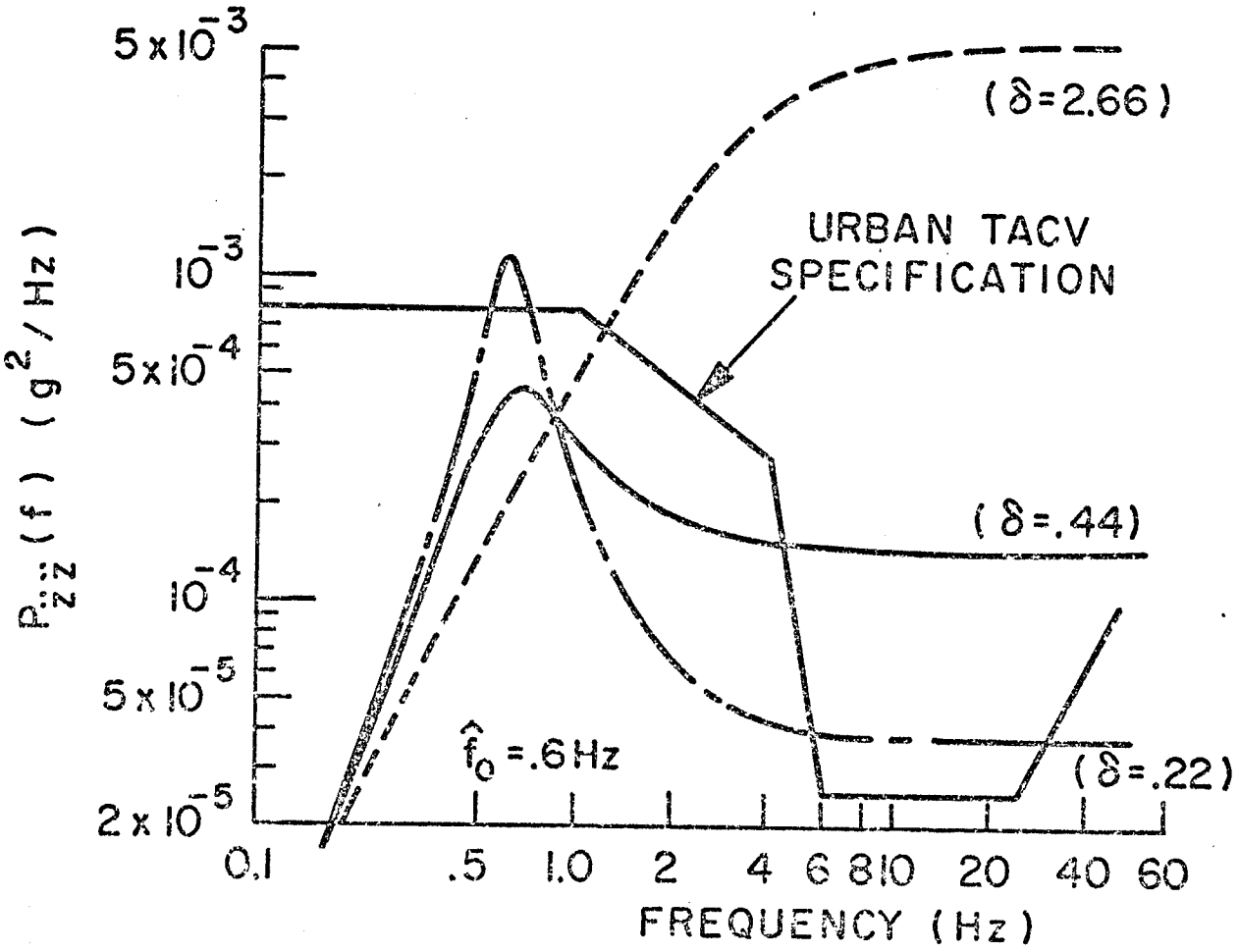
5 x 10⁻³
10⁻³
5 x 10⁻⁴
10⁻⁴
5 x 10⁻⁵
2 x 10⁻⁵
P_zz (f) (g²/Hz)
(δ=2.66)
URBAN TACV
SPECIFICATION
(δ=.44)
(δ=.22)
f̂₀ =.6Hz
0.1
.5
1.0
2
4
6
8
10
20
40
60
FREQUENCY (Hz)

FIG. 4

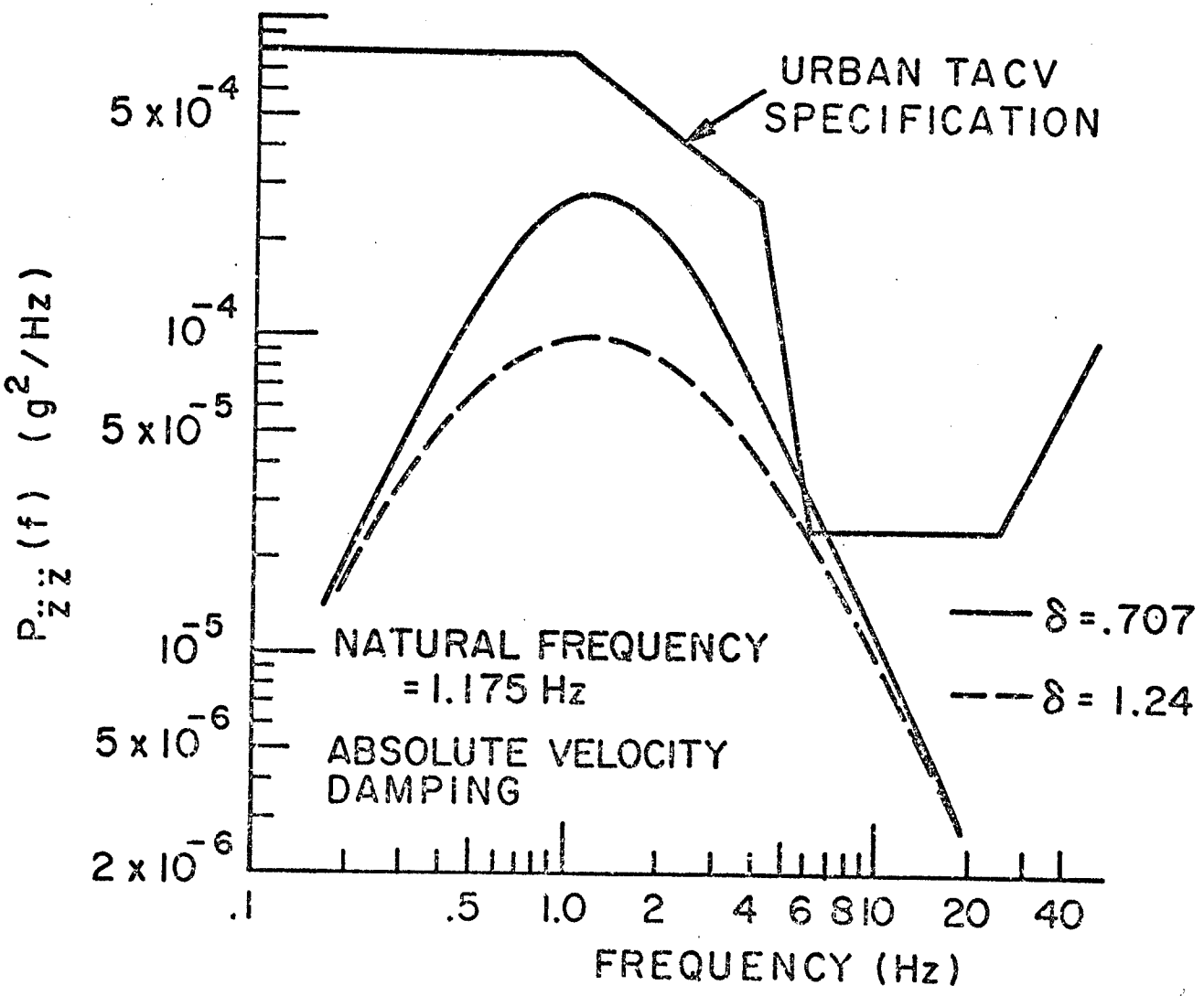
URBAN TACV
SPECIFICATION
5 x 10⁻⁴
10⁻⁴
5 x 10⁻⁵
10⁻⁵
5 x 10⁻⁶
2 x 10⁻⁶
P_żż (f) (g²/Hz)
NATURAL FREQUENCY
= 1.175 Hz
ABSOLUTE VELOCITY
DAMPING
δ = .707
δ = 1.24
.1
.5
1.0
2
4
6
8
10
20
40
FREQUENCY (Hz)

FIG. 5

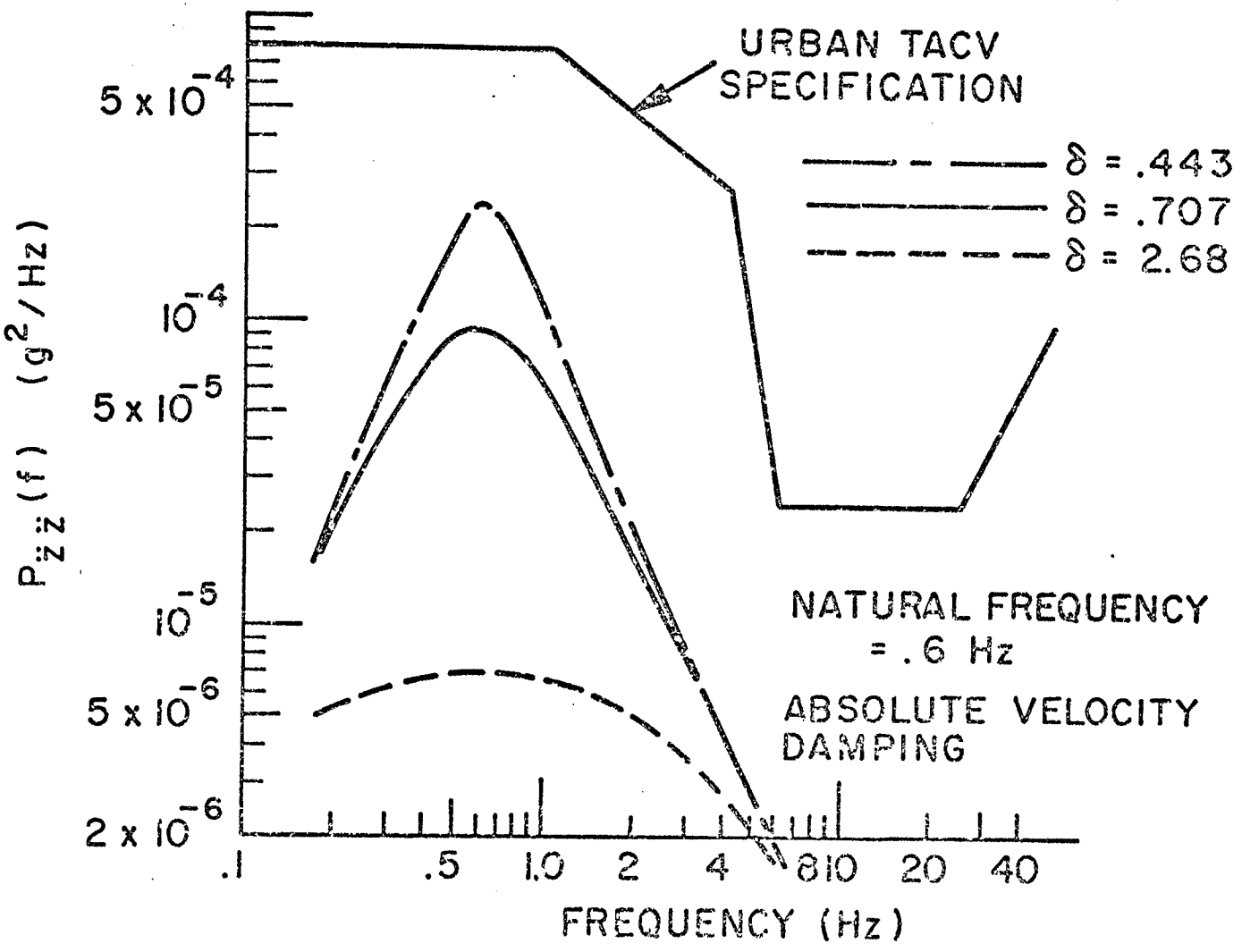
URBAN TACV
SPECIFICATION
δ = .443
δ = .707
δ = 2.68
NATURAL FREQUENCY
= .6 Hz
ABSOLUTE VELOCITY
DAMPING
5 x 10⁻⁴
10⁻⁴
5 x 10⁻⁵
10⁻⁵
5 x 10⁻⁶
2 x 10⁻⁶
P_żż(f) (g²/Hz)
.1
.5
1.0
2
4
8
10
20
40
FREQUENCY (Hz)

FIG. 6

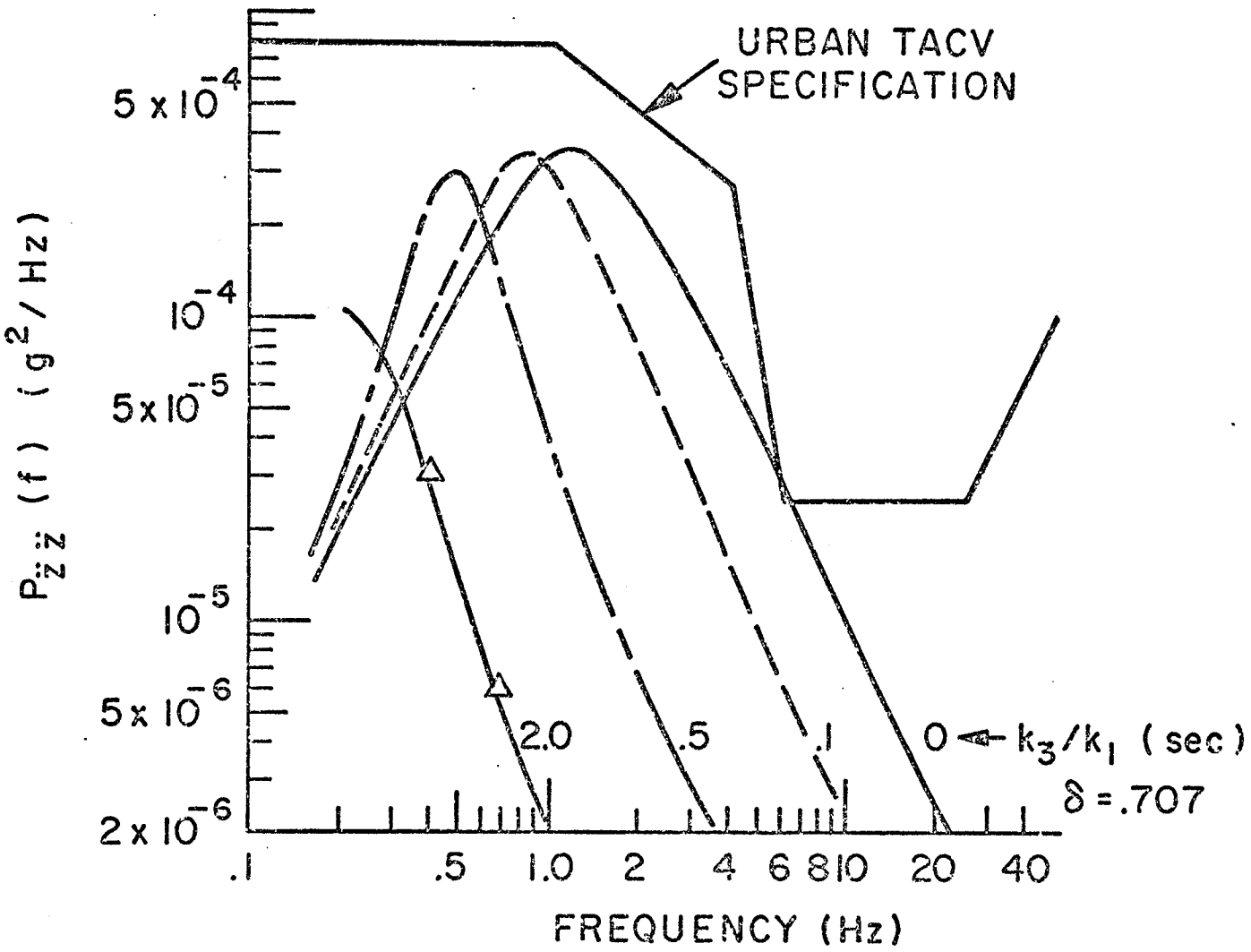
URBAN TACV
SPECIFICATION
5×10^{-4}
10^{-4}
5×10^{-5}
10^{-5}
5×10^{-6}
2×10^{-6}
$P_{\ddot{z}\ddot{z}}(f)$ (g^2/Hz)
2.0
.5
.1
0 ← k_3/k_1 (sec)
$\delta = .707$
.1
.5
1.0
2
4
6
8
10
20
40
FREQUENCY (Hz)

FIG. 7

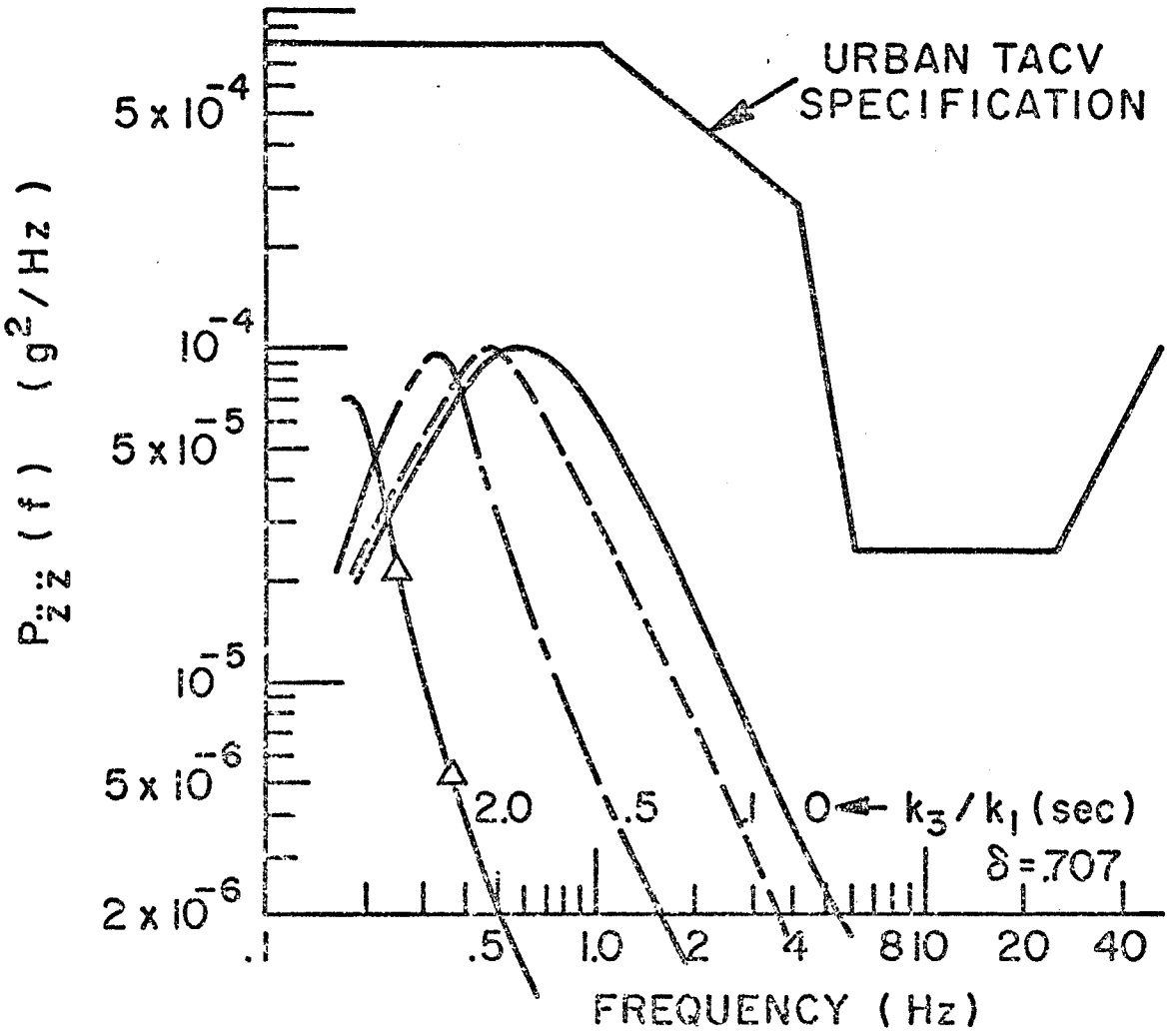
URBAN TACV
SPECIFICATION
5×10^{-4}
10^{-4}
5×10^{-5}
10^{-5}
5×10^{-6}
2×10^{-6}
$P_{\ddot{z}\ddot{z}}(f)$ (g^2/Hz)
2.0
.5
0
k_3/k_1 (sec)
$\delta = .707$
.5
1.0
2
4
8
10
20
40
FREQUENCY (Hz)

FIG. 8

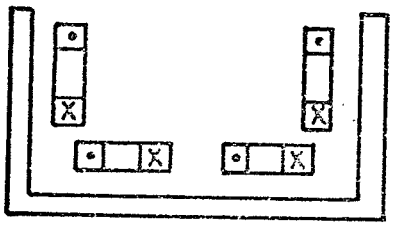

a) U-CHANNEL

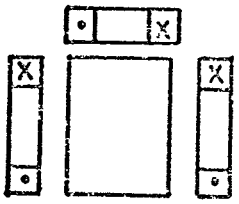

b) BOX BEAM

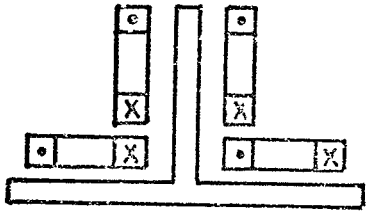

c) INVERTED T

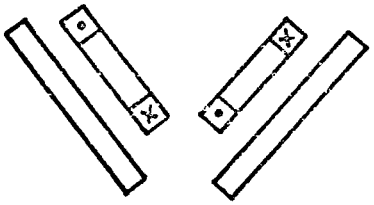

d) VEE

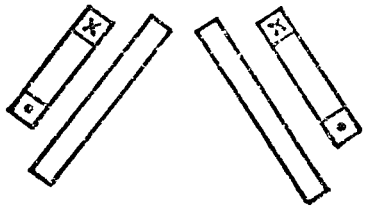

e) INVERTED VEE

FIG. 9

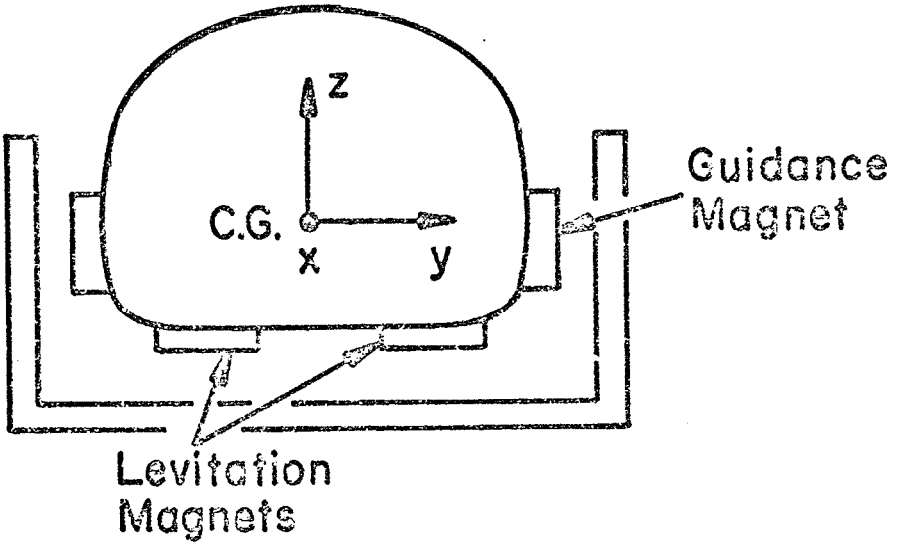

END VIEW - LARGER SCALE THAN
SIDEVIEW - NOT TO SCALE

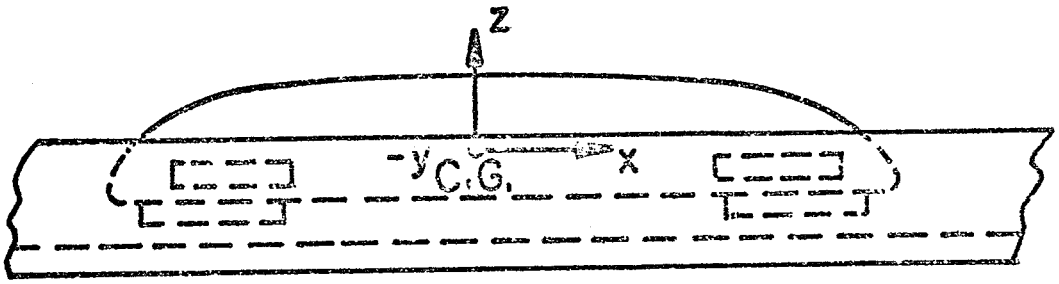

SIDE VIEW - NOT TO SCALE

FIG. 10

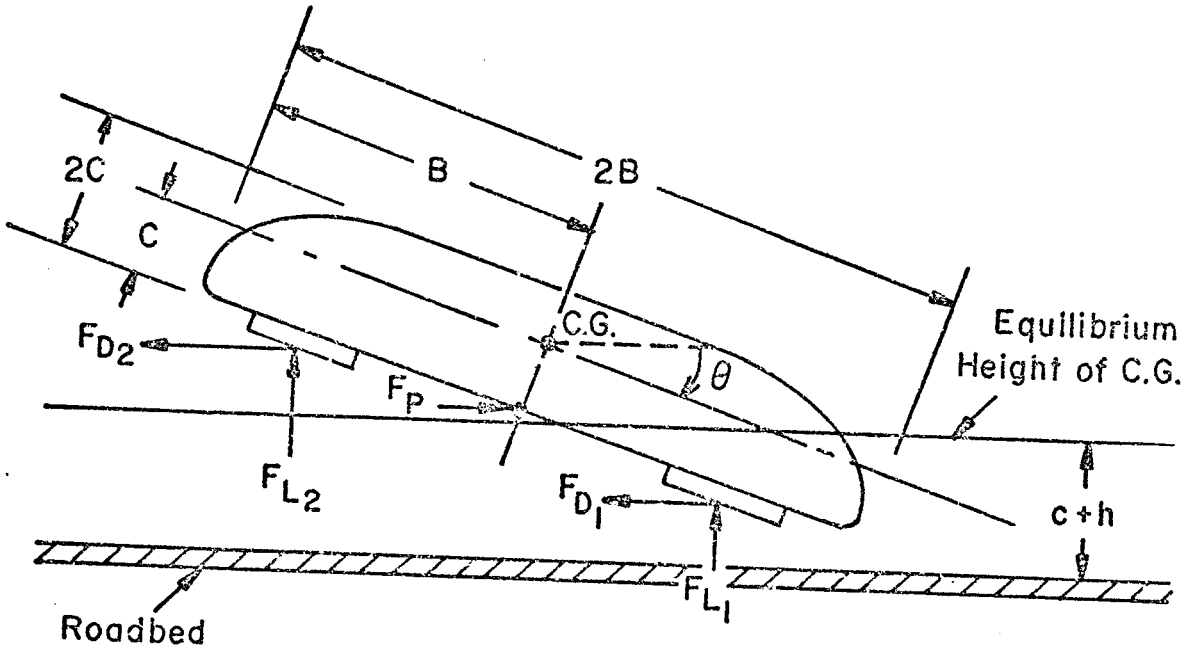
2C
C
B
2B
C.G.
θ
Equilibrium
Height of C.G.
F_{D_2}
F_P
F_{L_2}
F_{D_1}
c+h
F_{L_1}
Roadbed

Fig. 11

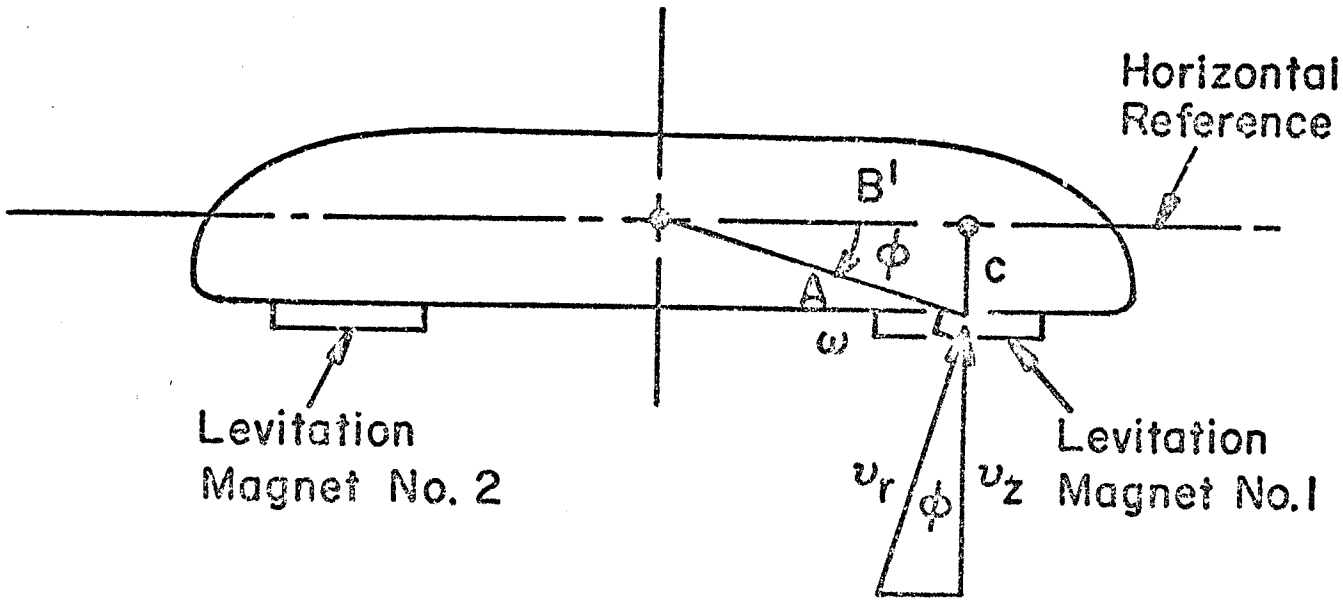
Horizontal
Reference
B'
φ
C
A
ω
Levitation
Magnet No. 2
v_r
φ
v_z
Levitation
Magnet No.1

Fig. 12

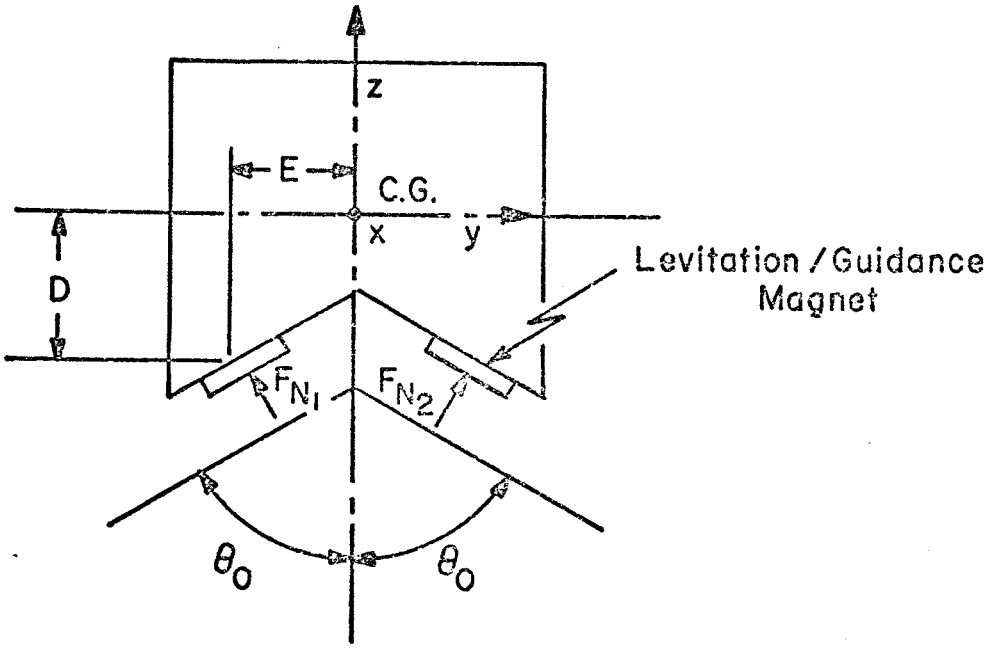

END VIEW - NOT TO SCALE

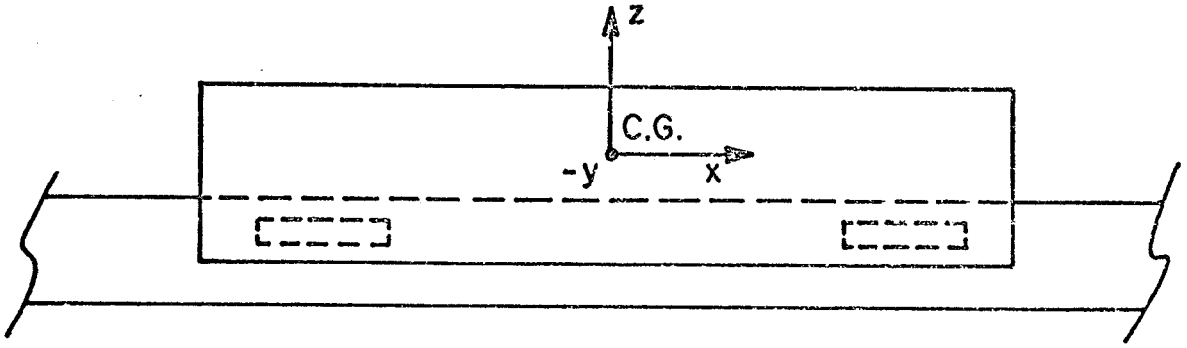

SIDE VIEW - NOT TO SCALE

Fig. 13

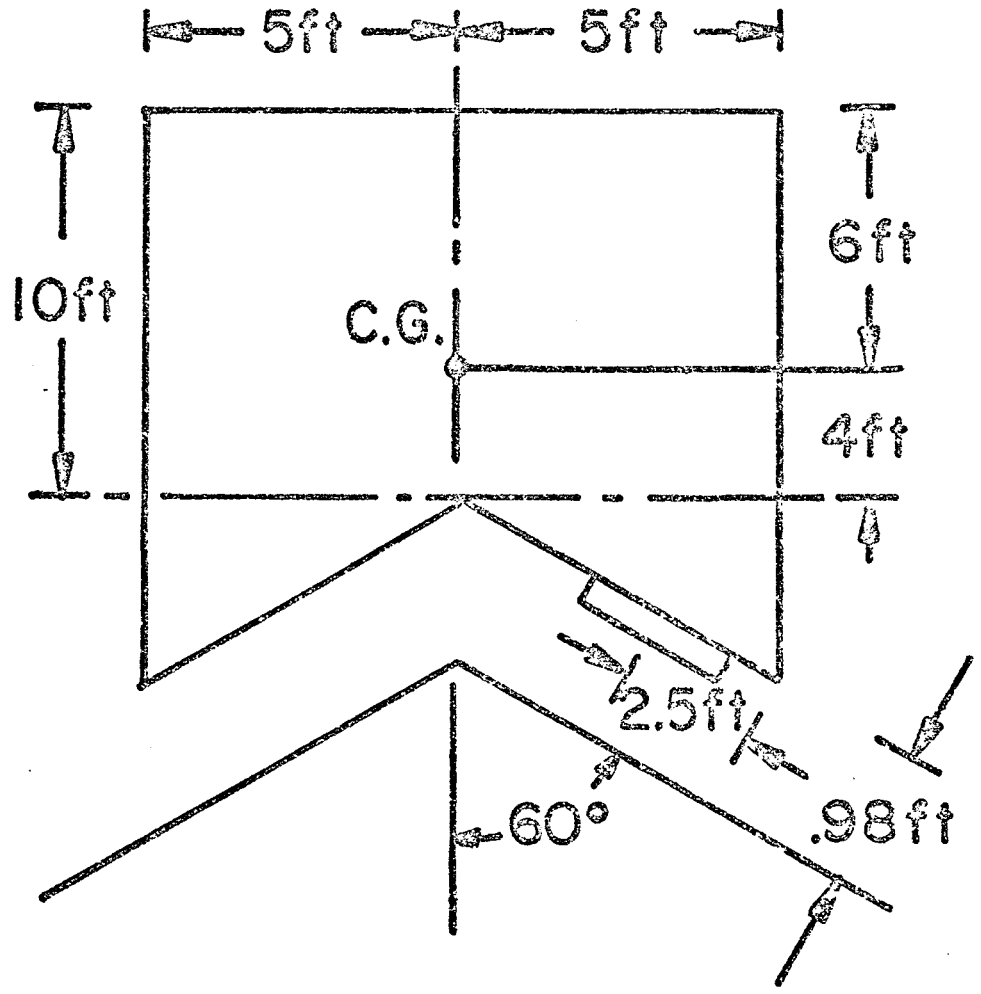

EXAMPLE VEHICLE DIMENSIONS

Fig. 14

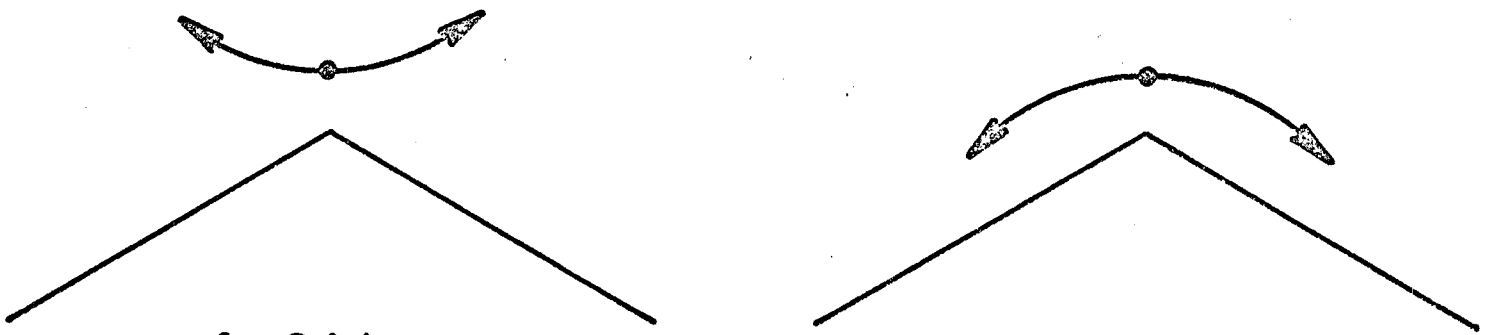

FUNDAMENTAL MODES FOR AN INVERTED VEE GUIDEWAY

Fig. 15

APPENDIX F

PASSIVE DAMPING

A. Conducting Plate

Let us examine the effects of a conducting plate placed between the levitation magnet and the guideway. The plate is attached to the vehicle, moving rigidly with the magnet. For steady motion, the plate has no effect. For oscillatory motion in the vertical direction (in addition to steady motion down the guideway) eddy currents are induced in the plate which damp the oscillations. Also, the eddy currents flowing in the plate produce a change in the guideway currents which provides additional damping.

Consider the high-speed limit. The guideway currents produce a magnetic field equivalent to that of the image of the levitation magnet (and of the eddy currents in the plate which will be considered later). As the vehicle oscillates in the vertical direction, the image oscillates in the opposite sense. The relative motion of the image and the plate induces eddy currents. The appropriate coordinate system is shown in Fig. F.1.

Let $z_o(t)$ be the height of the levitation magnet above the guideway, and $z_p(t)$ the height of the plate. At equilibrium $z_o = h$, $z_p = h'$, we let $z(t) = z_o(t) + z_p(t)$ be the distance between the image and the plate. If the vehicle is oscillatory in the vertical direction, then z_o is of the form

$$z_o(t) = h + h_1 \sin \gamma t \quad . \tag{1}$$

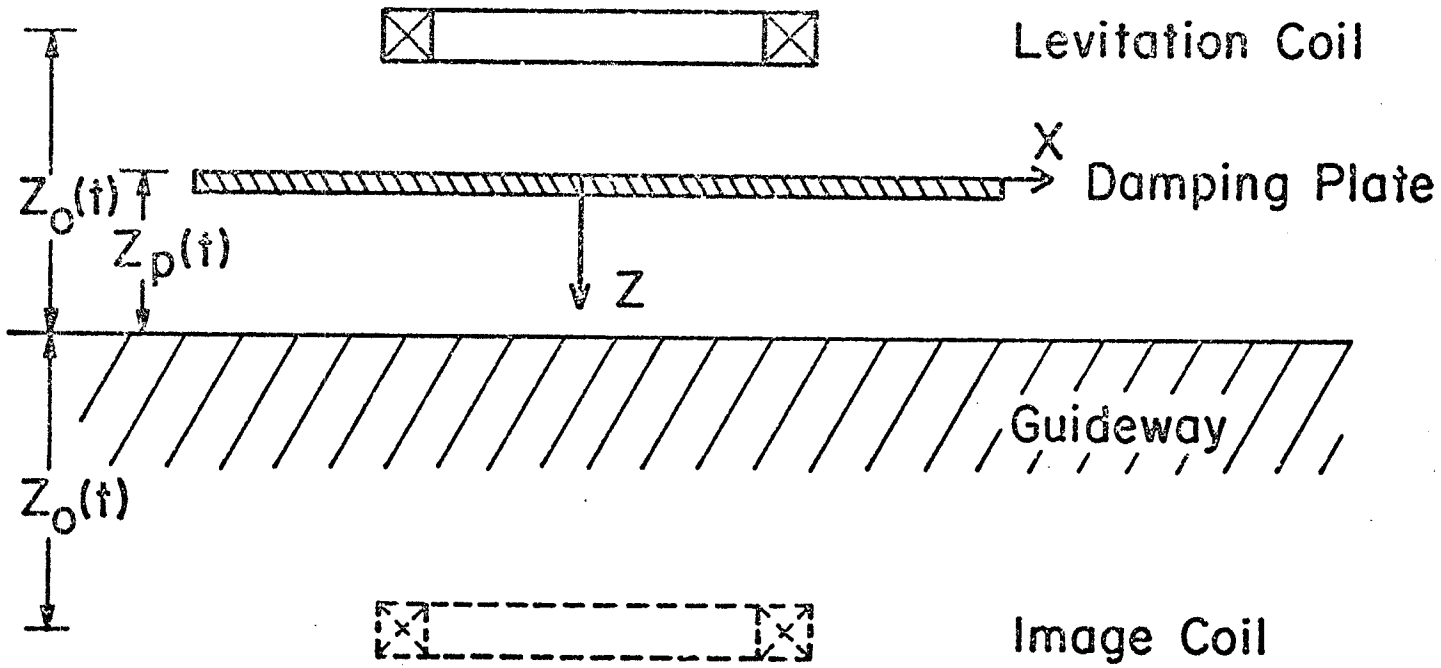

Fig. F.1. The use of a conducting plate for damping vehicle oscillation.

This implies that

$$z_p(t) = h' + h_1 \sin \gamma t \tag{2}$$

and that

$$z(t) = h + h' + 2h_1 \sin \gamma t \quad . \tag{3}$$

We assume that $h_1 \ll h'$, $h_1 \ll h$.

In the x-z frame of reference (rigidly attached to the plate, z pointing downward) the image moves in the vertical (z) direction according to (3). Since the motion in the x-z frame is purely vertical, the aspect ratio of the magnet does not play a dominant role. Hence, a calculation of the force on a long wire is relevant. Corrections for more realistic image magnets are given later. We also assume that the plate is thin so that the thin-plate model can be applied. The thickness of the plate is T_p and the conductivity is σ_p. From Eqs. (2.12) - (2.16) of Davis and Wilkie[15], we have

$$F_x = F_y = 0 \tag{4}$$

and

$$F_z = \frac{\mu_o I^2}{4\pi z(t)} - \frac{w_p \mu_o I^2}{2\pi} \int_o^\infty d\tau \, [z(t) + w_p \tau + z(t-\tau)]^{-2} \tag{5}$$

where $$w_p = 2/\mu_o \sigma_p T_p \quad . \tag{6}$$

The current in the long wire is I.

Now we write $z(t-T)$ as (see Eq. (3))

$$z(t-\tau) = z(t) + \Delta(t,\tau) \quad , \tag{7}$$

where

$$\Delta(t,\tau) = 2h_1 [\sin\gamma(t-\tau) - \sin\gamma t] \quad , \tag{8a}$$

$$= 2h_1 [\sin\gamma t\,(\cos\gamma\tau - 1) - \cos\gamma t \sin\gamma\tau] \quad . \tag{8b}$$

Assuming that h_1 is small, we expand the integrand of (5) in powers of $\Delta(t,\tau)$:

$$F_z = \frac{w_p \mu_o I^2}{\pi} \int_o^\infty \frac{d\tau\, \Delta(t,\tau)}{[2z(t) + w_p\tau]^3} + \cdots \quad . \tag{9}$$

To determine the damping forces, we need to retain only the terms proportional to velocty (i.e., $\propto \cos\gamma t$) in $\Delta(t,\tau)$. Thus, to first order in h_1

$$F_z = -\frac{2}{\pi} w_p \mu_o I^2 h_1 \cos\gamma t \int_o^\infty \frac{d\tau \sin\gamma\tau}{[2(h+h') + w_p\tau]^3} \quad . \tag{10}$$

It is straightforward to show that

$$F_z = -\frac{\mu_o I^2}{4\pi(h+h')} \frac{\dot{z}(t)}{w_p} I\left(\frac{2(h+h')\gamma}{w_p}\right) \quad , \tag{11}$$

$$I(x) = 1 - xf(x) \quad , \tag{12}$$

where [Handbook of Mathematical Functions][†]

$$f(x) = Ci(x)\sin x - si(x)\cos x \quad . \tag{13}$$

F_z is the damping force on the image in the x-z frame (z points downward). To find the damping force on the plate in a frame of reference where the guideway is stationary and a positive force points upward, we apply Newton's third law, giving one minus sign, and then

---

[†]Walter Gautachi and William F. Cahill, in Handbook of Mathematical Functions, edited by M. Abramowitz and J. A. Stegun (Natl. Bur. Std., Washington, D. C., 1964), Appl. Math. Sci. 55, p. 231.

we have another change of sign due to the difference in direction of a positive force. Hence, the force on the plate is given by (11). The total force on the vehicle is twice that given in (11), however, since the image of the plate in the guideway interacting with the levitation magnet gives (in the high-speed limit) a contribution identical to that of (11). Denoting the damping component of the lift by F_L^d, we have (for a long wire as the levitation magnet)

$$F_L^d = - \frac{\mu_o I^2}{\pi(h+h')} \frac{\dot{z}_o(t)}{w_p} I\left(\frac{2(h+h')\gamma}{w_p}\right) \quad . \tag{14}$$

[Note that we have written (14) in terms of $\dot{z}_o(t) = \gamma h_1 \cos \gamma t$, see Eq. (1).]

Next we make corrections to (14) for more realistic levitation magnets than a long wire. From Eq. (6.21a) of Davis and Wilkie[15], it can be shown that for $|\dot{z}(t)| \ll w_p$ or $2(h+h')\gamma/w_p \ll 1$ the damping force on the image of any levitation magnet is

$$F_z = - \frac{\dot{z}(t)}{w_p} F_I\,(2(h+h')) \quad , \tag{15}$$

where F_I is the force on the levitation magnet due to its image a distance $2(h+h')$ away. We can see that the long wire obeys the relationship by noting that $I(x) \to 1$ as $x \to 0$ and (for a long wire)

$$F_I = \frac{\mu_o I^2}{4\pi(h+h')} \quad . \tag{16}$$

Since we have not been able to find F_z for a realistic magnet for arbitrary $\dot{z}(t)$, we postulate that

$$F_z = -\frac{\dot{z}(t)}{w_p} F_I\,(2(h+h'))\; I\left(\frac{2(h+h')\gamma}{w_p}\right) \quad , \tag{17}$$

which reduces to (15) for $\frac{2(h+h')\gamma}{w_p} \ll 1$ and is identical to (14) for a long wire. Thus,

$$F_L^{\,d} = -\frac{4\dot{z}_o(t)}{w_p} F_I(2(h+h'))\; I\left(\frac{2(h+h')\gamma}{w_p}\right) \quad . \tag{18}$$

A damping time τ can be defined by

$$\frac{2m}{\tau} \equiv \frac{4}{w_p} F_I\,(2(h+h'))\; I\left(\frac{2(h+h')\gamma}{w_p}\right) \quad , \tag{19}$$

where m is the mass supported by one levitation magnet at equilibrium. Now, in the high-speed limit

$$mg = F_I(2h) \quad . \tag{20}$$

Substituting (20) into (19) gives

$$\frac{1}{\tau} = \frac{2g}{w_p} \frac{F_I\,(2(h+h'))}{F_I(2h)}\; I\left(\frac{2(h+h')\gamma}{w_p}\right) \quad . \tag{21}$$

For fixed γ, h and h', $1/\tau$ can be maximized with respect to w_p. We rewrite (21) as

$$\frac{1}{\tau} = \frac{g}{\gamma(h+h')} \frac{F_I(2(h+h'))}{F_I(2h)}\; [x\,I(x)]_{x = \frac{2(h+h')\gamma}{w_p}} \quad . \tag{22}$$

The maximum of $x\,I(x)$ is 0.41, occuring at $x = 1.7$. Hence

$$\left.\frac{1}{\tau}\right)_{max} = \frac{0.41g}{\gamma(h+h')} \frac{F_I(2(h+h'))}{F_I(2h)} \tag{23}$$

and

$$w_p)_{max} = 2(h+h')\gamma/1.7 \quad . \tag{24}$$

For a long wire, (23) becomes ($\gamma = 2\pi f$)

$$\tau = 4.9\pi f(h+h')^2/hg \quad . \tag{25}$$

For a 1 × 2m coil with h = 0.3m and h′ = 0.2m,

$$F_I(2(h+h'))/F_I(2h) = 0.38 \quad , \tag{26}$$

so that

$$\tau = 2.1 \text{ sec} \times (f/1 \text{ Hz}) \quad . \tag{27}$$

B. Tuned Coil

In place of the conducting plate, consider now a coil connected to a capacitor, C. Let L_d be the inductance of the coil, and R_d the resistance. The current induced in the coil is I_1. The height, $z_c(t)$, of this damping coil above the guideway is

$$z_c(t) = h' + z_1(t) \quad , \tag{1}$$

where $|z_1(t)| \ll h'$. Since the damping coil and the levitation coil move rigidly together, the height, $z_o(t)$, of the levitation coil is

$$z_o(t) = h + z_1(t) \quad . \tag{2}$$

The image of the levitation coil is a distance

$$z(t) = h + h' + 2z_1(t) \tag{3}$$

below the damping coil.

The current I_1 satisfies

$$L_d \frac{d^2 I_1}{dt^2} + R_d \frac{dI_1}{dt} + \frac{I_1}{C} = - \frac{d^2 \Phi}{dt^2} \quad , \tag{4}$$

where Φ is the flux through the damping coil due to the image of the levitation magnet. Let $M_d(z(t))$ be the mutual inductance between these two coils, so that (I = current in the levitation coil)

$$\Phi = M_d(z(t))\, I \quad , \tag{5}$$

$$= M_d(h + h')\, I + \frac{dM_d}{dz} 2z_1(t)\, I + \cdots \tag{6}$$

$\frac{dM_d}{dz}$ is evaluated at $z = h + h'$. Therefore,

$$\frac{d^2 \Phi}{dt^2} = \frac{dM_d}{dz}\, 2I \frac{d^2 z_1}{dt^2} \quad . \tag{7}$$

Substituting (7) into (4) gives

$$L_d \frac{d^2 I_1}{dt^2} + R_d \frac{dI_1}{dt} + \frac{I_1}{c} = - 2 \frac{dM_d}{dz}\, I \frac{d^2 z_1}{dt^2} \quad . \tag{8}$$

The dynamical motion of the mass m (mass supported at equilibrium by one levitation coil) is given by

$$m \frac{d^2 z_1}{dt^2} + m \omega_o^2 z_1 = 2I I_1 \frac{dM}{dz} + F(t) \quad , \tag{9}$$

where ω_o is the natural frequency (determined by the levitation coil interacting with its image) and F(t) is a perturbing force.

If F(t) is of the form

$$F(t) = F_o\, e^{i\omega t} \quad , \tag{10}$$

then it is straightforward to show that

$$z_1(t) = z_{10} e^{i\omega t} \quad , \tag{11}$$

where

$$z_{10} = \frac{F_o}{m}\left[\omega_o^2 - \omega^2 - \frac{k\omega_o^2\omega^2}{\omega_e^2 - \omega^2 + i\omega/\tau_e}\right]^{-1} \quad , \tag{12}$$

$$k = \frac{4I^2}{mL_d\omega_o^2}\left(\frac{dM_d}{dz}\right)^2 \quad , \tag{13}$$

$$\omega_e^2 = \frac{1}{L_d C} \quad , \tag{14}$$

and

$$\tau_e = L_d/R_d \quad . \tag{15}$$

For $\omega = \omega_o = \omega_e$, we have

$$z_{10} = -\frac{iF_o}{mk\omega_o^3\tau_e} \quad . \tag{16}$$

Defining a damping time by

$$\frac{1}{\tau} = \frac{|F_o|/|z_{10}|}{2m\omega_o} \quad , \tag{17}$$

we find

$$\tau = \frac{2}{k\omega_o^2\tau_e} \quad . \tag{18}$$

APPENDIX G

DYNAMIC RESPONSE AT AN EXPANSION JOINT IN THE TRACK

When the train coil passes over a cut in the track (such as might be encountered at an expansion joint), the coil will experience a momentary reduction in lift which will perturb its motion. Assuming no electrical conduction across the cut, calculations show that the lift on the coil is reduced about 40 percent when the coil is directly over the cut.

The vertical response of the coil is given by

$$\ddot{z} + \beta \dot{z} + \omega_o^2 z = F(t) \tag{G.1}$$

where $F(t)$ is the perturbing force (change in lift force) per unit mass as a function of time. The Fourier transform $z(\omega)$ is thus given by

$$z(\omega) = \frac{f(\omega)}{(\omega_o^2 - \omega^2) + i\beta\omega} \tag{G.2}$$

where

$$f(\omega) = \frac{1}{2\pi} \int F(t)\, e^{-i\omega t}\, dt \quad . \tag{G.3}$$

If we determine $F(t)$ from calculations of lift on a coil near the edge of a semi-infinite sheet, we obtain

$$F(t) = 0.4\, g\, e^{-2.78\, v^2 t^2} \tag{G.4}$$

where v is in meters/sec, t in seconds, g is the acceleration due to gravity, and $t = 0$ corresponds to the coil being symmetrically located above the joint. $f(\omega)$ is found to be

$$f(\omega) = A\, e^{-\beta\omega^2} \tag{G.5}$$

where $A = (0.2\, g) / (2.78\pi\, v^2)^{\frac{1}{2}}$ and $\beta = 1/(11.16\, v^2)$.

Now $z(t)$ is given by

$$z(t) = \int_{-\infty}^{\infty} \frac{A e^{-\beta\omega^2} e^{i\omega t} d\omega}{(\omega_o^2 - \omega^2) + i\beta\omega} \quad . \tag{G.6}$$

$e^{-\beta\omega_o^2} \approx 1$ over most of the speed range. It is also noted that we overemphasize the response if we take $e^{-\beta\omega^2} = 1$ in the integral. If we do this we may evaluate (G.6) by contour integration and obtain

$$z(t) = -\frac{2\pi A}{\omega_o} e^{-\beta t/2} \sin \omega_o t \tag{G.7}$$

where we have assumed the damping small enough that $\sqrt{\omega_o^2 - \beta^2/4} \approx \omega_o$. We note that the amplitude is independent of β.

If we have two levitation coils separated by the length of the vehicle, the coils receive their impulse at different times:

$$z(t) = -\frac{\pi A}{\omega_o} \left[e^{-\beta(t - t_o)/2} \sin \omega_o (t - t_o) \right.$$

$$\left. - e^{-\beta(t + t_o)/2} \sin \omega_o (t - t_o) \right] \quad . \tag{G.8}$$

If $\omega_o^2 = 54 \text{ sec}^{-2}$ (see Sec. 3.4) and $2 t_o/v$ corresponds to ~ 0.9 (length of revenue vehicle), then the amplitude of $z(t)$ is:

0.33 cm at v = 300 mph

1.04 cm at v = 130 mph

1.10 cm at v = 100 mph

0.84 cm at v = 50 mph .

APPENDIX H

MAGNET CALCULATIONS

1. The field near a conductor bundle is

$$B = \frac{\mu_o}{2\pi} I \cdot \frac{1}{r}$$

which for r = 2.5 cm and I = 3×10^5 amperes is

B = 24,000 gauss.

2. Wire diameter required for a critical field of 48,000 gauss, 300 ampere (safety factor of 2). From Airco's wire chart size: critical current density in 50 kG range is $\sim 10^5$ amperes/cm^2. Thus for

Copper/Superconductor cross-section = 2/1:

diameter = 0.873 mm ($\sim$ 0.035 in).

3. If the inner dewar is uniformly loaded from the superconducting wire then, assuming the dewar acts as a simple beam between any two supports, the maximum deflection becomes

$$y = \frac{5W\ell^3}{384\ EI} = 0.045"$$

where W = total load = 6,250 lb. (50% overload)

ℓ = length between supports (40 inches)

E = elastic modulus (26×10^6 psi)

I = moment of cross-section = $\frac{1}{12}(b_1h_1^3 - b_2h_2^3)$.

4. Maximum stress in this inner dewar occurs midway between the centers of the beam at the top or bottom and is

$$\sigma = \frac{M_c}{I} = \frac{W\ell^2}{8}\ \frac{c}{I}$$

where c is the half height of the beam. Evaluating this stress for both stainless steel and aluminum (dimensions of aluminum beam 2.75 in × 4.00 in)

$$\sigma_{S.S.} = 13{,}400 \text{ psi}$$

$$\sigma_{Al} = 6{,}020 \text{ psi} \quad .$$

The fatigue strengths at 4.2°K for these materials are given in the Cryogenic Materials Data Handbook[35] as 165,000 psi (S.S.) and 47,000 psi (Al).

5. Inner G-10 Epoxy Fiberglass Column (Maximum Load). Since these tubes are in compression the buckling stress is

$$S' = 0.3\ Et/r = 109{,}000 \text{ psi}$$

where E is the modulus (2×10^6 psi), t the wall thickness (0.2"), and r the mean radius (1.1"). Since this value is significantly higher than the fatigue strength of 20,000 psi (10^7 cycles) the fatigue strength will be used to calculate the maximum load.

$$S = \frac{W}{A} = \frac{6{,}250 \text{ lb.}}{1.76 \text{ in}^2} = 3{,}550 \text{ psi}$$

where the value of W is taken to be 1.5 times the equilibrium weight. This value thus provides a significant safety factor. S is (1/5.6) times the fatigue strength (10^7 cycles).

6. The all important heat leak down the inner column from 77°K to 4.2°K is calculated to be

$$Q = \frac{KA\Delta T}{\ell} = 0.267 \text{ Btu/hr}$$

which corresponds to a helium boil-off rate of 0.116 ℓ/hr at 4.2°K.

7. Web thickness for stainless steel hinge. At 4.2°K the fatigue strength for 304 stainless steel is 150,000 psi so that the minimum thickness of the web, for an axial load of 6,250 lb. and a length of 2 inches is

$$t = \frac{6,250}{150,000} \times \frac{1}{2} = 0.021 \text{ inches.}$$

However, there will also be a lateral load that will degrade this performance. For this reason we will consider a web of 0.080 thickness until the additional design features of the hinge are considered.

8. Now the maximum moment which should be permitted while still maintaining elastic behavior of the hinge web is

$$M = \frac{2}{3} \sigma d t^2$$

where for our case, σ is the fatigue strength 150,000 psi, d is the length of the web (2 inches) and t is one half the web thickness:

$$M = 320 \text{ lb.-in.}$$

Heim[36] shows that the maximum angle that the hinge can be actuated while still observing elastic behavior is

$$\Phi_{max} = \frac{2\sigma y(1-\nu^2)}{E} \left(\frac{t}{r}\right)^2 f\left(\frac{t}{r}\right)$$

where ν = Poisson's ratio

E = elastic modulus

r = web radius

$$f\left(\frac{t}{r}\right) = \int_o^r \frac{d\left(\frac{x}{r}\right)}{\left\{1 + \frac{t}{r} - \left[1 - \left(\frac{x}{r}\right)^2\right]^{\frac{1}{2}}\right\}^3} \quad .$$

Evaluating this expression for the above hinge we obtain, for r = 0.25"

$$\Phi_{max} = 0.0236 \text{ radians } (13.5^o) \quad .$$

However, even this value needs to be reduced by the factor $(1 - P/2dt\sigma y)$ which accounts for the axial force, P, that must be transmitted. This factor is 0.74 for the 6,250 lb. load on the hinge just described, reducing the maximum angle to 10.1^o. This value is less than that obtained by the shrinkage of the inner dewar, 13.3^o, but presumably this could be corrected by lengthening the column or narrowing the hinge web or relocation of the support columns--all acceptable from the present design considerations.

9. Radiation loss through superinsulation. The radiation through the superinsulation can be characterized by an effective K in the equation $\dot{Q} = KA\Delta T$ but penetration of the superinsulation by the support columns, fill lines, and current leads will degrade this value. Nevertheless

$$\dot{Q} = 430 \text{ mw/dewar } (0.68 \ell \text{ He/hr/dewar}) .$$